Calhoun
Institutional Archive of the Naval Postgraduate School

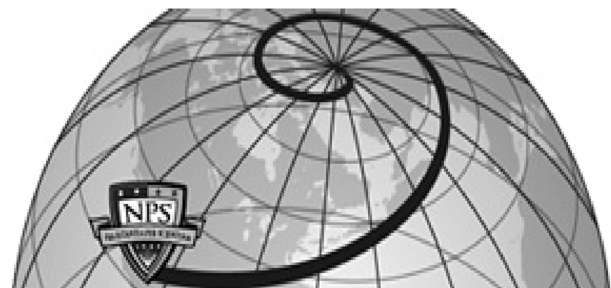

Calhoun: The NPS Institutional Archive

DSpace Repository

Theses and Dissertations 1. Thesis and Dissertation Collection, all items

2022-09

A STUDY FOCUSING ON THE EFFECTS OF HTOL STRESS ON THE LUMINESCENCE SPECTRUM OF GAN DIODES TO CHARACTERIZE COMPONENT DEGRADATION

Kavanagh, Shawn R.

Monterey, CA; Naval Postgraduate School

http://hdl.handle.net/10945/71072

This publication is a work of the U.S. Government as defined in Title 17, United States Code, Section 101. Copyright protection is not available for this work in the United States.

Downloaded from NPS Archive: Calhoun

Calhoun is the Naval Postgraduate School's public access digital repository for research materials and institutional publications created by the NPS community. Calhoun is named for Professor of Mathematics Guy K. Calhoun, NPS's first appointed -- and published -- scholarly author.

Dudley Knox Library / Naval Postgraduate School
411 Dyer Road / 1 University Circle
Monterey, California USA 93943

http://www.nps.edu/library

NAVAL POSTGRADUATE SCHOOL

MONTEREY, CALIFORNIA

THESIS

A STUDY FOCUSING ON THE EFFECTS OF HTOL STRESS ON THE LUMINESCENCE SPECTRUM OF GAN DIODES TO CHARACTERIZE COMPONENT DEGRADATION

by

Shawn R. Kavanagh

September 2022

Thesis Advisor:	Todd R. Weatherford
Second Reader:	Matthew A. Porter

Approved for public release. Distribution is unlimited.

THIS PAGE INTENTIONALLY LEFT BLANK

REPORT DOCUMENTATION PAGE			*Form Approved OMB No. 0704-0188*
Public reporting burden for this collection of information is estimated to average 1 hour per response, including the time for reviewing instruction, searching existing data sources, gathering and maintaining the data needed, and completing and reviewing the collection of information. Send comments regarding this burden estimate or any other aspect of this collection of information, including suggestions for reducing this burden, to Washington headquarters Services, Directorate for Information Operations and Reports, 1215 Jefferson Davis Highway, Suite 1204, Arlington, VA 22202-4302, and to the Office of Management and Budget, Paperwork Reduction Project (0704-0188) Washington, DC, 20503.			
1. AGENCY USE ONLY ***(Leave blank)***	**2. REPORT DATE** September 2022	**3. REPORT TYPE AND DATES COVERED** Master's thesis	
4. TITLE AND SUBTITLE A STUDY FOCUSING ON THE EFFECTS OF HTOL STRESS ON THE LUMINESCENCE SPECTRUM OF GAN DIODES TO CHARACTERIZE COMPONENT DEGRADATION			**5. FUNDING NUMBERS**
6. AUTHOR(S) Shawn R. Kavanagh			
7. PERFORMING ORGANIZATION NAME(S) AND ADDRESS(ES) Naval Postgraduate School Monterey, CA 93943-5000			**8. PERFORMING ORGANIZATION REPORT NUMBER**
9. SPONSORING / MONITORING AGENCY NAME(S) AND ADDRESS(ES) N/A			**10. SPONSORING / MONITORING AGENCY REPORT NUMBER**
11. SUPPLEMENTARY NOTES The views expressed in this thesis are those of the author and do not reflect the official policy or position of the Department of Defense or the U.S. Government.			
12a. DISTRIBUTION / AVAILABILITY STATEMENT Approved for public release. Distribution is unlimited.			**12b. DISTRIBUTION CODE** A

13. ABSTRACT (maximum 200 words)

Wide bandgap (WBG) semiconductor technology allows devices to be operated at higher voltages, currents, temperatures, and frequencies than does conventional silicon-based narrow bandgap semiconductors. These characteristics are advantageous to military applications, such as uses in power converters, weapons, and radar systems. Notably, WBG semiconductors have advantages where cooling and space availability for components are concerns, such as unmanned underwater platforms. The ability to monitor the health and performance of these devices passively and remotely would reduce the man-hours required for preventative maintenance; it would also reduce the needs for invasive troubleshooting and needless component replacement. This thesis demonstrates the abilities to measure and analyze the electroluminescence spectrum of WBG devices using a custom-built high-temperature operating life (HTOL) test setup incorporating the ability to sample light spectroscopy.

14. SUBJECT TERMS semiconductor, wide bandgap, WBG, electroluminescence spectrum, spectroscopy, high-temperature operating life, HTOL, gallium nitride, GaN, high voltage, power			**15. NUMBER OF PAGES** 107
			16. PRICE CODE
17. SECURITY CLASSIFICATION OF REPORT Unclassified	**18. SECURITY CLASSIFICATION OF THIS PAGE** Unclassified	**19. SECURITY CLASSIFICATION OF ABSTRACT** Unclassified	**20. LIMITATION OF ABSTRACT** UU

NSN 7540-01-280-5500 Standard Form 298 (Rev. 2-89) Prescribed by ANSI Std. 239-18

THIS PAGE INTENTIONALLY LEFT BLANK

Approved for public release. Distribution is unlimited.

A STUDY FOCUSING ON THE EFFECTS OF HTOL STRESS ON THE LUMINESCENCE SPECTRUM OF GAN DIODES TO CHARACTERIZE COMPONENT DEGRADATION

Shawn R. Kavanagh
Lieutenant, United States Navy
BS, Pennsylvania State University, 2015

Submitted in partial fulfillment of the
requirements for the degree of

MASTER OF SCIENCE IN ELECTRICAL ENGINEERING

from the

NAVAL POSTGRADUATE SCHOOL
September 2022

Approved by: Todd R. Weatherford
Advisor

Matthew A. Porter
Second Reader

Douglas J. Fouts
Chair, Department of Electrical and Computer Engineering

THIS PAGE INTENTIONALLY LEFT BLANK

ABSTRACT

Wide bandgap (WBG) semiconductor technology allows devices to be operated at higher voltages, currents, temperatures, and frequencies than does conventional silicon-based narrow bandgap semiconductors. These characteristics are advantageous to military applications, such as uses in power converters, weapons, and radar systems. Notably, WBG semiconductors have advantages where cooling and space availability for components are concerns, such as unmanned underwater platforms. The ability to monitor the health and performance of these devices passively and remotely would reduce the man-hours required for preventative maintenance; it would also reduce the needs for invasive troubleshooting and needless component replacement. This thesis demonstrates the abilities to measure and analyze the electroluminescence spectrum of WBG devices using a custom-built high-temperature operating life (HTOL) test setup incorporating the ability to sample light spectroscopy.

THIS PAGE INTENTIONALLY LEFT BLANK

TABLE OF CONTENTS

I. INTRODUCTION 1
- A. MOTIVATION 2
- B. RESEARCH OBJECTIVES 3
- C. RELATED WORK 4
- D. THESIS ORGANIZATION 5

II. BACKGROUND 7
- A. MATERIAL PROPERTIES OF GALLIUM NITRIDE 7
- B. GAN PN JUNCTION DIODES 9
- C. ELECTROLUMINESCENCE OF GALLIUM NITRIDE 12
  - 1. Band-to-band Recombination and Excitonic Recombination 12
  - 2. Non-Radiative Recombination 13
  - 3. Quantum Efficiency 14

III. HTOL STRESS TEST AND EL SPECTRAL ANALYSIS SYSTEM DESIGN 17
- A. SYSTEM OVERVIEW 17
- B. HIGH-CURRENT EL-ENABLED HTOL SYSTEM DESIGN 18

IV. INITIAL ELECTRICAL AND OPTICAL CHARACTERIZATION OF GAN PN DIODES AND RELIABILITY TESTING METHODOLOGY 25
- A. FABRICATION AND PACKAGING OF TESTED DEVICES 25
- B. INITIAL ELECTRICAL AND OPTICAL CHARACTERIZATION OF GAN PN DIODES 27
  - 1. NRL GaN PN 27
  - 2. HTOL System Validation using Commercial Device 29
  - 3. Initial Optical and Electrical Characterization of Commercial Devices 31
- C. EXPERIMENT METHODOLOGY AND TEST PLAN 38
  - 1. NRL GaN PN 38
  - 2. HTOL System Validation Methodology 39
  - 3. Testing Methodology for Commercial GaN PN diodes 39

V. EXPERIMENTAL RESULTS 41
- A. RESULTS OF INITIAL STRESS TEST OF NRL GAN DIODE 41
- B. RESULTS OF SECOND STRESS TEST OF DEVICE N1 43

C. RESULTS OF HTOL SYSTEM VALIDATION TESTING OF COMMERCIAL GAN PN DIODES ... 49
D. RESULTS OF INITIAL STRESS TEST OF DEVICE C2 ... 51
E. RESULTS OF SECOND STRESS TEST OF DEVICE C2 ... 59
F. RESULTS OF STRESS TEST ON DEVICE C3 ... 62
G. ANALYSIS OF STRESS TEST RESULTS ON COMMERCIAL DEVICES ... 65

VI. CONCLUSION AND FUTURE WORK ... 69
A. CONCLUSION ... 69
B. FUTURE WORK ... 70

APPENDIX A. LABVIEW HTOL INITIALIZATION PANES ... 73

APPENDIX B. LABVIEW SPECTROSCOPY ADDITION ... 75

APPENDIX C. COMMERCIAL DEVICE SPECTRAL DATA VS. INTENSITY PRE AND POST STRESS ... 77

LIST OF REFERENCES ... 83

INITIAL DISTRIBUTION LIST ... 87

LIST OF FIGURES

Figure 1. Applications of WBG Semiconductors GaN and SiC in Relation to Silicon. Source: [6]. 2

Figure 2. On-state Resistance vs. Breakdown Voltage of Semiconductor Materials. Source: [6]....................9

Figure 3. PN Junction (a) Unbiased (b) Forward Biased (c) Reverse Biased. Source: [17]....................11

Figure 4. Depiction of Direct and Indirect Bandgap Photon and Phonon Emission. Source: [7]....................13

Figure 5. Block Diagram of Update HTOL Sub-systems with Communication Paths....................18

Figure 6. Image of HTOL and EL Spectral Analysis System. (A) Control PC, (B) Programmable Power Supplies, (C) Back-UPS, (D) Keysight B1500A, (E) Legacy HTOL Modules, (F) HOTL EL Capable Module....................19

Figure 7. Image of the HTOL and EL Spectral Analysis Module. (A) DUT Chamber with PLA Lid Installed, (B) Module Power Supply Enclosures, (C) Upgraded Parallel Wired Switch Matrices....................21

Figure 8. Updated HTOL System TEC Convergence 10C to 120C 22

Figure 9. Updated HTOL System TEC convergence 120C to 10C 22

Figure 10. Top and Bottom Views of 3D-printed DUT Chamber Lid....................23

Figure 11. Fiber Cable and DUT Chamber with PLA Lid Installed (left), Prototyping of Spectrometer Integration to DUT Chamber with Device Installed in Cradle (right) 24

Figure 12. NRL Device Mounted on Custom-milled PCB in 3D-printed Polyethylene Carbon Fiber Cradle....................27

Figure 13. Initial Forward Bias Curves for N1 Device 28

Figure 14. Initial Reverse Bias Curves for N1 Device....................29

Figure 15. Initial Forward Bias Curves for Validation of Updated HTOL System with Device C1....................30

Figure 16. Initial Forward Bias Curves for Validation of Updated HTOL System with Device C1 30

Figure 17. Initial EL Spectra Data for Device C1 31

Figure 18. Device C2 Initial Stress Test Peak Spectra at 30C Varying Current 32

Figure 19. Device C2 Post Initial Stress Test Peak Spectra at 1.0A Varying Temperature 33

Figure 20. Initial Forward Bias Curves for C2 Device Stress Test 34

Figure 21. Initial Reverse Bias Curves for C2 Device Stress Test....34

Figure 22. Device C3 Initial Stress Test Peak Spectra at 30C Varying Current 35

Figure 23. Device C3 Initial Stress Test Peak Spectra at 1A Varying Temperature 36

Figure 24. Initial Forward Bias Curves for C3 Device Stress Test 37

Figure 25. Initial Reverse Bias Curves for C2 Device Stress Test....38

Figure 26. Image of Commercial Device with Sidewall Cut away to Allow Positioning Fiber Cable to Couple Light from the Die....39

Figure 27. Post Stress Forward Bias Curves for Device N1 41

Figure 28. Post Stress Reverse Bias Curves for Device N1 42

Figure 29. Device N1 Anode Voltage over Time for 100mA....43

Figure 30. Initial Forward Bias Curves for Second Test of N1 Device 44

Figure 31. Initial Reverse Bias Curves for Second Test of N1 Device....44

Figure 32. Forward Bias of Device N1 at Hour 8, Before Failure 45

Figure 33. Forward Bias of Device N1 at Hour 10, Before Failure 46

Figure 34. Reverse Bias of Device N1 at Hour 8, Before Failure....47

Figure 35. Forward Bias Device N1 at Hour 10, Before Failure 47

Figure 36. Anode Voltage of N1 Device at 1A over Time 48

Figure 37. Post-Stress Forward Bias Curves for Validation of Updated HTOL System with Device C1....49

Figure 38. Post-Stress Reverse Bias Curves for Validation of Updated HTOL System with Device C1 50

Figure 39. Degradation to Band-to-band Peak of Device N1 over Time 50

Figure 40. Device C1 Final Three Hours of EL Spectra Data for Validation of Updated HTOL System 51

Figure 41. Device C2 Forward Bias Curves Post Initial Stress Test 52

Figure 42. Device C2 Reverse Bias Curves Post Initial Stress Test 53

Figure 43. Device C2 EL Spectra Data for First Three Increments of Stress Test 54

Figure 44. Device C2 Final Three Hours of EL Spectrum Data Post Stress Test 55

Figure 45. Device C2 Post Initial Stress Test Peak Spectra at 1.0A Varying Temperature 56

Figure 46. Device C2 Post Initial Stress GaN EL Spectra at 30C Varying Currents 57

Figure 47. Device C2 Forward Bias Curves for Second Stress Test 58

Figure 48. Device C2 Reverse Bias Curves for Second Stress Test 58

Figure 49. Device C2 Forward Bias Curves Post Second Stress Test 59

Figure 50. Device C2 Reverse Bias Curves Post Second Stress Test 60

Figure 51. Device C2 Final Three Hours of EL Spectra Data Post Second Stress 60

Figure 52. Device C2 Post Second Stress Test GaN Peak Spectra at 30C Varying Current 61

Figure 53. Device C2 Post Second Stress Test GaN Peak Spectra at 1.0A Varying Temperature 62

Figure 54. Forward Bias Curves for Device C3 Post Stress Test 63

Figure 55. Reverse Bias Curves for Device C3 Post Stress Test 63

Figure 56. Device C2 Post Second Stress Test GaN Peak Spectra at 30C Varying Current 64

Figure 57. Device C3 Post Second Stress Test GaN Peak Spectra at 1A Varying Temperature 65

Figure 58. Device C2 Intensity vs. Intensity for Pre-stress (left) and Post-stress (right) at 1a and Varying Temperature 66

Figure 59. Device C2 Wavelength vs. Intensity for Pre-stress (left) and Post-stress (right) at 1a and Varying Temperature 66

Figure 60. Device C3 Intensity vs. Temperature for Pre-stress (left) and Post-stress (right) at 1 A and Varying Temperature 67

Figure 61. Device C3 Wavelength vs. Temperature for Pre-stress (left) and Post-stress (right) at 1A and Varying Temperature 68

Figure 62. Screen Capture of HTOL EL Spectra Testing System Main User Interface in LabVIEW..73

Figure 63. Screen Capture of HTOL EL Spectra Testing Parameters Setup Panel In LabVIEW...73

Figure 64. Screen Capture of HTOL EL Spectra Testing Sub-system Setup Panel in LabVIEW 74

Figure 65. Screen Capture of HTOL EL Spectra Testing System Spectrometer Integration SubVI Front Panel in LabView 75

Figure 66. Screen Capture of HTOL EL Spectra Testing System Spectrometer Integration Block Diagram in LabVIEW..75

Figure 67. Device C2 Pre-stress Band-to-band Peak Intensity vs. Wavelength 77

Figure 68. Device C2 Post-stress Band-to-band Peak Intensity vs. Wavelength........78

Figure 69. Device C2 Post Second Stress Band-to-band Peak Intensity vs. Wavelength 79

Figure 70. Device C3 Pre-stress Band-to-band Peak Intensity vs. Wavelength 80

Figure 71. Device C3 Post-stress Band-to-band Peak Intensity vs. Wavelength........81

LIST OF TABLES

Table 1. Material and Electrical Properties of Semiconductors. Source: [15]...........8

THIS PAGE INTENTIONALLY LEFT BLANK

LIST OF ACRONYMS AND ABBREVIATIONS

A.U.	arbitrary unit
BFOM	Baliga Figure of Merit
DC	direct current
DUT	device under test
EL	electroluminescence
EMI	electromagnetic interference
FET	field effect transistor
GaN	gallium nitride
GCU	general control unit
GPIB	general purpose interface bus
GUI	graphical user interface
HEMT	high-electron-mobility transistor
HTOL	high-temperature operating life
I-V	current-voltage
I-V-T	current-voltage-temperature
LED	light emitting diode
MOCVD	metalorganic chemical vapor deposition
MOSFET	metal-oxide-semiconductor field-effect transistor
PN	P-type-N-type
NPS	Naval Postgraduate School
NRL	Naval Research Laboratory
SiC	silicon carbide
SRH	Shockley-Read-Hall
TEC	thermoelectric cooler
USB	universal serial bus
USW	undersea warfare
UUV	unmanned undersea vehicle
WBG	wide bandgap

THIS PAGE INTENTIONALLY LEFT BLANK

ACKNOWLEDGMENTS

I would like to thank all the professors and staff in the Electrical and Computer Engineering and Undersea Warfare departments for the academic and professional development I received during my time at the Naval Postgraduate School. Thank you, Dr. Todd Weatherford, for the opportunity to work on such an interesting and hands-on project and thank you to Mr. Matthew Porter for all of the technical advice and for making yourself available for questions and help at literally all hours of the day. Thank you to all my fellow students for the comradery and good times had during our time together, especially all my lab mates from Room 512a. Finally, I would like to thank my wife Lindsay, my daughter Kaylee, and my friend Sierra for all their encouragement and support along the way. I could not have made it through this experience without your help.

THIS PAGE INTENTIONALLY LEFT BLANK

I. INTRODUCTION

As technology advances, the demand for high-power electronics is at an all-time high. Combat system components, such as sonar and radar, and directed energy weapons, as well as the growing Naval interest in unmanned vehicles and systems, require more energy and can handle greater energy than legacy systems. While current technology is acceptable, lighter, more compact, and more efficient power converters are required to meet the rising energy density demand [1]. Weight is a growing concern for ships; furthermore, unmanned platforms have even stricter constraints for weight and size. As power requirements continue to rise for sensors and combat systems equipment, the sizing of power supplies and switching devices offered by current silicon-based technology will rise as well. Wide bandgap (WBG) semiconductors, like gallium nitride (GaN), offers a potential solution with much smaller footprint, greater energy density and much higher efficiency [2].

Unmanned vehicles require complex power systems. In the case of underwater unmanned vehicles (UUVs), these systems include battery management systems, power conditioning circuits for radar, sonar, and communications systems, as well as propulsion and computing power systems [3]. These systems consume valuable space within the confines of an underwater system, and the efficiency of these systems determines the duration for which the vehicle they serve can remain on station. Increasing the efficiency of the necessary electronic systems, while shrinking their footprint, would allow more real estate for propulsion power (storage mediums such as batteries) and mission packages. Increasing the power density and efficiency of these systems would thus allow the vehicle to remain on station for longer, allowing it to conduct longer missions in a clandestine manner.

At the heart of any unmanned underwater system, whether it is a static sea-bed system or vehicle, lies its power supply. Increasing the amount of available power increases the potential of these systems, allowing them to collect more sensor data and execute more complex mission sets, which extends their operational usefulness. This requires advances

in power electronics and further miniaturization of existing systems, as existing systems are near the limit of current silicon-based technology that is reliable and available [4].

A. MOTIVATION

The size and weight of power supplies are dictated by the components required to supply equipment with the necessary voltages and currents to ensure proper operation. As the demand for power increases, so does the size of the power supplies. This can be mitigated to some extent by utilizing higher switching frequencies of power converters, allowing for the use of smaller passive electrical components, such as capacitors, inductors, and resistors. As switching frequencies rise, the efficiency of the power converter decreases due to the increased switching losses of semiconductor devices. This is where semiconductors composed of WBG materials, such as silicon carbide (SiC) and GaN, are more well suited, shown in Figure 1. The properties of WBG devices allow for power circuits to operate at much higher frequencies and power densities due to intrinsically lower switching and conductions losses in comparison to similarly rated Si power devices. The higher thermal conductivities of SiC and GaN allow for higher temperature operation as well, reducing the need for active cooling systems or large heat sinks [5].

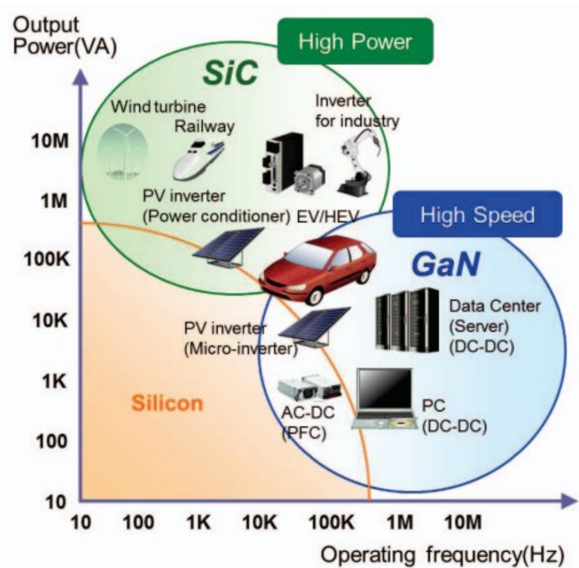

Figure 1. Applications of WBG Semiconductors GaN and SiC in Relation to Silicon. Source: [6].

As technology advances, autonomous vehicles are being used more and more within our military. Deploying a UUV for long-duration missions will rely on the power density of that vehicle, as well as the reliability of its systems. GaN power devices will provide an edge in power density and efficiency over the current silicon technology in use today. Recent development of high-quality native bulk GaN substrates will allow for the fabrication of high-voltage and high-current vertical GaN devices that will approach the theoretical performance limit of GaN. These devices will have the added benefit of strong electroluminescence from the high-quality PN junctions in vertical GaN, which offer possibilities for thermal and sensing benefits [7]. Along with the attractive power density, thermal properties, and efficiency of GaN devices, the electroluminescence (EL) spectra can also be utilized as a signal for analysis of system control, performance, and health measurements, provided the connection between the electrical properties and EL properties of the devices is known. These properties offer great prospects for achieving the promise of vertical GaN devices. Ongoing research into the development of such devices means that the reliability of high-power vertical GaN devices has been relatively unexplored to date. Such studies are needed to ensure the long-term performance of GaN devices for military applications.

B. RESEARCH OBJECTIVES

This thesis examines the high-temperature operating life (HTOL) reliability performance of novel vertical GaN PN diodes. To accomplish this, a custom programmable stress-measure-stress HTOL system is developed. This system can perform automatic temperature control of devices with up to 288 W of continuous device-under-test (DUT) power loss during testing and biasing devices at currents greater than 12 A. The designed system is based upon earlier work performed at NPS on the development of a compact stress-measure-stress HTOL system for the reliability testing of GaN Schottky diodes at lower current and temperature magnitudes. In addition, the updated system design includes the ability to dynamically measure EL spectra of DUTs during testing.

Utilizing the updated HTOL system, we examine the HTOL reliability of vertical GaN 1.2 kV PN junction power diodes. The diodes used in this work include devices

fabricated at the Naval Research Laboratory (NRL) and devices obtained from a commercial source. Four commercial devices are tested at varying current density levels from 200 A/cm^2 to 1 kA cm^2 and a range of device die temperature setpoints. Characteristics and light spectrum data measured during the stress-measure-stress testing are used evaluate and analyze the effects of induced stress on device performance.

Through HTOL and EL spectrum analysis, we demonstrate the ability to passively monitor device health and performance utilizing emitted light spectra. Forward bias stress testing and analysis of how the emitted light spectrum changes over time with stress can assist in monitoring device health and performance. This would allow for preventative maintenance before a device fails, which would prevent the unexpected loss of a piece of equipment or asset. Identifying specific defects in devices before they are manufactured can also aid in predicting expected lifetime, as well as potentially aid in changing the growth processes to make GaN more easily manufactured, more reliable, and thus more affordable to produce.

C. RELATED WORK

While GaN is a great example of a WBG semiconductor, the maturity of the material growth is not currently on the level of that of SiC. One of the reasons is how difficult it is to manufacture low-defect components. Growth of pure GaN substrates is difficult and cost prohibitive. These issues have led to research on GaN devices in which the GaN is grown heteroepitaxially on other substrates, such as sapphire, silicon and SiC. While devices are successfully manufactured in this manner, they suffer high levels of material defects and stress due to the differences in the crystal lattice structure and thermal properties of the epitaxially deposited GaN and the substrate. Specifically, threading dislocations, which propagate through the material during the deposition process, can lead to low yield and premature failure [8]. Recent advances in technology have allowed for growing low-defect, large-area wafers of bulk GaN, but it is still a maturing technology and is costly [9]. Due to the recent availability of large-area bulk GaN substrates, a large amount of recent work has demonstrated the feasibility of high-voltage, high-current vertical GaN devices.

In 2015, Kizilyalli, Bui-Quang, Disney, Bhatia and Aktas fabricated vertical GaN PN diodes grown on bulk GaN substrate with sufficiently low-defect density to permit use in power electronics. In-house reliability testing revealed high-quality devices capable of maintaining low-leakage current at up to 1200 V of applied reverse bias and could withstand forward bias currents up to 20 kA/cm^2 [10].

In 2021, LT Clemmer at the Naval Postgraduate School (NPS) performed research on the reliability of GaN Schottky diodes using the predecessor HTOL system in use for this research. His work demonstrated the use of the purpose-built autonomous HTOL system to take in-situ measurements of voltage, temperature and current between periods of electrical stressing on commercial-grade palladium/gallium nitride PN diodes. This research proved the usefulness of the HTOL system for conducting stress testing on components [11].

In 2019, ENS Broeg at NPS performed research relating the effects of various currents and temperatures on the EL output of GaN power diodes. Vertical GaN-on-GaN diodes were subjected to varying currents and temperatures, from 100 mA to 5 A and 20 C to 100 C, respectively, and the emitted light was analyzed using a spectrometer through various light filters via a fiber optic cable [12]. In 2022, LT Robinson conducted further research on both GaN and SiC, using a similar GaN power diode as well as a custom-built SiC power module, analyzing the EL spectra from the power modules MOSFET body diode [7].

D. THESIS ORGANIZATION

This thesis is organized as follows. Relevant information on WBG semiconductors and EL, focusing on GaN, is reviewed in Chapter II. An overview of the HTOL system design and experimental approach, as well as information on the vertical GaN power devices tested, is provided in Chapter III. For the HTOL and EL collected data, discussions of observations between I-V characteristics and EL spectra are reviewed in Chapter IV. The experimental results and findings are presented in Chapter V. Lastly, conclusions and recommendations for experimental modification/alteration for future work are given in Chapter VI.

THIS PAGE INTENTIONALLY LEFT BLANK

II. BACKGROUND

A. MATERIAL PROPERTIES OF GALLIUM NITRIDE

While silicon (Si) has demonstrated its reliability for decades and is widely available, easily manufactured and used in a wide array of devices, the material properties of Si limit the achievable tradeoff between the on-state resistance, breakdown voltage and switching speed of Si power devices [13]. Specifically, the material limited tradeoff between on-state resistance and breakdown voltage requires large-area devices for large current ratings, which limits device switching speed, resulting in greatly reduced converter power densities [14]. Materials that can overcome these limits are WBG semiconductors; their properties result in higher critical electric fields at breakdown and low intrinsic carrier concentrations at elevated temperatures, and they have high electron and acceptable hole mobility.

WBG semiconductors have a bandgap of greater than 2.2 eV, with a bandgap energy of 3.4 eV for GaN. The high critical electric field of GaN, 3.3×10^6 V/cm, means that GaN devices may have a narrower drift region, reducing on-state resistance, which in turn lowers conduction losses. The high electron mobility, 2000 cm^2/Vs, decreases the required area and allows for operating devices at higher switching speeds, which means a power device may operate at higher frequencies. A list of the material properties of GaN and SiC in comparison to those of silicon are shown in Table 1.

Table 1. Material and Electrical Properties of Semiconductors. Source: [15].

Parameter	Symbol	Unit	Si	SiC	GaN
Bandgap	E_c	eV	1.12	3.2	3.43
Relative Dielectric Constant	ϵ_s	-	11.9	10	9.5
Electron Mobility	μ_n	$cm^2/(V.s)$	1500	700	2000
Peak Electron Velocity	v_{peak}	$10^7 \cdot cm/s$	1	2	2.5
Critical Electric Field	E_c	MV/cm	0.3	3.0	3.3
Baliga Figure of Merit (BFOM)	$\epsilon_s \mu_n E_c^2$	W/cm^2	1	392*	1416*
* Normalized to Si					

The Baliga Figure of Merit (BFOM) is a standard that was developed to aid in designing semiconductor devices and optimize design parameters to minimize conduction losses [16]. The ideal on-state resistance for minimizing conduction loss is derived from equation (1). R_{DSon} is the on-state resistance, which is determined by the values of the breakdown voltage, V_B; the critical electrical field, E_{crit}; the electron mobility, μ; and the relative permittivity, ε_s [16].

$$R_{DS_{on}} = \frac{4V_B^{\ 2}}{\varepsilon_s \mu E_{crit}^{\ 3}} \tag{1}$$

A graphical representation of on-state resistance vs. breakdown voltage for different semiconductor materials is shown below in Figure 2. This shows GaN as having greater potential over SiC, given its lower on-state resistance and higher breakdown voltage. Though advances in manufacturing have been made in recent years, the technical complexities involved in the growth of low-defect bulk GaN substrate and device growth are limiting factors for the ability of GaN to reach its BFOM and thereby achieve its full usefulness in power electronics applications.

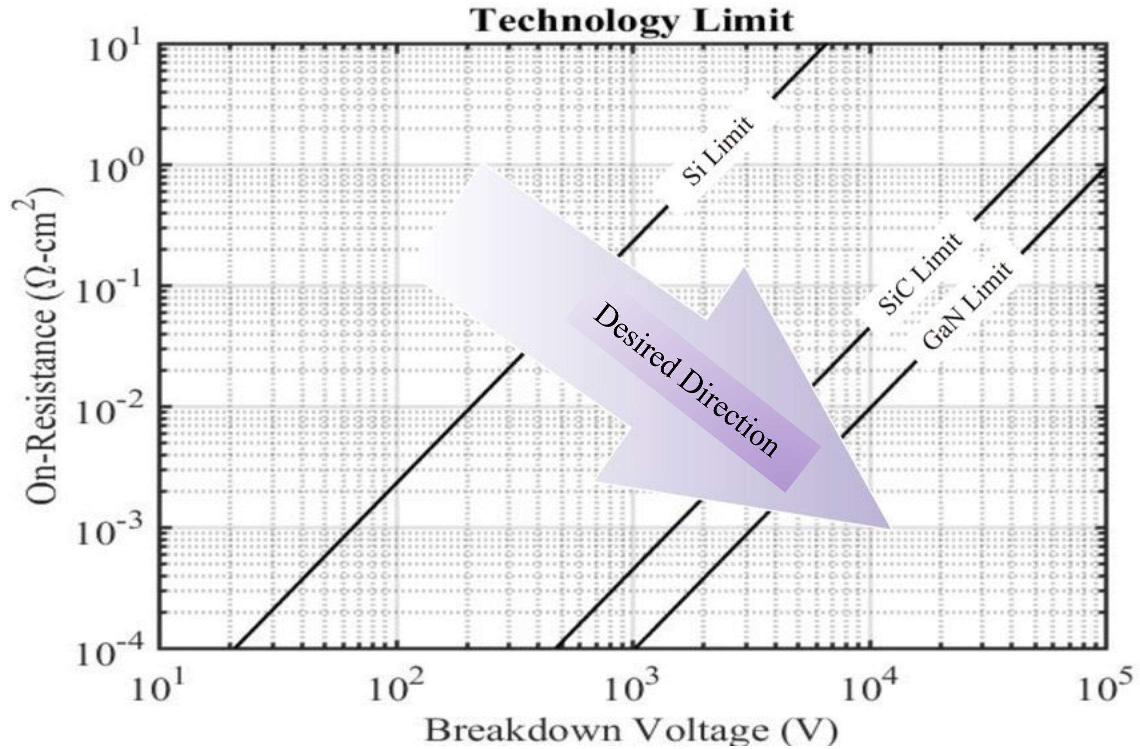

Figure 2. On-state Resistance vs. Breakdown Voltage of Semiconductor Materials. Source: [6].

While the bandgap energy, electron mobility, and electron saturation velocity of GaN are higher than those of Si and SiC, the thermal conductivity of GaN is 1.3 W/cmK, lower than that of SiC at 3.7 W/cmK [15]. However, the larger bandgap energy and greater electron mobility lead to GaN devices having much lower on-state resistances and higher switching frequencies, as well as low leakage current; these features make GaN an attractive material for the future of power electronics.

B. GAN PN JUNCTION DIODES

In this study, we examine the relationship between the electrical properties and EL of vertical GaN PN diodes. A PN diode is formed from the junction between p-type and n-type semiconductor material. The p-type region is doped with acceptor impurities to create a higher concentration of holes, while the n-type region is doped with donor impurities to increase the concentration of electrons. This creates a potential barrier via the formation of an electrostatic dipole through buildup of ionized dopants near the

junction in a region called the depletion region. The direction of current flow through the device is dictated by the height of the potential barrier and is comprised of drift current and diffusion current.

Once formed, the potential barrier prevents free electrons and holes from diffusing between the PN junction until a forward or reverse bias is applied. Biasing of the diode affects the height of the potential barrier and thus the conduction state of the diode, as shown in Figure 3. If a reverse bias is applied, with a potential on the p-type region being lower than that on the n-type region, the depletion region grows and the potential barrier of the junction increases. In this state, very little current flows through the diode [17].

When a PN junction is forward biased, a positive potential on the p-type material relative to the n-type material lowers the potential barrier of the junction, and holes are injected from the p-type to the n-type side of the junction (and vice-versa for electrons). This produces a net current flow through the diode as diffusion current, due to injected minority carriers becoming greater than the opposing drift current in the depletion region and the device conducts [17]. The relationship between drift, diffusion and net current flow through the device is shown by equation (2). The term V is the potential applied across the device, q is the absolute value of electron charge, T is temperature in degrees Kelvin and k is the Boltzmann's constant.

$$I = I_0(e^{qV/kT} - 1) \tag{2}$$

Total current through the device is derived from equation (3), where A is the area of the diode, W is the width of the device, n_i is the intrinsic carrier concentration, N_D is the donor concentration, D_P is the hole diffusion constant, W is the width of the depletion region, and τ is the effect minority carrier lifetime [17]. The left side of the bracketed term describes diffusion current, while the right side describes recombination current in the depletion region.

$$I = qAn_i \cdot [\frac{n_i}{N_D}\sqrt{\frac{D_P}{\tau}}(e^{qV/kT} - 1) + \frac{W}{2\tau}(e^{qV/2kT} - 1)] \tag{3}$$

I_0, representing saturation current, can be derived from equation (4). When a PN junction is reverse biased, the left- and right-side exponential terms drive the $(e^{qV/kT}-1)$ terms to a very small negative value and become insignificant, simplifying down to the terms left in equation (4).

$$I_0 = -qAn_i\left(\frac{n_i}{N_D}\right)\sqrt{\frac{D_P}{\tau}} + \frac{W}{2\tau} \tag{4}$$

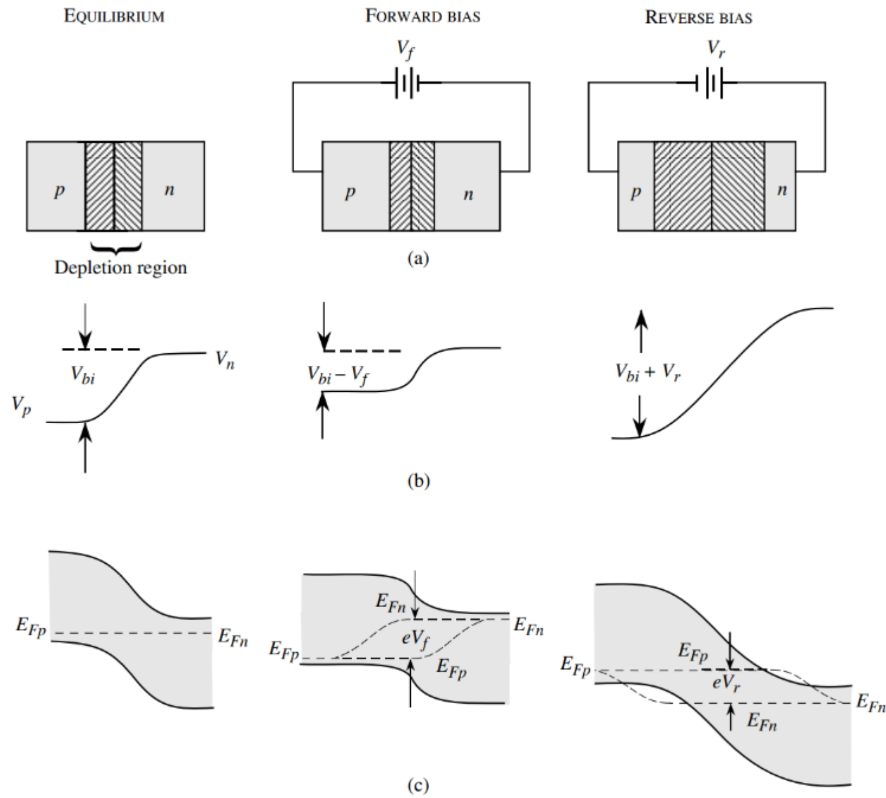

Figure 3. PN Junction (a) Unbiased (b) Forward Biased (c) Reverse Biased. Source: [17].

C. ELECTROLUMINESCENCE OF GALLIUM NITRIDE

Due to the direct bandgap of GaN, the efficiency of light emission from GaN PN devices is high, making these devices a good material for optoelectronic devices intended to emit near-UV wavelengths. GaN is used for LEDs as well as power electronics. Light emission from GaN devices under electrical bias, or EL, occurs through several mechanisms. The primary mechanisms are electron and hole recombination as well as excitonic recombination. Secondary mechanisms of light emission occur through electron and hole recombination via trap or doping states [17].

1. Band-to-band Recombination and Excitonic Recombination

Radiative recombination in GaN devices is categorized by band-to-band recombination, stimulated emission, excitonic recombination, and trap emission. In the case of band-to-band recombination, an electron from the conduction band drops into the valence band and combines with a hole emitting excess energy in the form of a photon, shown in Figure 3. In the case of stimulated emission, an incoming photon interacts with an electron, scattering the electron into the conduction band and causing emission of a photon. Trap emission results from the presence of defects in the semiconductor material, where a hole or electron becomes "trapped" and recombines with its counterpart, resulting in emitted photons [17].

Electron hole interactions that do not result in recombination can form excitons, electrically neutral quasi-particles resembling a hydrogen atom [18]. WBG materials such as GaN have large exciton binding energies, around 100 meV, allowing excitons to exist at room temperature in low-doped material [19]. In lightly doped direct bandgap material such as GaN, the decay of excitons is another major contributor to emitted light. Both excitonic emission and band-to-band recombination are subject to temperature dependence due to the change in electronic structure, specifically the fundamental bandgap, as a function of temperature. The change in bandgap as a function of temperature can be captured by the Varshni equation shown in Equation (4), where $E_g(0)$ is the bandgap energy at 0 degrees Kelvin, T is junction temperature in degrees Kelvin,

and α and β are properties of the semiconductor material. As temperature increases, the bandgap energy decreases, resulting in the emission of higher wavelength photons.

$$E_g(T) = E_g(0) - \frac{\alpha T^2}{1 + \beta T} \tag{4}$$

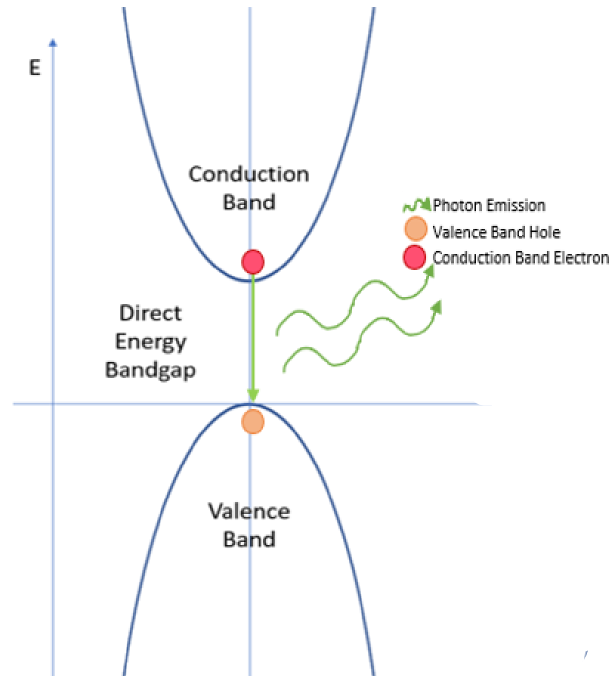

Figure 4. Depiction of Direct and Indirect Bandgap Photon and Phonon Emission. Source: [7].

2. Non-Radiative Recombination

Non-radiative recombination occurs due to energy transitions mediated by phonons rather than photons, as illustrated in Figure 4 [20]. Two significant types of non-radiative recombination include Shockley-Read-Hall (SRH) recombination and Auger recombination. SRH recombination is a multi-step process in which an electron or hole is trapped in a defect, and then recombination occurs when another hole or electron is trapped nearby; this type of recombination generally occurs in a semiconductor during

instances of low carrier concentration. This recombination results in the generation of phonons into the surrounding crystal structure rather than the emission of a photon [21]. Auger recombination results from electron-electron scattering in which the energy is transferred to another electron in the conduction or valence band rather than the energy being emitted as a photon. This process occurs more frequently in areas of a device where there is a high carrier concentration, due to the necessity for there to be an abundance of carriers in the vicinity of the original instance of electron-hole recombination [22].

3. Quantum Efficiency

Not all excitonic and radiative recombination interactions result in a photon being emitted from a diode. Non-radiative recombination and Auger recombination will reduce the number of photons produced for a given bias. In addition, some photons will be absorbed or reflect within the physical boundaries of the semiconductor once emitted. The ratio of the radiative recombination rate to the total recombination rate (sum of the radiative and non-radiative terms) is referred to as the internal quantum efficiency (IQE). The ratio of the emitted photon flux to the total drive current is termed the external quantum efficiency (EQE) and captures the effect of internal reflection and absorption in the semiconductor prior to emission. Commercially produced LEDs utilized for lighting and communication applications boast EQEs of up to 75% for shorter wavelengths, with that number tapering off as the wavelengths become longer [23]. In the case of power semiconductors, this is not necessarily engineered for, but with appropriately packaged direct-bandgap semiconductor diodes, we can study the intensity of the light emitted vs. the current applied to these devices and the effects of electrical and thermal stresses on them.

Using diodes that are manufactured to minimize dislocations and have sufficiently low defect density, carrier recombination can be described using the ABC model developed by Piprek [23]. In equation (5), I_{rad} is the current contributing to radiative recombination, while I is the current applied to the device, n is the carrier density, A represents SRH effects, B represents radiative recombination, C represents Auger recombination, and η_i, represents the IQE. Each of the coefficients A, B and C exhibit

temperature dependence, with B and C decreasing in magnitude with rising temperature and A increasing with rising temperature. This decrease in magnitude associated with B and C dominates the equation as temperature of the junction rises, causing the characteristic droop in IQE [23].

$$\eta_i = \frac{I_{rad}}{I} = qV\left(\frac{Bn}{A + Bn + Cn^2}\right) \tag{5}$$

THIS PAGE INTENTIONALLY LEFT BLANK

III. HTOL STRESS TEST AND EL SPECTRAL ANALYSIS SYSTEM DESIGN

A. SYSTEM OVERVIEW

The HTOL system with EL spectrum analysis was designed based off of the system previously implemented by LT Clemmer in 2019 [11]. The system was originally designed to conduct automated "stress-measure-stress" experiments with no user action required other than to install the device under test (DUT) and perform system initialization procedures. During initialization, the user defines the stress current and temperature to be applied to the DUT, humidity tolerance for the system, test duration and measurement intervals for spectrum collection and current-voltage-temperature measurements (I-V-T). The original system was designed in a modular rack-mounted configuration to allow testing of multiple batches of devices at once, removal of the racks for DUT installation and removal, and system troubleshooting. This thesis extends the capabilities of the original stress-measure-stress system via a redesign of the DUT chamber, TEC-enabled thermal controller and automated switch matrix. In addition, automated measurement of in-situ DUT electroluminescence was enabled via the addition of an Ocean Optics spectrometer to the measurement loop. Due to the addition of the OsTech TEC controller and Ocean Insight spectrometer, the testing system developed in this thesis is situated external to the server rack housing previous editions of the HTOL system. A block diagram of the overall system layout is shown below in Figure 5.

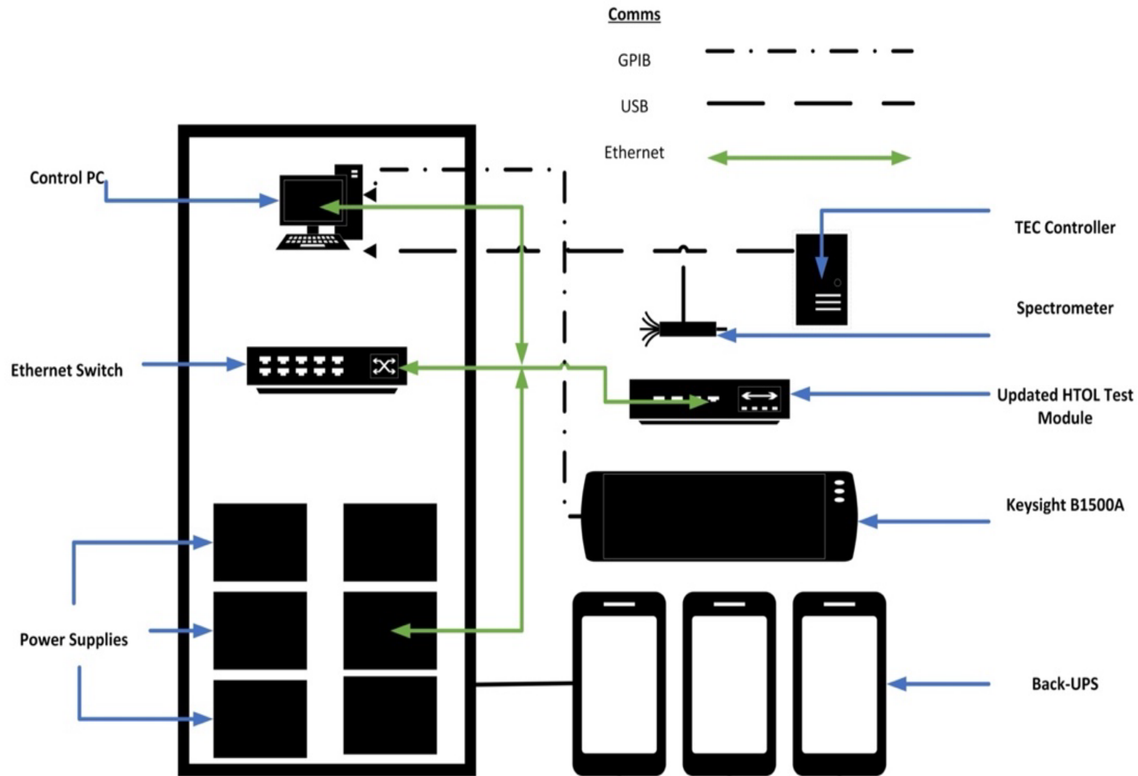

Figure 5. Block Diagram of Update HTOL Sub-systems with Communication Paths

B. HIGH-CURRENT EL-ENABLED HTOL SYSTEM DESIGN

The HTOL and EL spectrum test system module was constructed with design modifications to allow higher stress temperatures and faster rise/fall times of device temperature as well as integration of a spectrometer to take spectrum measurements during the stress cycle. The rest of the system is inherited from the original HTOL system in which the modifications were built upon, described in Clemmer's work [11]. The inherited part of this system is controlled by a PC using a custom designed LabVIEW program that automatically controls all the sub-systems of the setup. A Netgear 24-port gigabit switch, a Keysight B1500A semiconductor parameter analyzer, multiple SPD3000x Siglent programmable DC power supplies and BR1500G APC back-UPS are reused for the system design of this thesis. The PC is the central control unit for the subsystems and is where system data measurements are stored. The Netgear switch manages communications among all the subsystems with the exceptions of the Keysight B1500A, a Model 305v2

OsTech thermoelectric cooler (TEC) controller and Ocean Insight HR4000 spectrometer. The Keysight B1500A utilizes a GBIP bus to perform and communicate the I-V-T measurements, while the OsTech TEC controller and the Ocean Insight spectrometer each utilize a direct USB connection to the control computer for temperature control and spectrum measurements, respectively. Siglent power supplies provide stress current and voltage for the DUTs, while APC back-UPS provide power conditioning and reliability. The entire system, including two of the legacy HTOL modules, is shown in Figure 6.

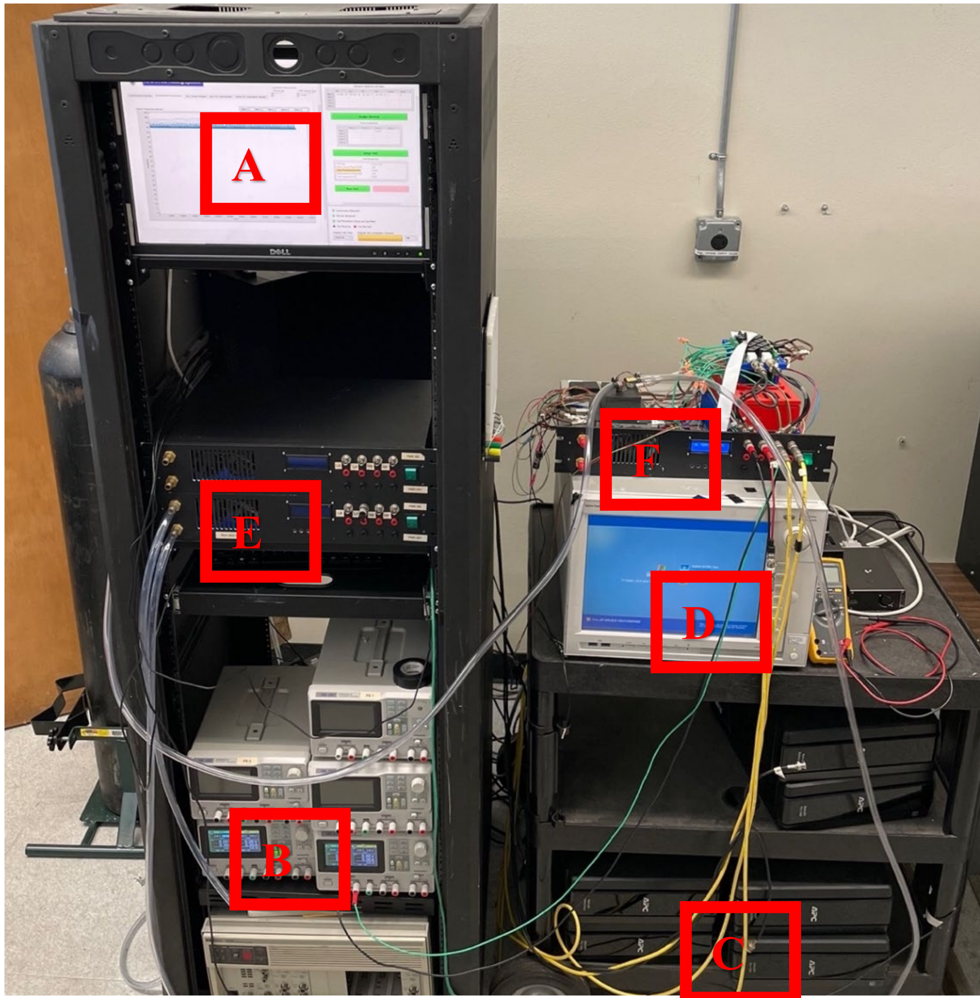

Figure 6. Image of HTOL and EL Spectral Analysis System. (A) Control PC, (B) Programmable Power Supplies, (C) Back-UPS, (D) Keysight B1500A, (E) Legacy HTOL Modules, (F) HOTL EL Capable Module

The testing module can perform testing on up to four devices at a time, collecting I-V-T measurement data and EL spectrum data. The test module is supplied 120 V AC/60 Hz suppled from the APC back-UPS, feeding a 5-V, 30-A DC power supply and a 24-V, 15-A power supply through a front-panel LED switch. These supply power to the three major sub-systems, the OsTech TEC controller, the custom-designed switch matrix and an Mbed NXP LPC1768 microcontroller that acts as a general control unit (GCU). The GCU controls the switch matrix permitting the B1500A to sequentially perform I-V-T sweeps on devices at intervals controlled by the LabVIEW program run from the PC. The GCU also controls humidity in the DUT chamber by sensing chamber humidity and actuating an external solenoid operated valve that admits dry nitrogen to keep humidity within tolerances.

The switch matrix allows for automated control of I-V-T measurements between multiple devices during the test cycle. For the design used in this thesis, two switch matrices of the original module design were assembled and wired in parallel to allow for testing power devices at higher currents without compromising the integrity of the dual-pole single-throw switch, which are rated at 8 A each. This allows devices to be stressed at currents up to 16 A each, shown in Figure 7.

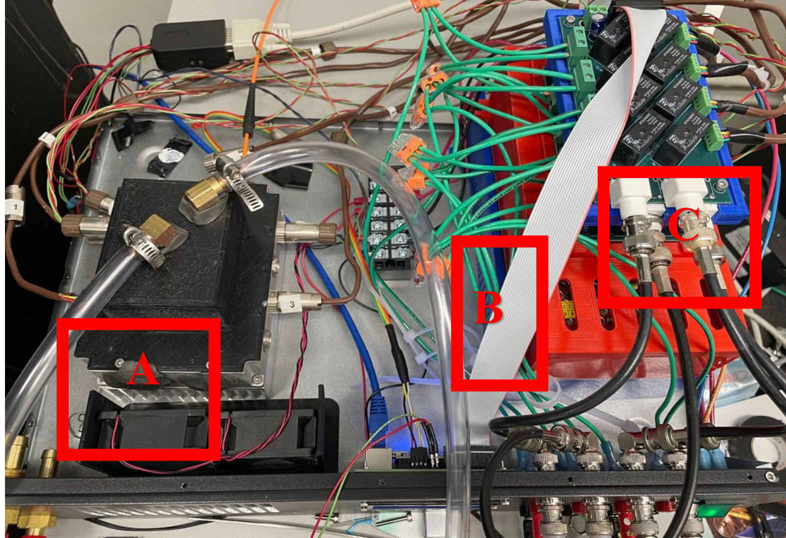

Figure 7. Image of the HTOL and EL Spectral Analysis Module. (A) DUT Chamber with PLA Lid Installed, (B) Module Power Supply Enclosures, (C) Upgraded Parallel Wired Switch Matrices

Temperature control is accomplished using the Model 305v2 OsTech TEC controller. The OsTech utilized has an output of 12 A and 20 V, with the ability to control temperature between -25 C and 150 C. The unit utilizes a 10K Ω thermistor to sense temperature and varies current and voltage to the TEC as necessary to maintain a desired temperature. The thermistor is wired to the DUT chamber and secured to the surface of the cold plate atop the TEC. Control power for the TEC is wired to the DUT chamber, and a single 288-W TEC plate is mounted in the center of the DUT underneath a cold plate to allow heat transfer between devices and the TEC. The actual range of temperature achievable by the TEC utilized was between 10 C and 120 C. Temperature rise and fall times were 119 seconds and 205 seconds, respectively, for a 10 C to 120 C step (and vice versa), which are shown in Figure 8 and Figure 9, respectively.

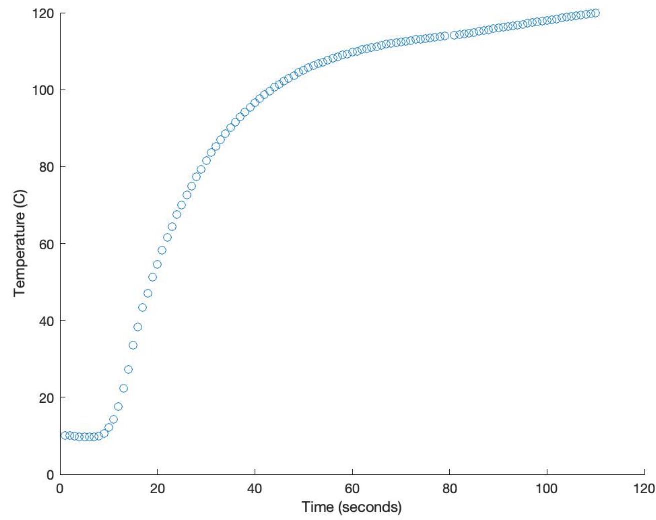

Figure 8. Updated HTOL System TEC Convergence 10C to 120C

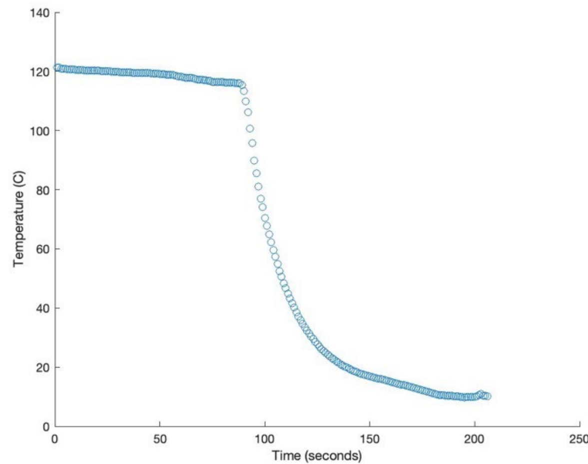

Figure 9. Updated HTOL System TEC convergence 120C to 10C

Humidity control is accomplished using a Honeywell HIH7120 humidity sensor, which is mounted on a custom-designed board and housed within the DUT chamber. The sensor sends data to the GCU, which is sent to a board external to the module that controls a solenoid-operated valve. This valve cycles as necessary to keep relative humidity within the DUT chamber within 5% of the user-specified humidity input into the GUI by purging the DUT chamber with dry nitrogen gas at a purity of 99.8%. A

modification to the DUT chamber lid was necessary to accommodate the addition of fiber optic cables entering the DUT chamber. A custom-designed lid was developed and manufactured from polylactic using a 3D printer, shown below in Figure 10. The lid was designed with ports for admitting the dry nitrogen gas to the chamber as well as a pocket where desiccant can be installed to aid in keeping humidity low in the DUT chamber and slow the consumption of nitrogen during testing.

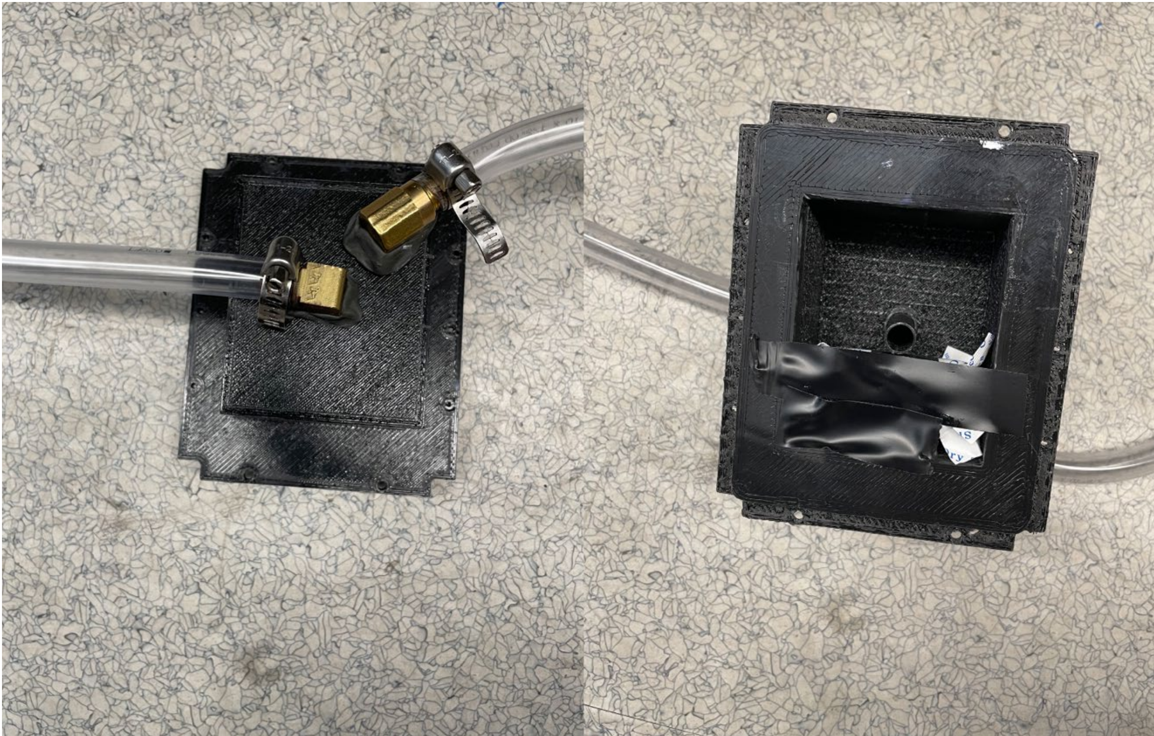

Figure 10. Top and Bottom Views of 3D-printed DUT Chamber Lid

The EL spectrum can be sampled for open packaged devices with the Ocean Insight HR4000. This spectrometer is capable of sampling wavelengths from 200 nm to 1100 nm. The sampling frequency is determined by a customized LabVIEW VI built with wrappers to a c-library supplied by the manufacturer. The spectrum subVI, which is shown in Appendix B, is integrated with the HTOL program that controls operation of the test module, with light being sampled via a fiber optic cable secured near the junction of an open package device.

Figure 11. Fiber Cable and DUT Chamber with PLA Lid Installed (left), Prototyping of Spectrometer Integration to DUT Chamber with Device Installed in Cradle (right)

As discussed earlier, the entire system operates autonomously after it is initialized by the user. Devices to be stressed are installed in the DUT chamber, where they are secured to the cold plate using custom-designed cradles that were created using a 3D printer with carbon fiber-impregnated polypropylene for heat resistance. Once devices are installed, the custom-designed 3D-printed lid is installed to seal the DUT chamber. The LabVIEW GUI is then used to set stress test parameters such as stress current and temperature, as well as test duration and the intervals and temperatures at which I-V-T sweeps and spectral data are collected. Additional user interfaces and initialization panels can be viewed in Appendix A.

IV. INITIAL ELECTRICAL AND OPTICAL CHARACTERIZATION OF GAN PN DIODES AND RELIABILITY TESTING METHODOLOGY

A. FABRICATION AND PACKAGING OF TESTED DEVICES

A total of four devices were tested using the updated HTOL system. A vertical GaN PN diode fabricated by the NRL was used to validate operation of the thermal upgrades to the HTOL system, as well as prepare for future experiments utilizing similarly packaged GaN devices. Three other commercial vertical GaN PN diodes were used to validate and test the optical updates to the HTOL system. The NRL device was from a lot manufactured for use in research and development in an Advanced Research Projects Agency-Energy (ARPA-E) project aimed at developing GaN diodes with 20kV breakdown voltage for use in power grid protection systems. The fabrication and design of the NRL device were as follows. A 10-um thick n-drift layer was grown via MOCVD, with an estimated effective donor concentration of 10^{16} cm^{-3}, followed by MOCVD growth of a 400-nm-thick p-type layer. The estimated acceptor doping concentration of the p-type layer was $1x10^{18}$ cm^{-3}. A thin p+ cap was grown to aid ohmic contact formation to the p-type anode layer. Edge termination of the devices was accomplished via N implantation. Ni/Au metallization was utilized for the backside ohmic contact and a Ti/Ni/Au alloy was used to form the ohmic contact to the p-type region. The devices used in this study had an effective anode area of 400 um x 400 um.

The NRL device used in this work was packaged in a SMD10003 surface mount style metal package with gold wire bonds for the anode and backside ohmic contact for the cathode. The NRL device was mounted on a break-out board that was designed and produced using a Roland Modela MDX-40A mill on FR-4 copper clad boards. Copper tracks were milled out to provide mounting surfaces for soldering the package anode and cathode contacts to the PCB. The cavity of the NRL device provided was sealed with an epoxy compound to hermetically seal the component for use in a power converter, so EL spectrum data were not collected for this device.

In addition, three commercial GaN PN devices were tested; these devices were also vertically grown on bulk GaN substrate through MOCVD. The commercial devices were similar to the NRL device in vertical structure, with an estimated drift layer thickness of 8 um and estimated drift layer donor level of $7x10^{15}cm^{-3}$. The estimated area of the anode contact of the commercial devices was 1.2 mm x 0.4 mm. These devices were packaged in TO-257 open-cavity metal packages. One sidewall of the packaging was cut away to allow fiber optic placement to collect EL spectrum data during the HTOL stress testing. No surface-mount PCB was required for these packages, as the posts were sufficient to deliver power to the device. Both the commercial and NRL devices were mounted in the DUT chamber using custom-designed cradles using rapid prototyping with a 3D printer and printed from a polyethylene and carbon fiber blend filament to provide adequate heat resistance. These cradles, pictured below in Figure 11, ensured each device would remain in contact with the heat transfer surface within the DUT chamber. In the case of the NRL device, a gap existed between the bottom of the SMD10003 package and the heat transfer surface within the DUT chamber. To overcome this, sheets of aluminum nitride were sandwiched between the bottom of the device and the heat transfer surface, with thermal paste used to provide a good thermal contact. An example of this configuration is pictured below in Figure 12. The 3D-printed cradles also provided a method for positioning a fiber optic cable to collect EL spectrum data from the open-cavity TO-257 commercial devices.

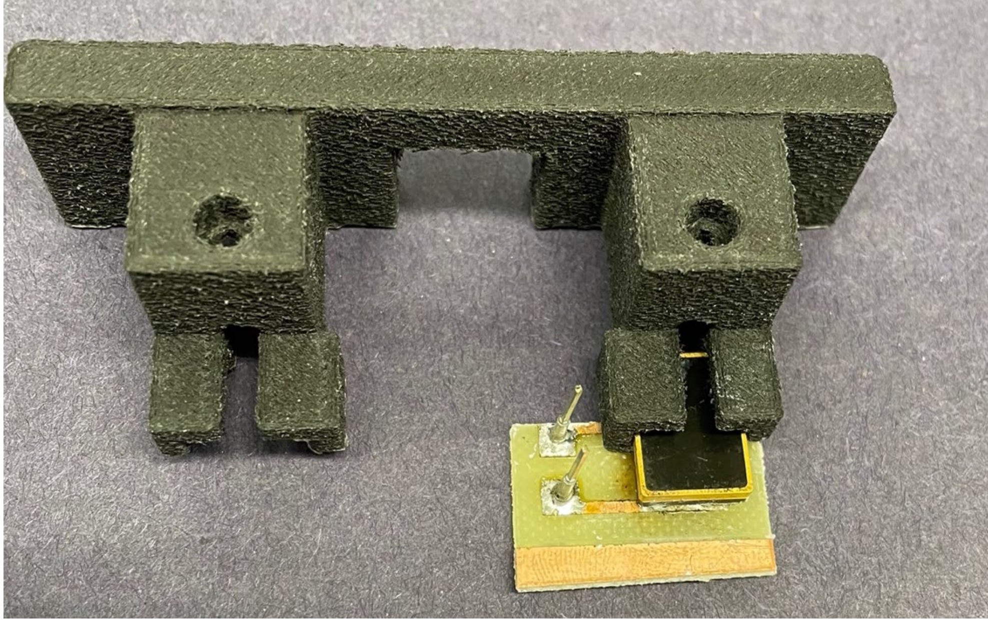

Figure 12. NRL Device Mounted on Custom-milled PCB in 3D-printed Polyethylene Carbon Fiber Cradle

B. INITIAL ELECTRICAL AND OPTICAL CHARACTERIZATION OF GAN PN DIODES

Each device tested in this work was characterized electrically using the Keysight B1500A semiconductor analyzer. I-V-T measurements were conducted at 20 C increments, from 30 C to 110 C, with the devices mounted within the DUT chamber. Initial forward and reverse measurements varied in range and are specified for each device that was tested. Generally, forward measurements covered 0 V up to 5 V, and reverse measurements ranged from 0 V to 200 V.

The devices tested are referred to throughout the rest of the document by the following serialization scheme: the NRL device is N1, and the commercial devices are referred to as C1 for the EL spectrum validation test and C2 and C3 for the follow-on stress tests.

1. NRL GaN PN

The initial I-V-T sweep is shown below in Figure 13 and Figure 14. Because the device was hermetically sealed with epoxy, no spectral data were obtained for this test.

Initial on-state resistance calculated from data at 30 C was 3.1 Ω, while initial I-V-T sweeps show reverse leakage current as tens of nanoamps.

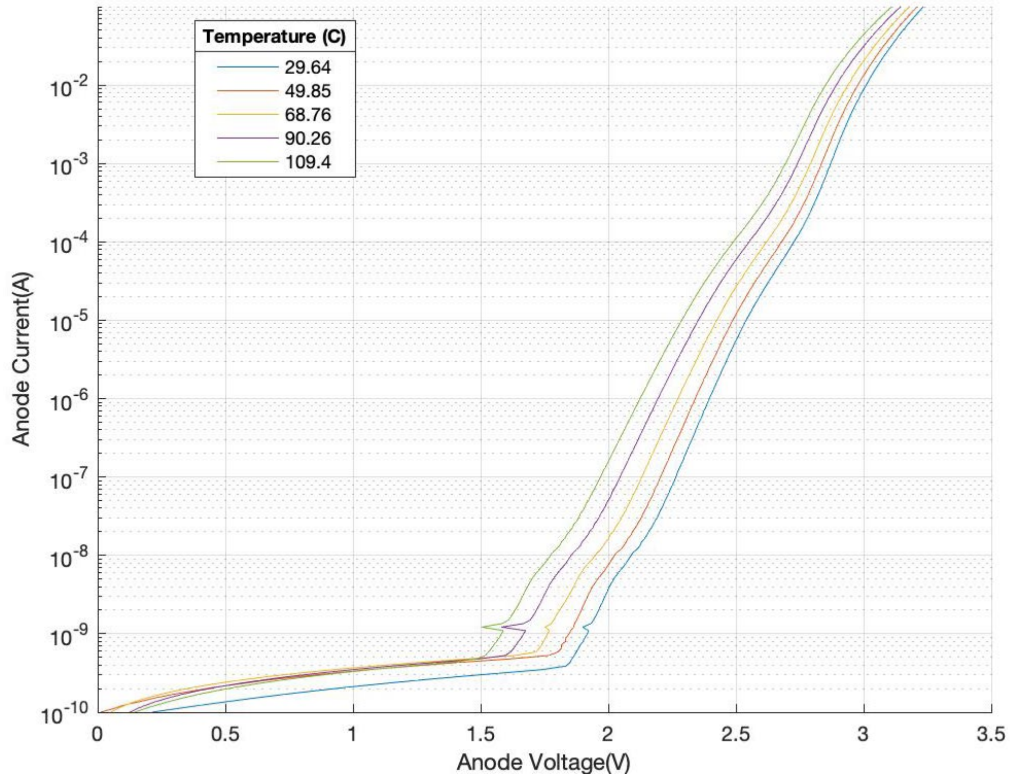

Figure 13. Initial Forward Bias Curves for N1 Device

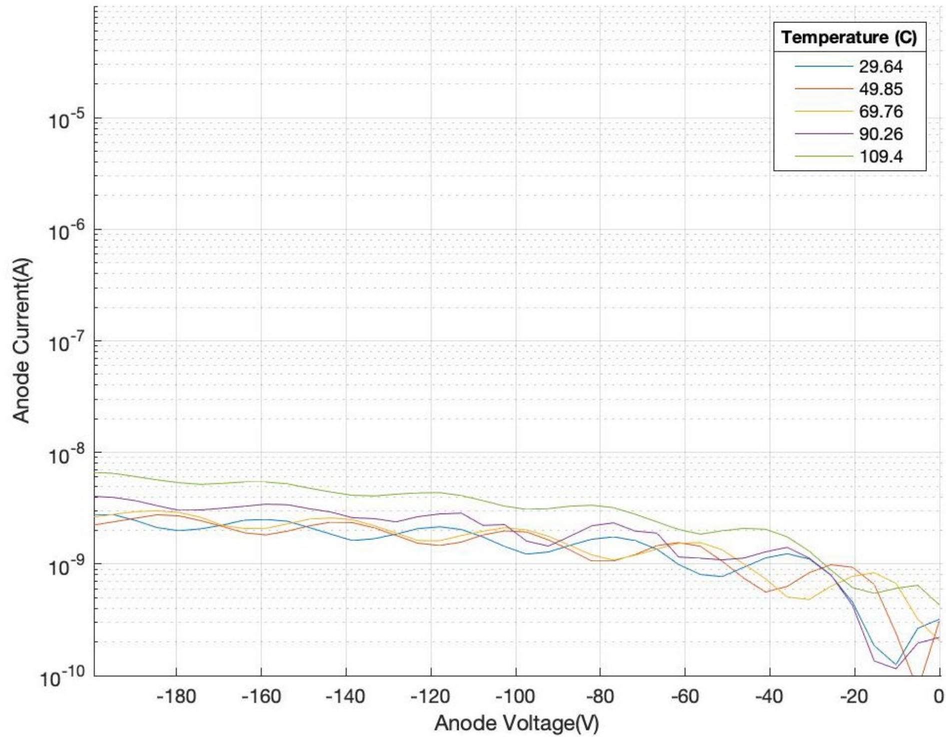

Figure 14. Initial Reverse Bias Curves for N1 Device

2. HTOL System Validation using Commercial Device

A GaN power diode was used as the commercial device tested to validate the optical features of the updated HTOL system. A TO-257 open package style device was installed in the DUT chamber in the customized cradle. The fiber optic cable was positioned to couple light from the diode to the fiber. Figure 15 and Figure 16 show the initial I-V-T measurement prior to the stress cycle, with on-state resistance calculated from data at 30 C was 3.76 Ω, with reverse leakage current in the hundreds of picoamps range. Figure 17 displays the band-to-band peak and peaks due to carbon impurity.

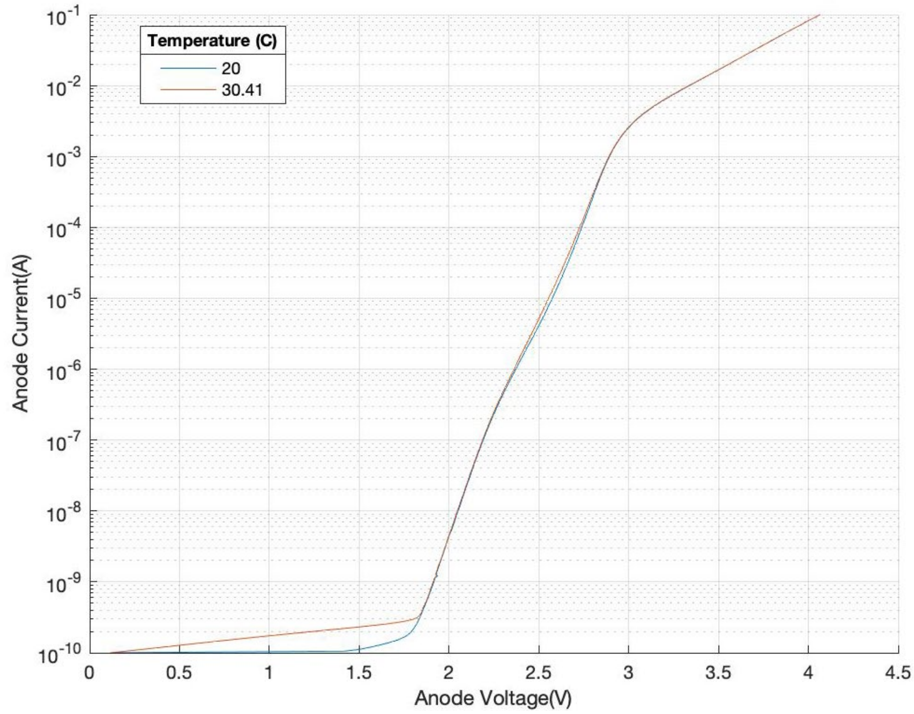

Figure 15. Initial Forward Bias Curves for Validation of Updated HTOL System with Device C1

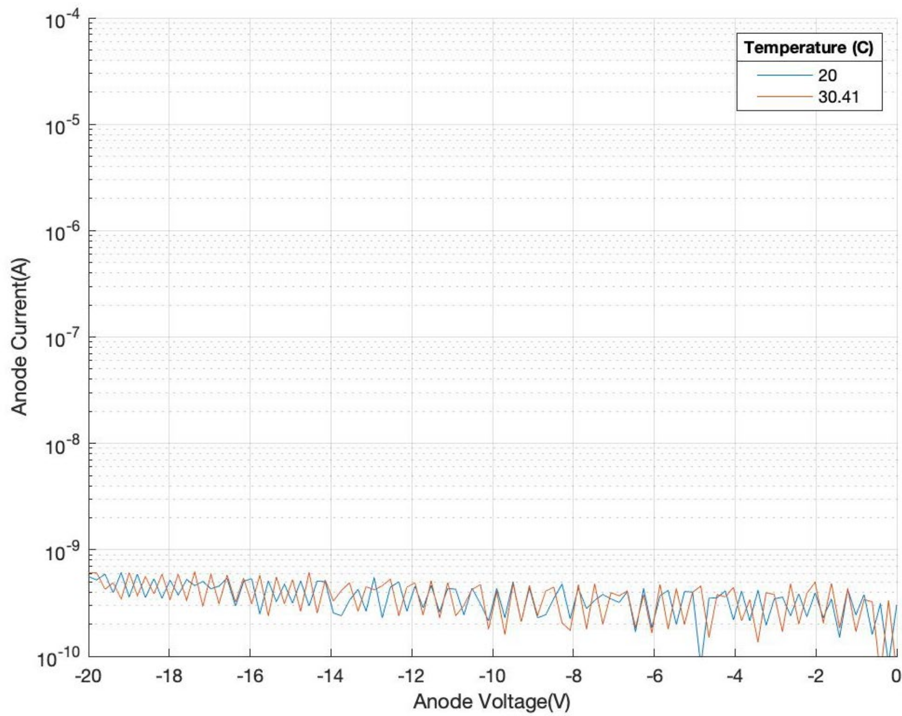

Figure 16. Initial Forward Bias Curves for Validation of Updated HTOL System with Device C1

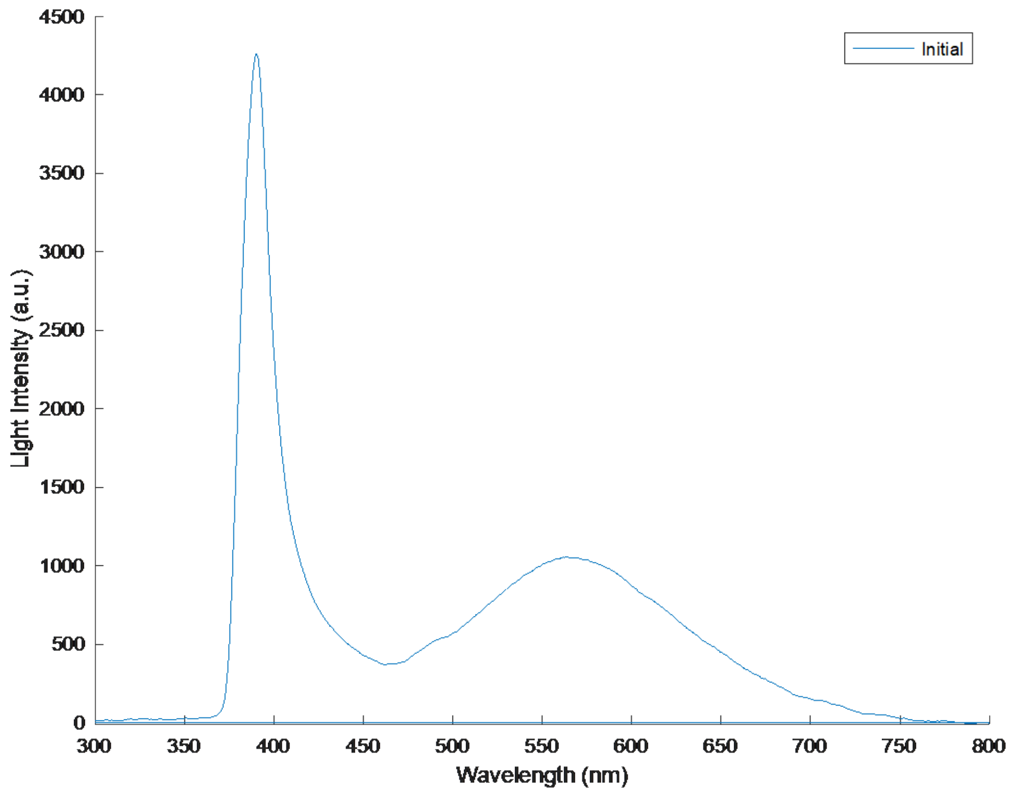

Figure 17. Initial EL Spectra Data for Device C1

3. Initial Optical and Electrical Characterization of Commercial Devices

A commercial GaN power diode, device C2, was used to run a long-duration constant-current stress test. Initial EL spectrum measurements were taken ranging from 100 mA to 3 A with TEC set to a constant temperature of 30 C, as shown in Figure 18. The band-to-band peak intensity grows with current intensity, with a slight increase in peak wavelength over the current range, from approximately 488 nm to 490 nm. The second peak, centered around 560nm, is from carbon impurities that are an artifact from the manufacturing process [7].

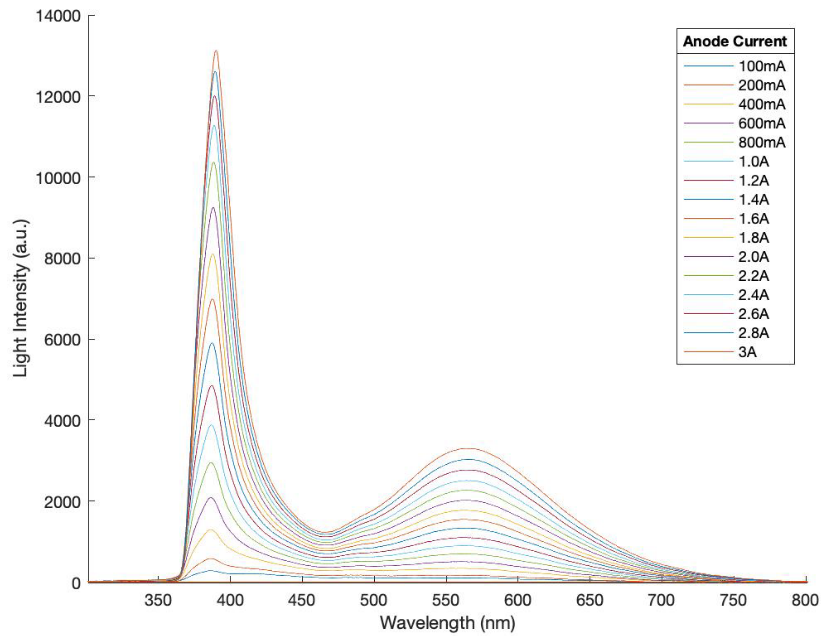

Figure 18. Device C2 Initial Stress Test Peak Spectra at 30C Varying Current

Additional EL spectrum measurements were taken at a constant current of 1 A, and TEC temperature was varied from 30 C to 120 C, shown below in Figure 19. Again, the band-to-band and carbon impurity peaks are observed, with intensity decreasing over the temperature range. This is due to increased amounts of recombination at higher temperatures, with non-radiative recombination suppressing the photons emitted from the diode.

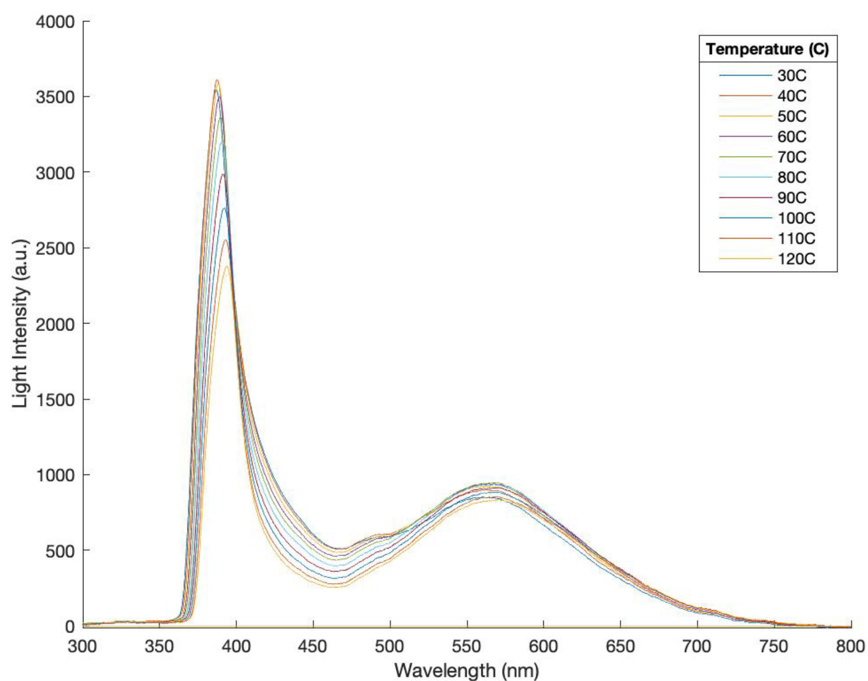

Figure 19. Device C2 Post Initial Stress Test Peak Spectra at 1.0A Varying Temperature

The I-V-T data collected for this test are not typical of a GaN PN diode. Troubleshooting the test setup seemed to indicate a poor electrical connection to the Keysight B1500A semiconductor analyzer, adding unexpected series resistance to the signal path and affecting the test data. The malfunction was not discovered until the test was completed, due to disruptions in day-to-day operations because of pandemic mitigation procedures. A subsequent stress test after all connections were checked on the same device delivered I-V curves expected for a GaN PN diode. On-state resistance calculated from data taken at 30 C was 6.03 Ω, markedly higher than previous values obtained for GaN PN diodes, and demonstrates the presence of some series resistance in the signal path to the diode. Initial reverse leakage currents range from hundreds of nanoamps to microamps, with reverse bias curves being affected in the same manner as the forward bias curves.

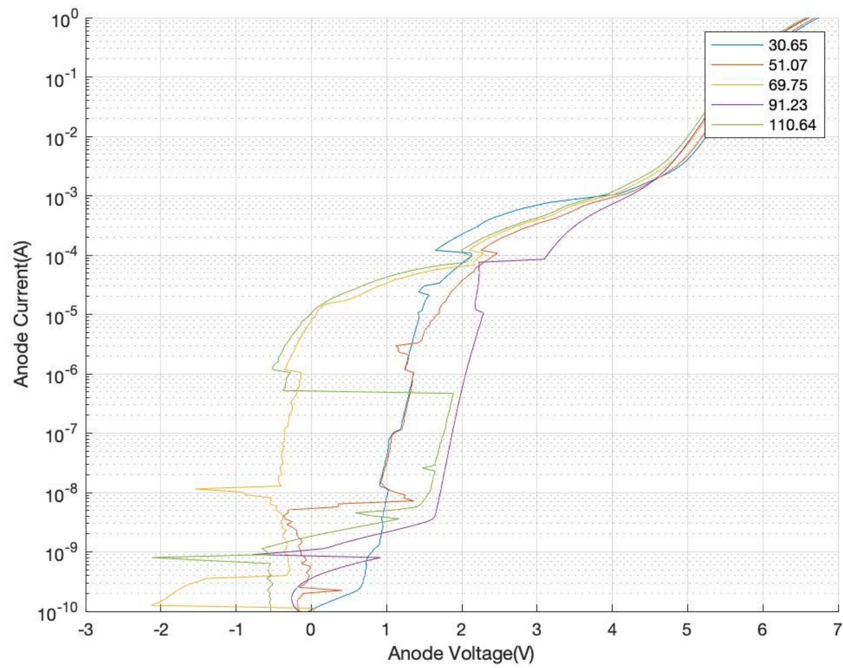

Figure 20. Initial Forward Bias Curves for C2 Device Stress Test

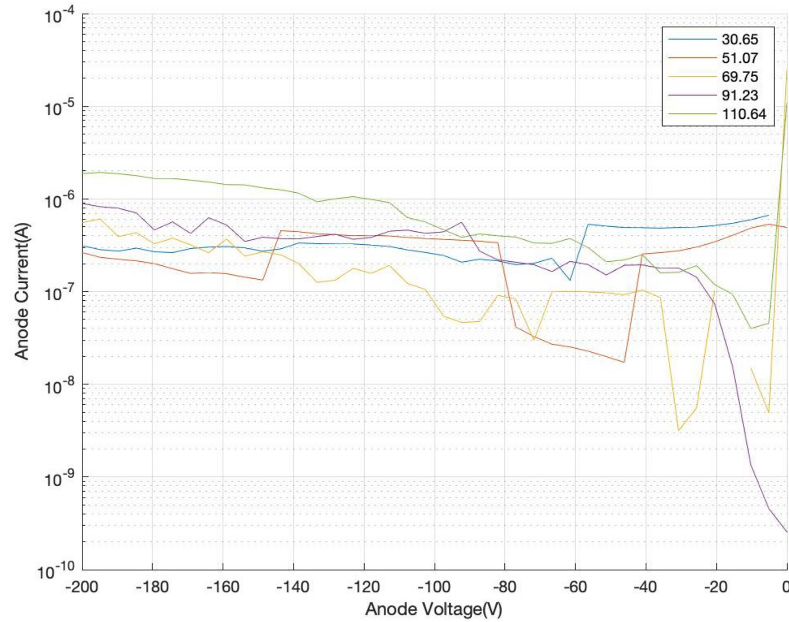

Figure 21. Initial Reverse Bias Curves for C2 Device Stress Test

Another commercial GaN power diode, device C3, was used to run a long-duration constant-current stress test. Initial EL spectrum measurements were taken ranging from 100 mA to 3 A with TEC set to a constant temperature of 30 C, as shown in Figure 22. The band-to-band peak and carbon impurity peak are of similar intensity with slightly different magnitudes due to the way the devices must be removed and installed when testing a new device.

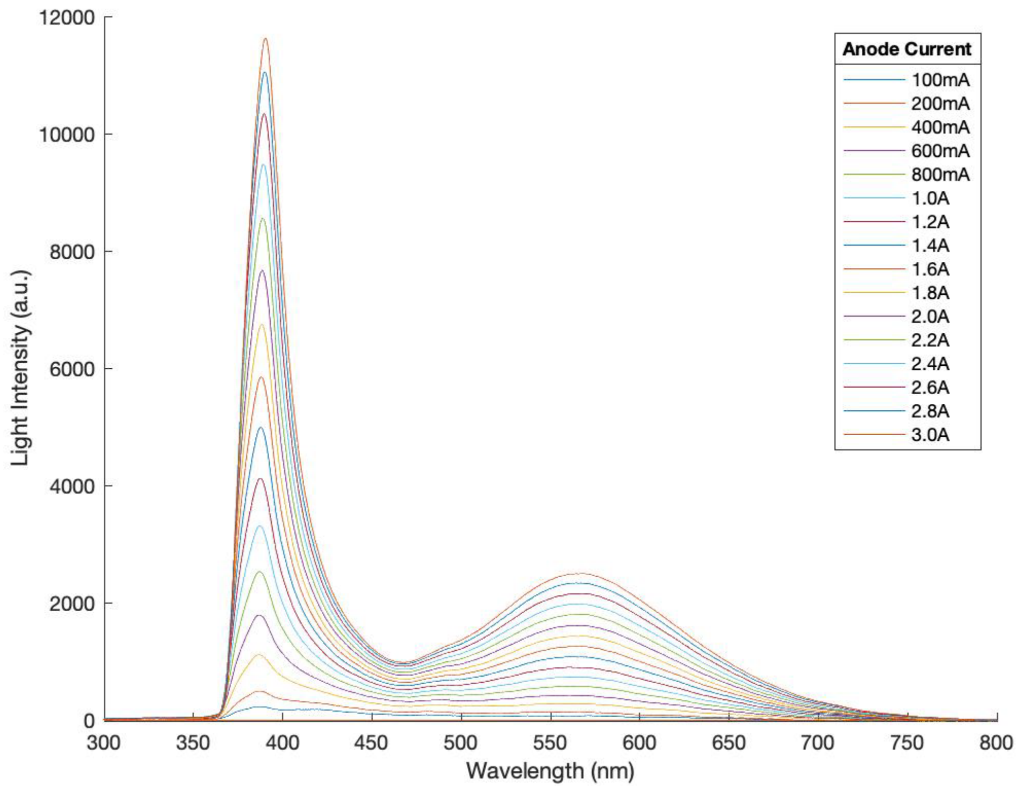

Figure 22. Device C3 Initial Stress Test Peak Spectra at 30C Varying Current

Additional EL spectrum measurements were taken at a constant current of 1A, and TEC temperature was varied from 30 C to 110 C, shown below in Figure 23. Again, the band-to-band and carbon impurity peaks are observed, with intensity decreasing over the temperature range. This decrease is due to increased amounts of recombination at

higher temperatures, with non-radiative recombination suppressing the photons emitted from the diode.

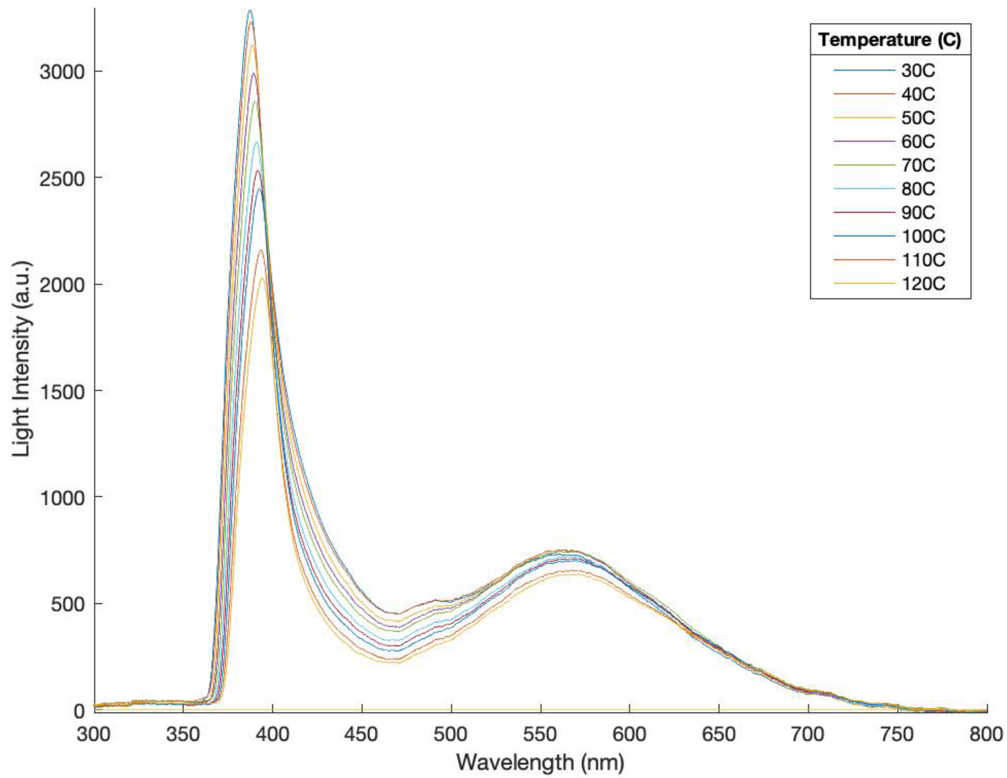

Figure 23. Device C3 Initial Stress Test Peak Spectra at 1A Varying Temperature

Initial I-V-T data were collected for device C3, with the expected characteristics of a PN diode observed for both the forward and reverse measurements, shown in Figure 24 and Figure 25. Initial on-state resistance calculated from data at 30 C was 3.04 Ω, with reverse leakage current at 30 C being 3.5 nA.

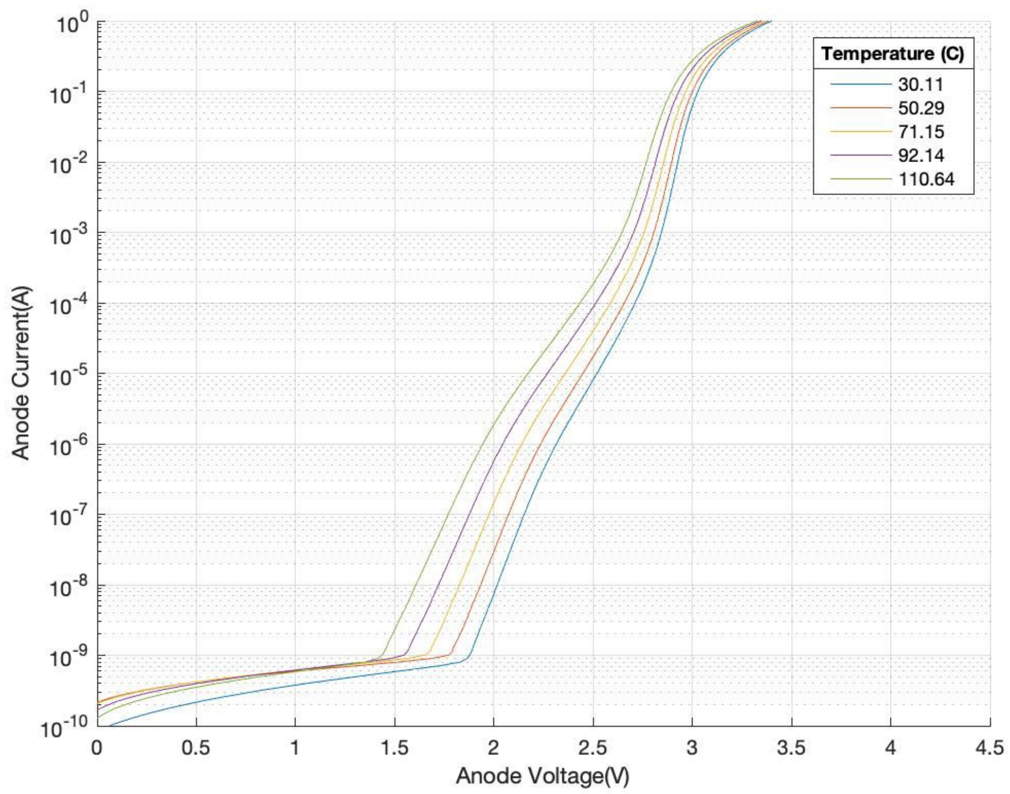

Figure 24. Initial Forward Bias Curves for C3 Device Stress Test

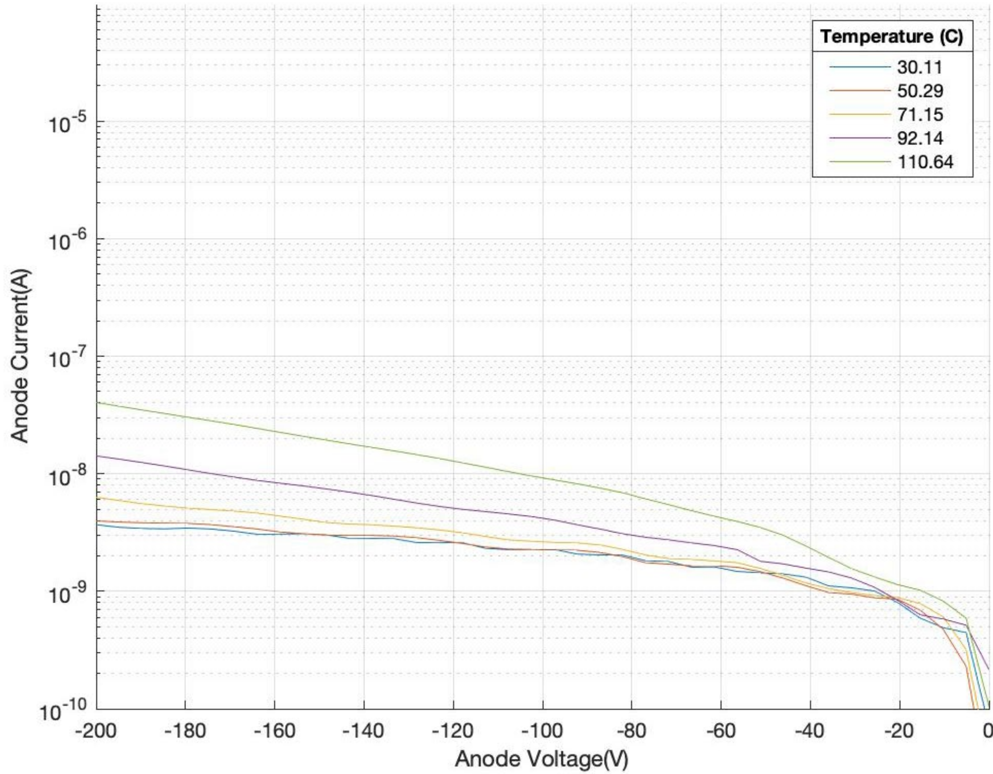

Figure 25. Initial Reverse Bias Curves for C2 Device Stress Test

C. EXPERIMENT METHODOLOGY AND TEST PLAN

1. NRL GaN PN

The N1 device was installed in the DUT chamber, and the updated HTOL system was initialized to perform a 336-hour constant-current stress test. Stress temperature was set to 90 C, with I-V-T measurements taken every two hours at the temperatures specified above. The programmable power supply was set to deliver a constant current of 1 A, or 625 A/cm2.

To further test the capability of the updated HTOL system, the N1 device was tested again with the same initialization parameters as above, except for stress time and stress current. Stress time was set to 168-hrs, and the constant stress current was increased to 1.5 A, or 937 A/cm^2. Initial forward and reverse I-V-T measurements were taken before the stress cycle, shown below in Figure 15 and Figure 16, and again every two hours during the test.

2. HTOL System Validation Methodology

A commercial GaN PN, specifically, device C1, was prepared by cutting the sidewall to allow a fiber to be placed near the PN junction to collect EL spectrum data, pictured in Figure 26. The lid to the DUT chamber was installed, and the updated HTOL system was initialized to conduct a 36-hour constant-current stress test. Stress current temperature was set to 90 C, and humidity control was set to 10%. I-V-T measurements were collected every hour, and EL spectral data were collected every half hour in the middle of the one-hour constant current stress cycle. The programmable power supply was set to deliver a constant current of 1 A, or 208 A/cm^2.

Figure 26. Image of Commercial Device with Sidewall Cut away to Allow Positioning Fiber Cable to Couple Light from the Die

3. Testing Methodology for Commercial GaN PN diodes

a. Tests Performed on Device C2

Device C2 was prepared and installed in a similar fashion to the validation test run on C1. Initial I-V-T measurements were taken, and the updated HTOL system was initialized to conduct a 168-hour constant-current stress test with stress temperature set to 90 C, with I-V-T measurements taken every two hours and EL spectrum measurements

taken midway through the stress cycle at one hour. The stress current was set to 3A, or 625 A/cm^2, and EL spectrum measurement current was set to 1 A, or 208 A/cm^2.

After the initial test was completed on device C2, the device was allowed to rest for 144 hours. EL spectrum data was taken again across varying temperatures and currents, and a second 168-hour constant-current test with stress temperature set to 100 C was initialized, with I-V-T and EL spectrum measurements taken in the same fashion as those performed during the initial stress test on device C2.

b. Tests Performed on Device C3

Device C3 was prepared and installed in the DUT chamber in the same manner as devices C1 and C2. Initial I-V-T measurements were taken, and the updated HTOL system was initialized to conduct a 84-hour constant-current stress test with stress temperature set to 110 C; I-V-T measurements were taken every two hours, and EL spectrum measurements were taken midway through the stress cycle at one hour. The stress current was set to 3 A, or 625 A/cm^2, and EL spectrum measurement current was set to 1 A, or 208 A/cm^2.

V. EXPERIMENTAL RESULTS

A. RESULTS OF INITIAL STRESS TEST OF NRL GAN DIODE

The post stress I-V-T measurements show clear degradation of the device, with changes in both forward and reverse I-V characteristics shown in Figure 27 and Figure 28. Pre-stress on-state resistance calculated from data at 30 C was 3.1 Ω, and post-stress on-state resistance was 3.079 Ω.

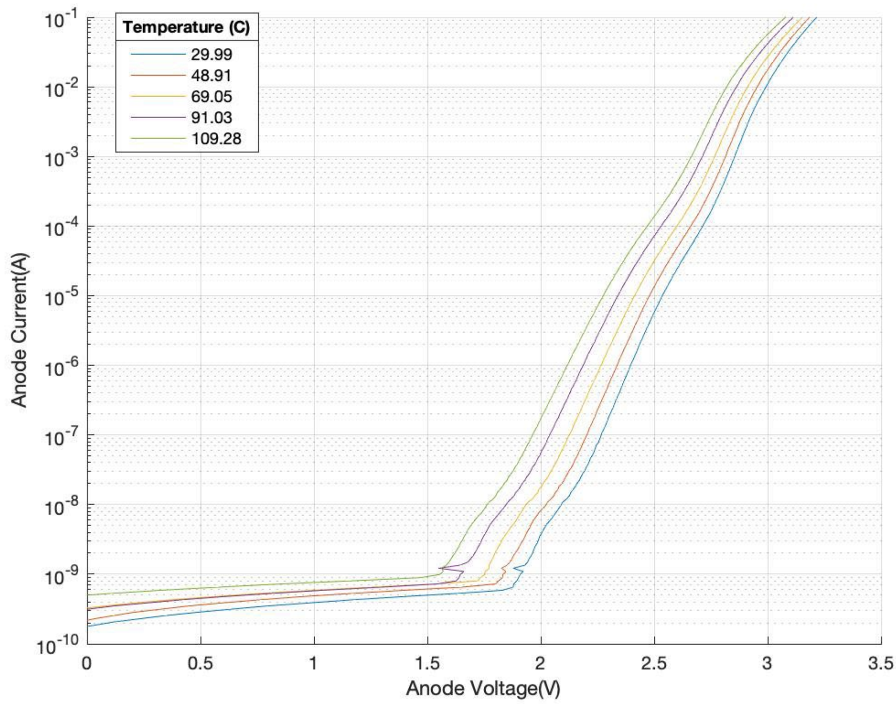

Figure 27. Post Stress Forward Bias Curves for Device N1

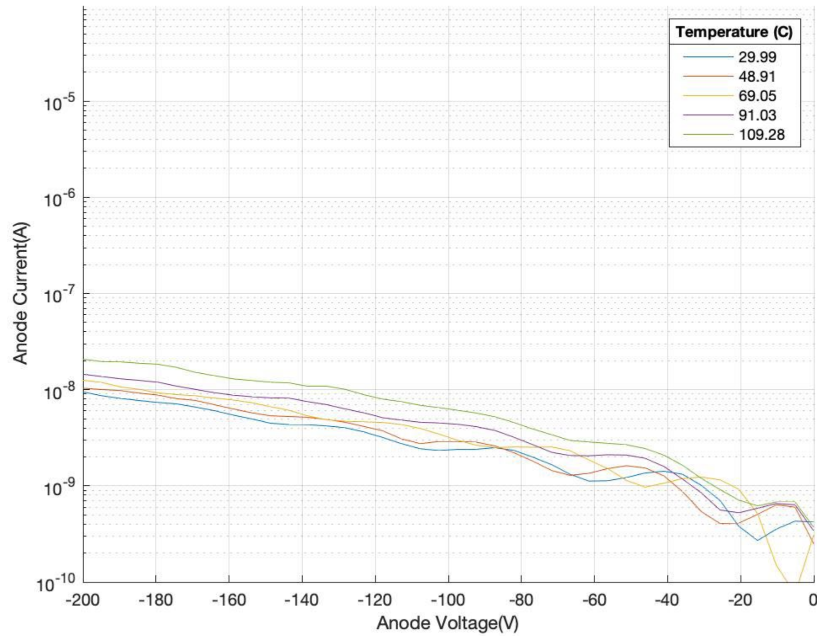

Figure 28. Post Stress Reverse Bias Curves for Device N1

Reverse leakage current increased in magnitude, with initial values ranging from 2 nA to 7 nA over the temperature range from the pre-stress measurements in Figure 6 and post-stress values at 9 nA to 30 nA. In Figure 29, there is a slight excursion in anode voltage from 224 hours to 250 hours, which correlates to a rise in ambient humidity in the lab where the testing was conducted due to rainfall in the region. The lid to the DUT chamber was not installed for this test as the device was hermetically sealed with epoxy

type resin, and the change in humidity was not expected to affect the sealed device.

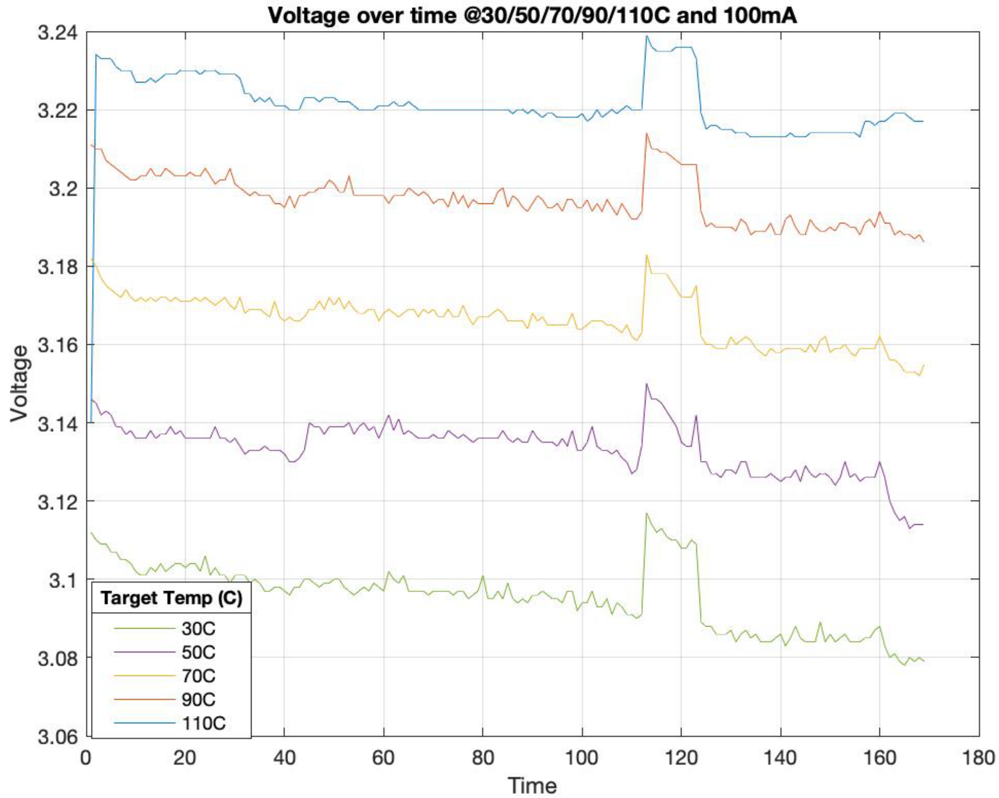

Figure 29. Device N1 Anode Voltage over Time for 100mA

B. RESULTS OF SECOND STRESS TEST OF DEVICE N1

The second stress test conducted on device N1 raised the current to 1.5 A, or 937 A/cm^2, this time utilizing a High-Power Source/Monitor Unit (HPSMU) installed in the Keysight B1500A, which allowed for taking I-V measurements out to 1A vice 100 mA. On-state resistance calculated from measurements collected before the second stress test was 3.31 Ω. Examining the initial forward bias curves between the first and second stress tests in Figure 13 and Figure 30 identified a slight shift in the I-V characteristics in the forward direction. More pronounced changes are observed in the reverse bias curves between the first and second stress tests shown in Figure 31, with leakage current being slightly elevated over 0 V to -200 V, likely due to the long duration of the stress test.

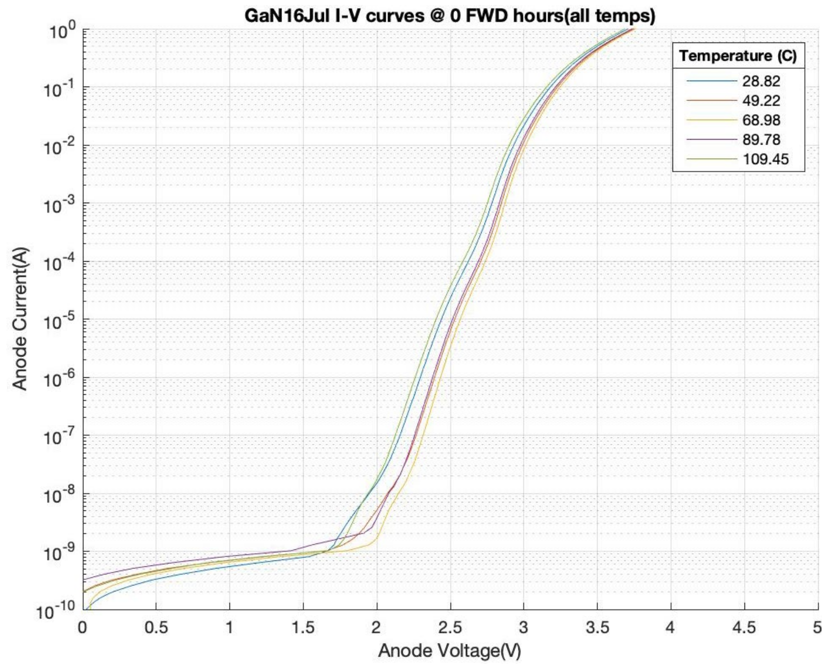

Figure 30. Initial Forward Bias Curves for Second Test of N1 Device

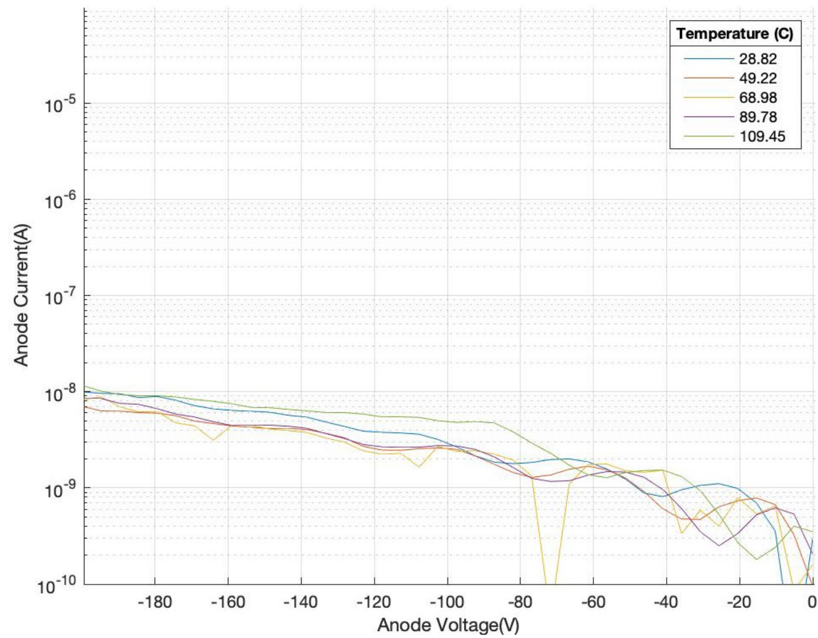

Figure 31. Initial Reverse Bias Curves for Second Test of N1 Device

Between eight to ten hours into the test, a temperature excursion occurred, and the device failed. I-V-T measurements at hour eight and hour ten show the 30 C

measurement having a greater current than the higher temperature measurements for a given voltage, with hour ten showing incorrect temperatures for the 70 C, 90 C and 110 C measurements, displayed in Figure 32 and Figure 33.

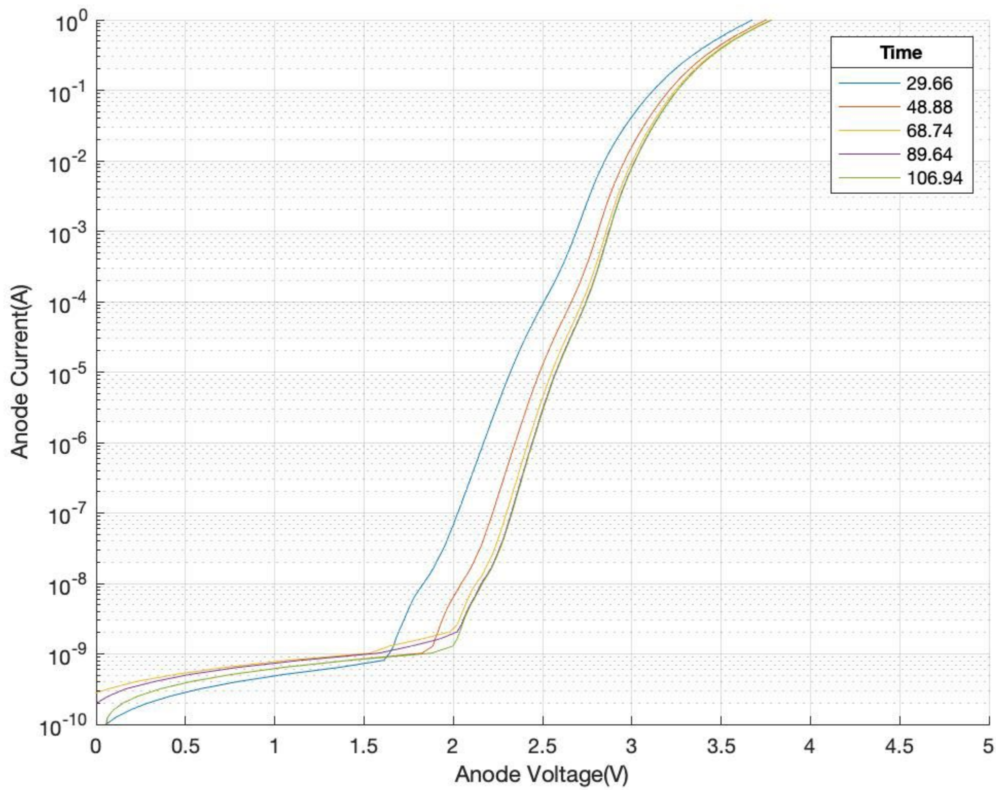

Figure 32. Forward Bias of Device N1 at Hour 8, Before Failure

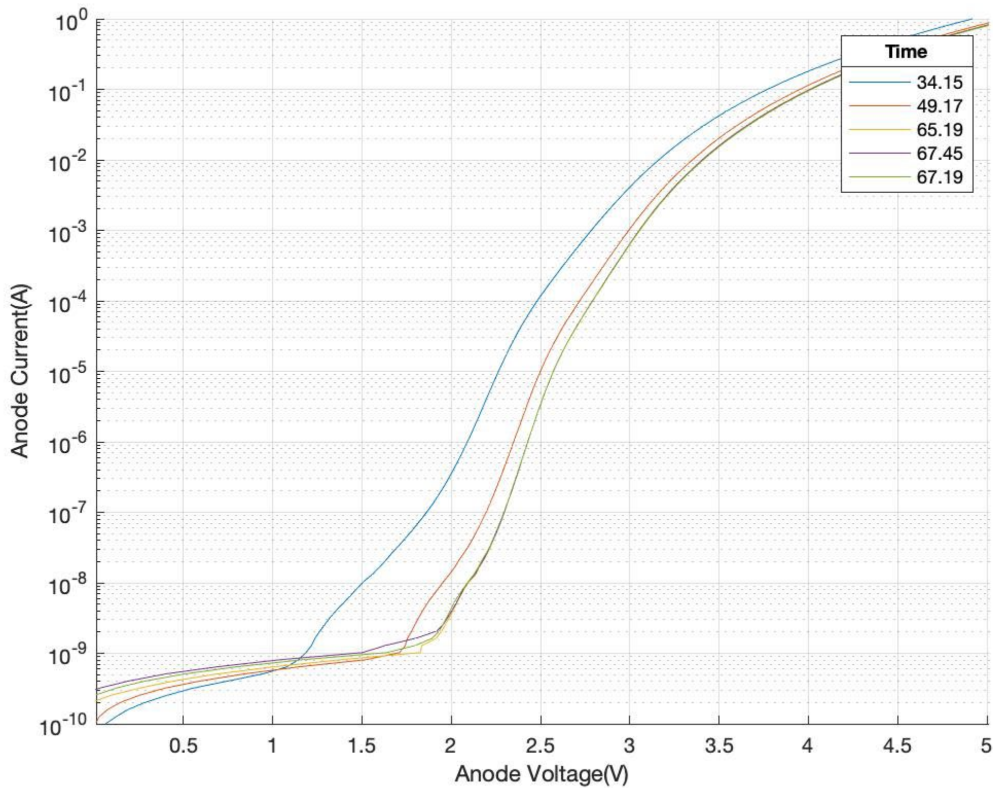

Figure 33. Forward Bias of Device N1 at Hour 10, Before Failure

Reverse I-V-T measurements at eight and ten hours, shown in Figure 34 and Figure 35. Respectively, show a clear degradation in the device as leakage current across the temperature range increases in comparison to the pre-stress measurement shown in Figure 31, from 7–10 nA and increasing to 70–100 nA from the start of the second stress test until device failure. On-state resistance calculated from data at 30 C before the last data set taken before failure was 4.14 Ω; after failure, the diode appeared as a short in resistance calculations.

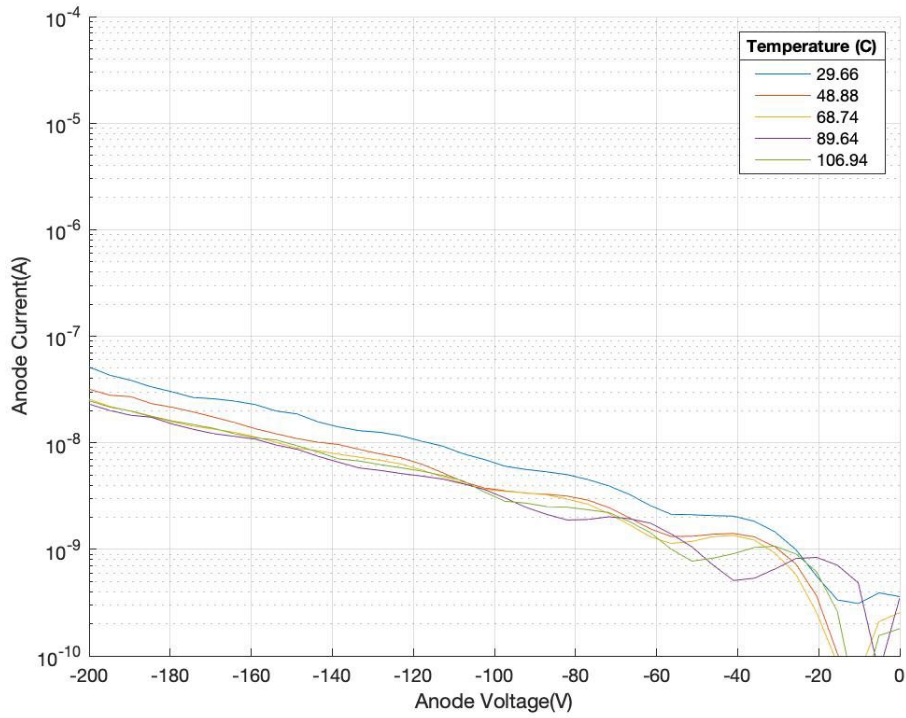

Figure 34. Reverse Bias of Device N1 at Hour 8, Before Failure

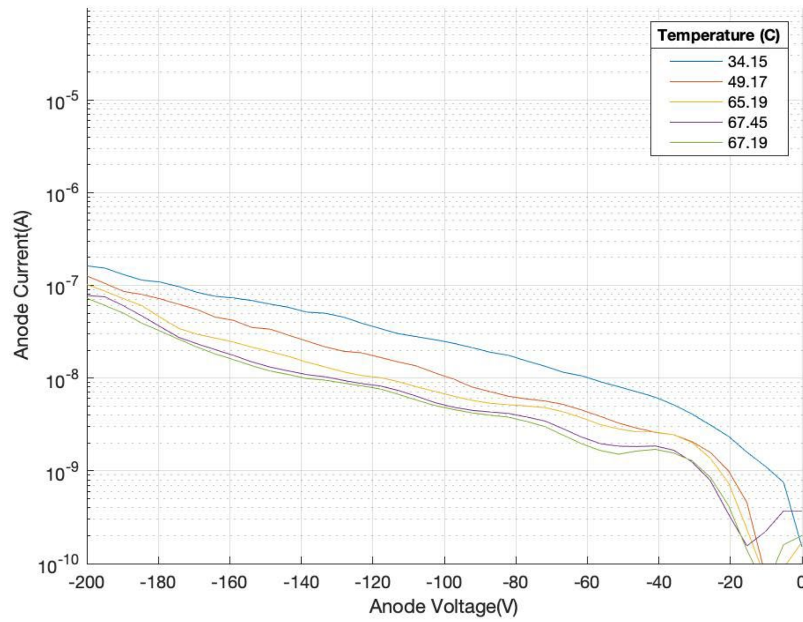

Figure 35. Forward Bias Device N1 at Hour 10, Before Failure

Anode voltage over time for measurements taken at 1 A is shown in Figure 36, with device N1 failing sometime between the measurement at hour 10 (Time 5) and hour 12 (Time 6).

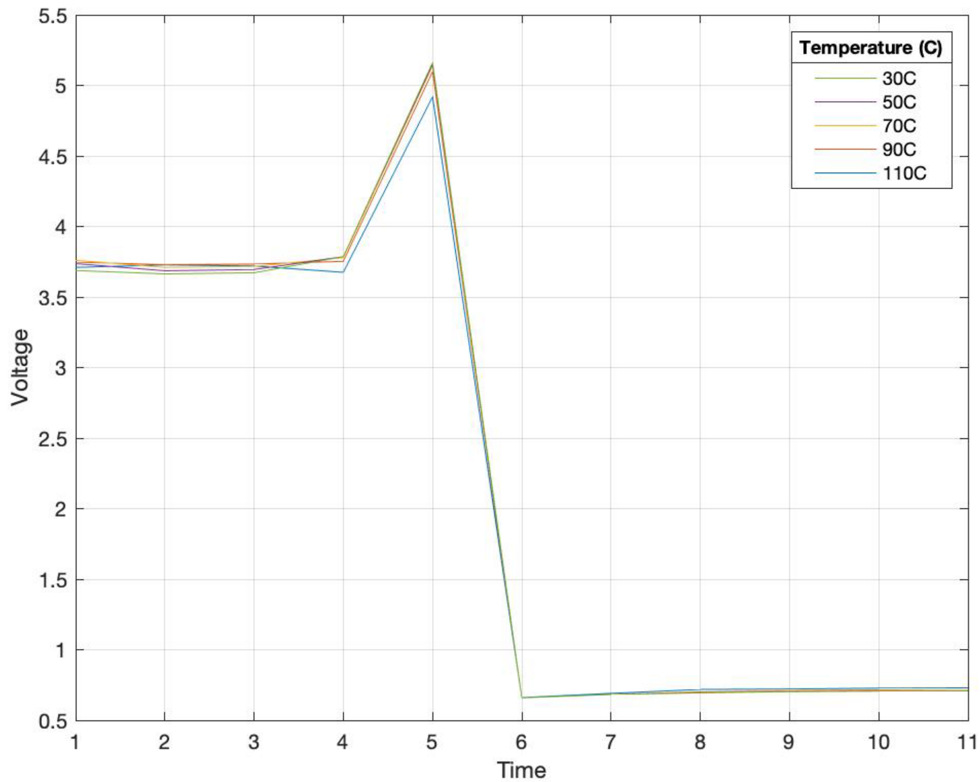

Figure 36. Anode Voltage of N1 Device at 1A over Time

This failure is likely due to the device losing contact with the heat sink. In this case, the method of heat conduction to the backplate became lossy, which caused a temperature excursion that overheated the device, melted the solder securing the device electrically and mechanically to the breakout board and displaced the temperature sensor that was placed near the junction of the package to the aluminum nitride wafers that thermally coupled the package to the heat sink. While the premature failure of the device precluded further data collection, it does prove the importance of the “stress-measure-

stress" methodology of testing to obtain data during the test period even if the device fails unexpectedly.

C. RESULTS OF HTOL SYSTEM VALIDATION TESTING OF COMMERCIAL GAN PN DIODES

The post-stress results for device C1 used for validating the EL spectrum collection sub-system show a slight change in the forward I-V characteristics of the device in Figure 37, with on-state resistance increasing from 3.72 Ω to 3.76 Ω post stress. The reverse leakage current shown in Figure 38 does not appear to have changed considerably, which is to be expected for the low-stress temperature and low-current that were applied to the device and the short duration of the test.

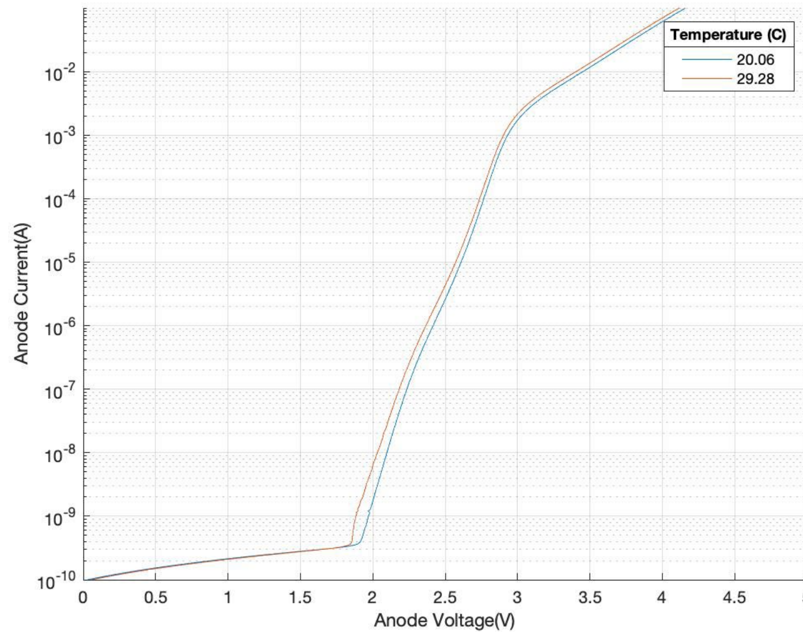

Figure 37. Post-Stress Forward Bias Curves for Validation of Updated HTOL System with Device C1

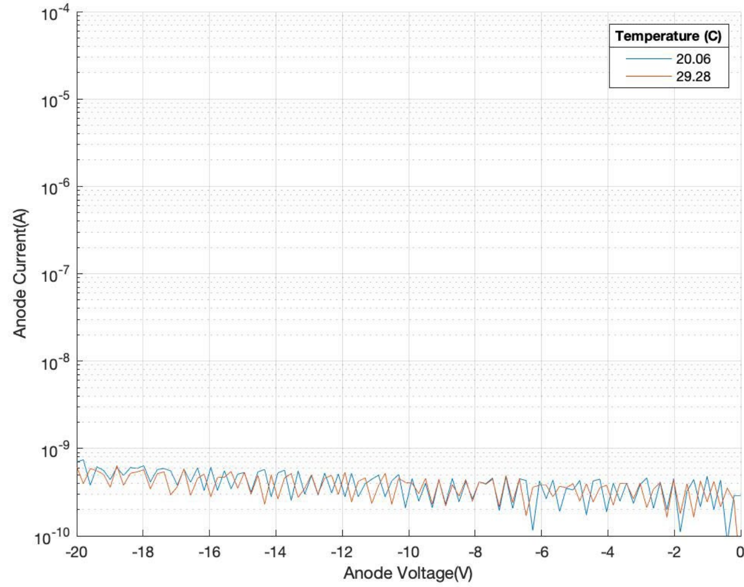

Figure 38. Post-Stress Reverse Bias Curves for Validation of Updated HTOL System with Device C1

The peak intensity of the EL spectra in Figure 39 trended slightly downward over the duration of the test, demonstrating that extended operation of the diode under stress conditions will degrade light output.

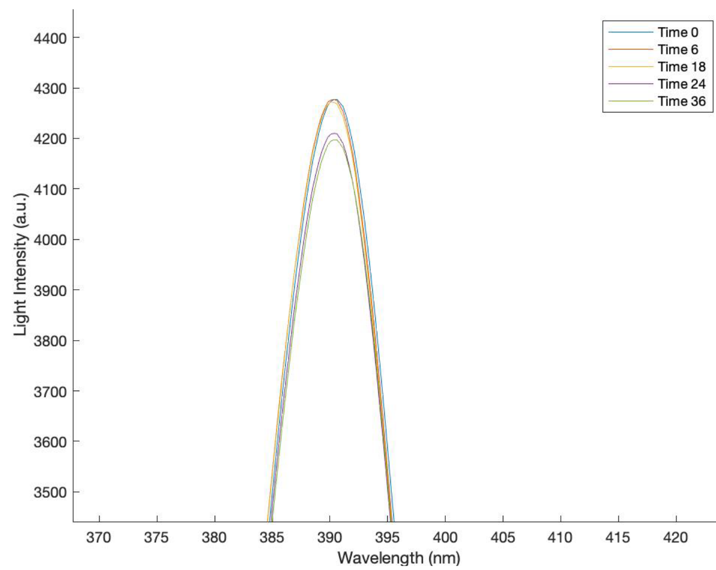

Figure 39. Degradation to Band-to-band Peak of Device N1 over Time

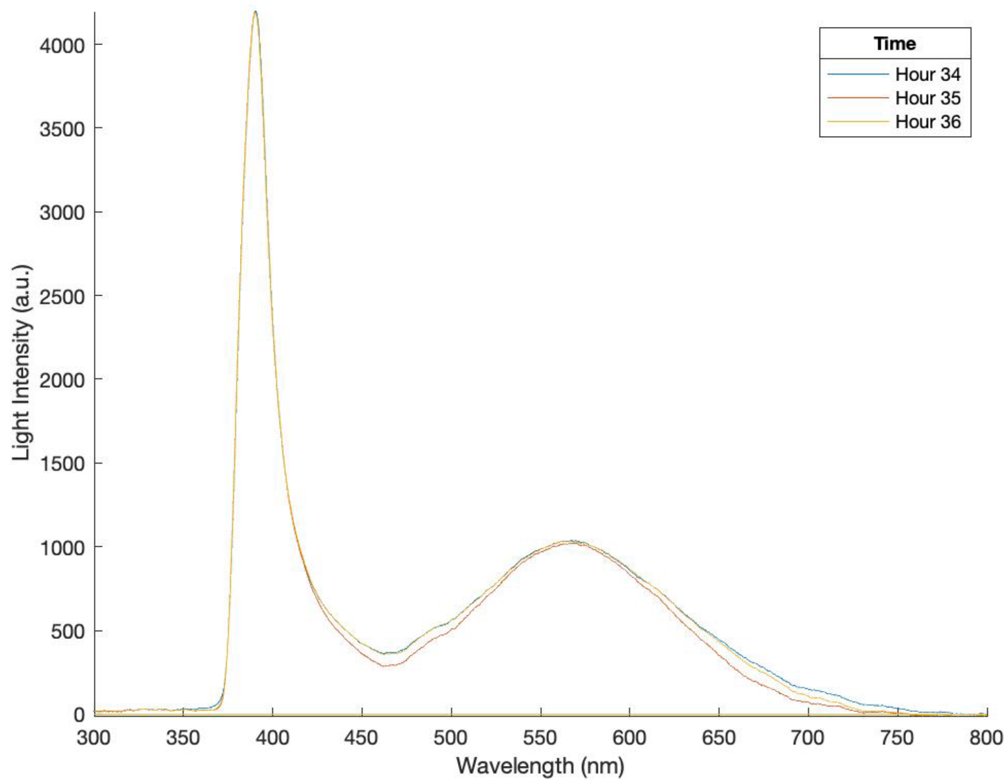

Figure 40. Device C1 Final Three Hours of EL Spectra Data for Validation of Updated HTOL System

D. RESULTS OF INITIAL STRESS TEST OF DEVICE C2

The electrical data for the initial stress test of device C2 are uncharacteristic of a PN diode, shown in Figure 41; these unexpected data were caused by a series high-resistance connection in the signal lines to the test module. Anode voltage for this device rose steadily over time, as measured by the LabVIEW VI, beginning at 4.16 V and ending at 5.54 V at 3.0 A after 168 hours of stress. The I-V curves, though uncharacteristic, do show a rise in anode voltage over time at 1 A, rising from approximately 6.8 V to 7.9 V.

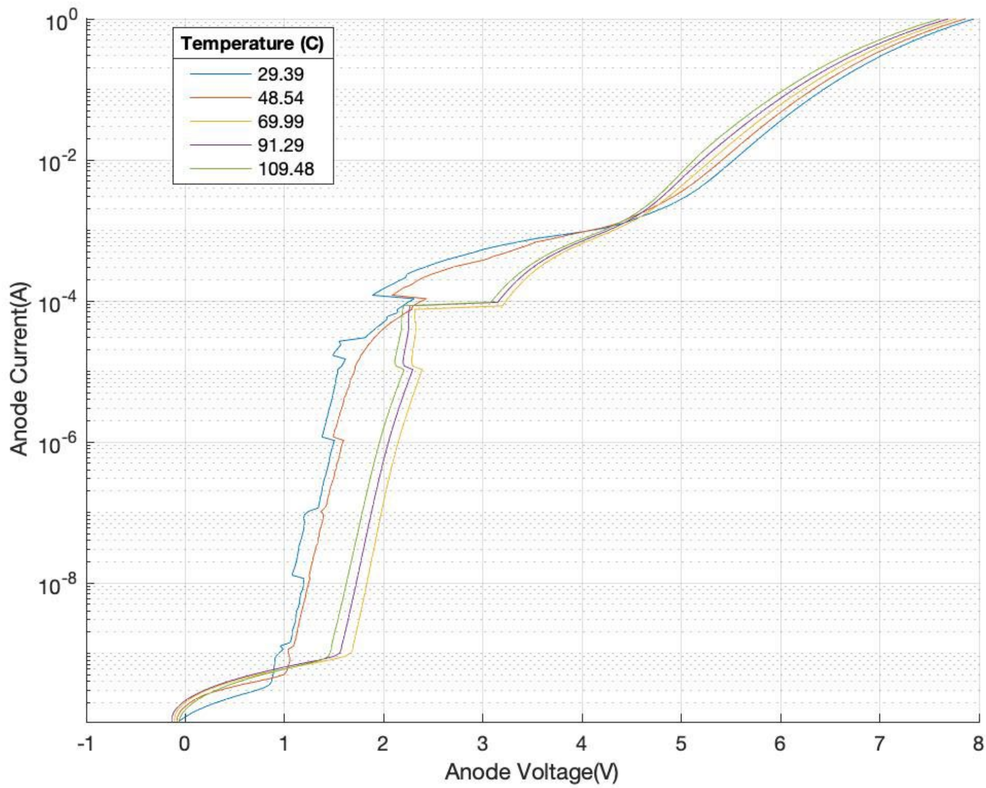

Figure 41. Device C2 Forward Bias Curves Post Initial Stress Test

The reverse bias curves show a marked increase in leakage current over the stress period, even with the high-resistance series connection issue that existed in the signal path, increasing from an initial value of 300 nA at 30C to 50 uA at 30 C post stress. Though this connection issue tainted the results, the reverse bias results in Figure 42 are very similar to those for the initial I-V-T sweeps done on the same device prior to the second stress test, shown in Figure 27.

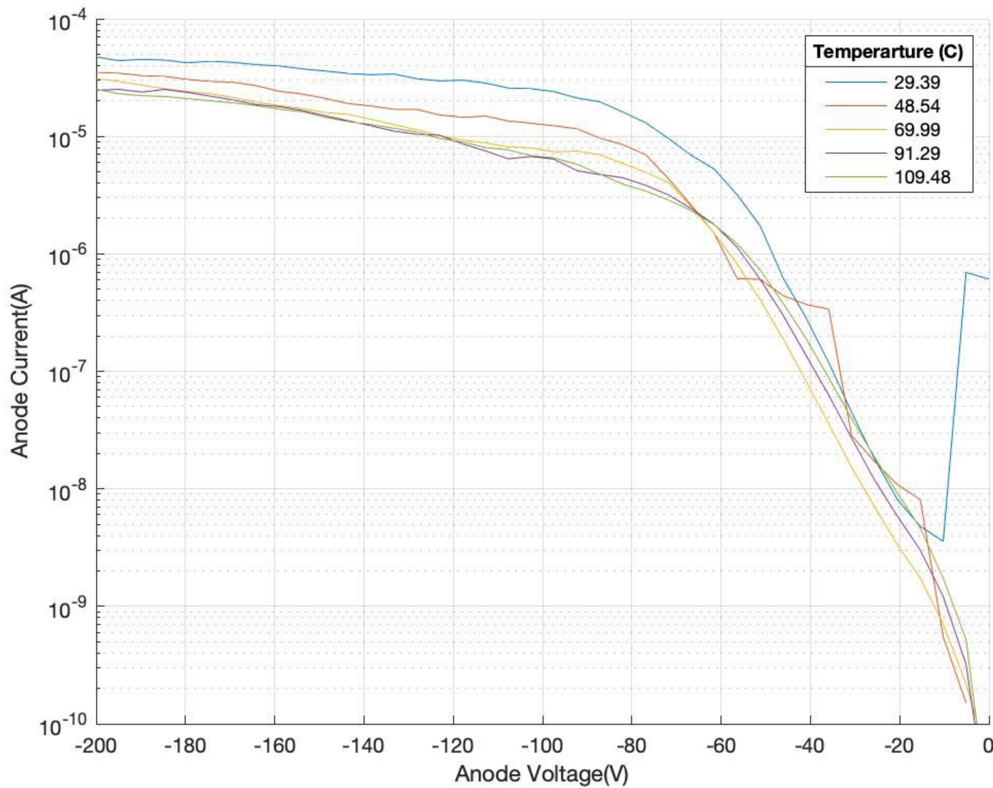

Figure 42. Device C2 Reverse Bias Curves Post Initial Stress Test

After 168 hours of stressing, the light intensity measured at 1 A and 90 C was considerably lower, with the last three hours of measurements in Figure 44 yielding 708.3 a.u., 632.2 a.u. and 553.5 a.u. compared to the initial three hours in Figure 43 of 1 A 90 C measurements 376.1 a.u., 320.8 a.u. and 246.5 a.u. This drop in intensity follows the increase in leakage current observed during the I-V measurements, suggesting that the induced stress caused migration of impurities and defects; these data show a correlation between electrical degradation and EL spectrum degradation.

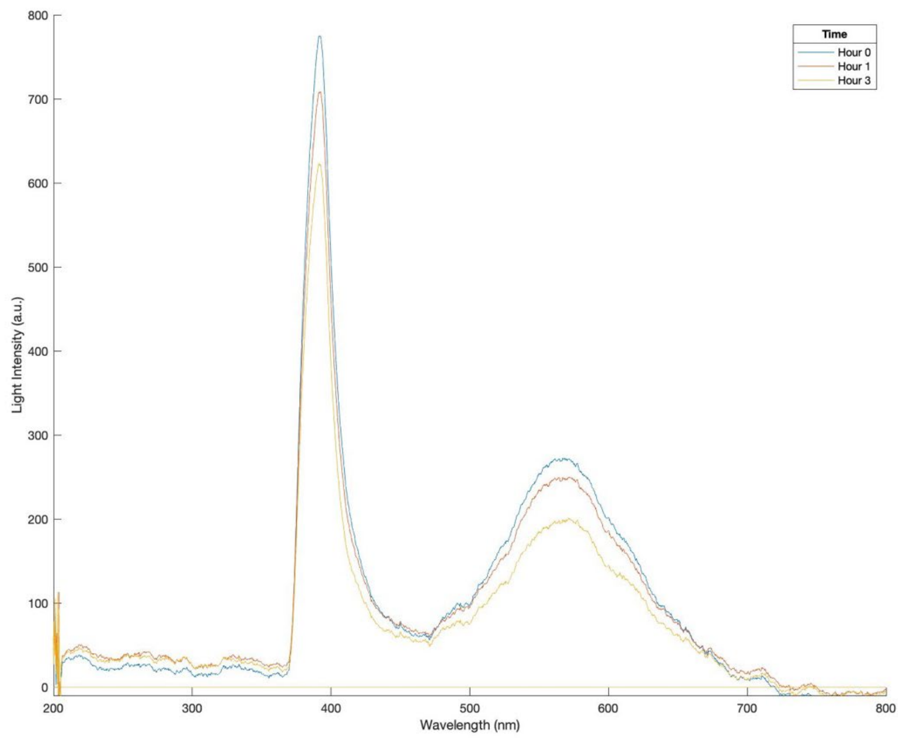

Figure 43. Device C2 EL Spectra Data for First Three Increments of Stress Test

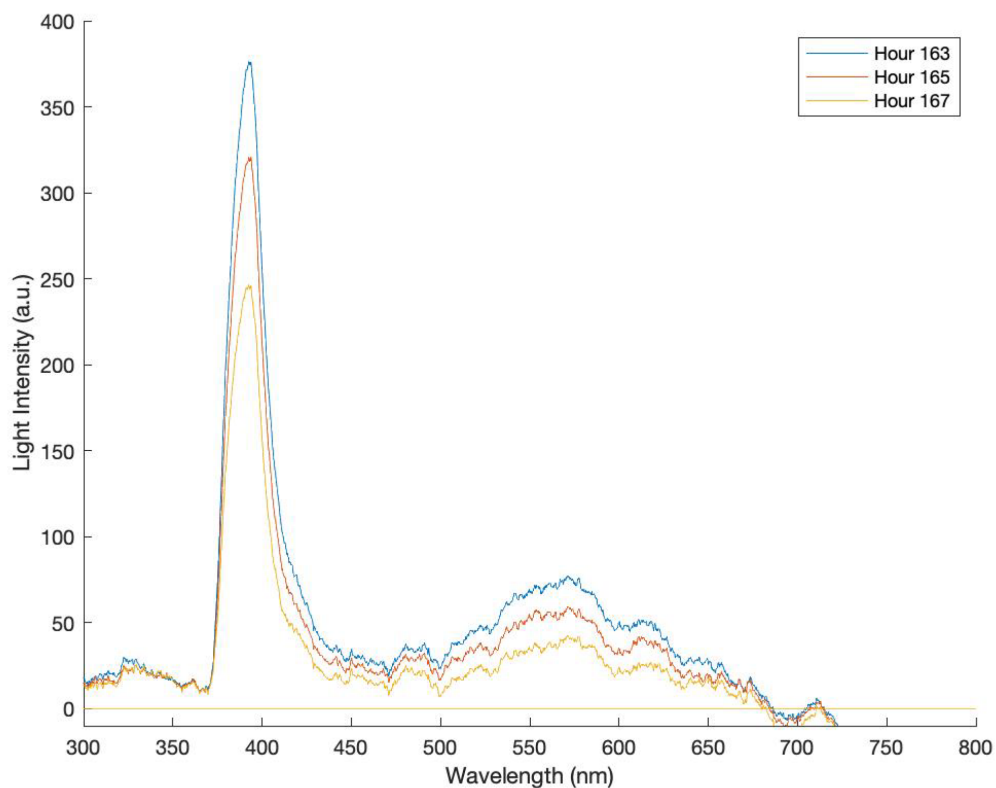

Figure 44. Device C2 Final Three Hours of EL Spectrum Data Post Stress Test

After the initial stress test was completed on device C2, the device was allowed to rest for a period of 144 hours. EL spectrum measurements were also taken at a constant current of 1 A, and TEC temperature was varied from 30 C to 110 C, shown below in Figure 45.

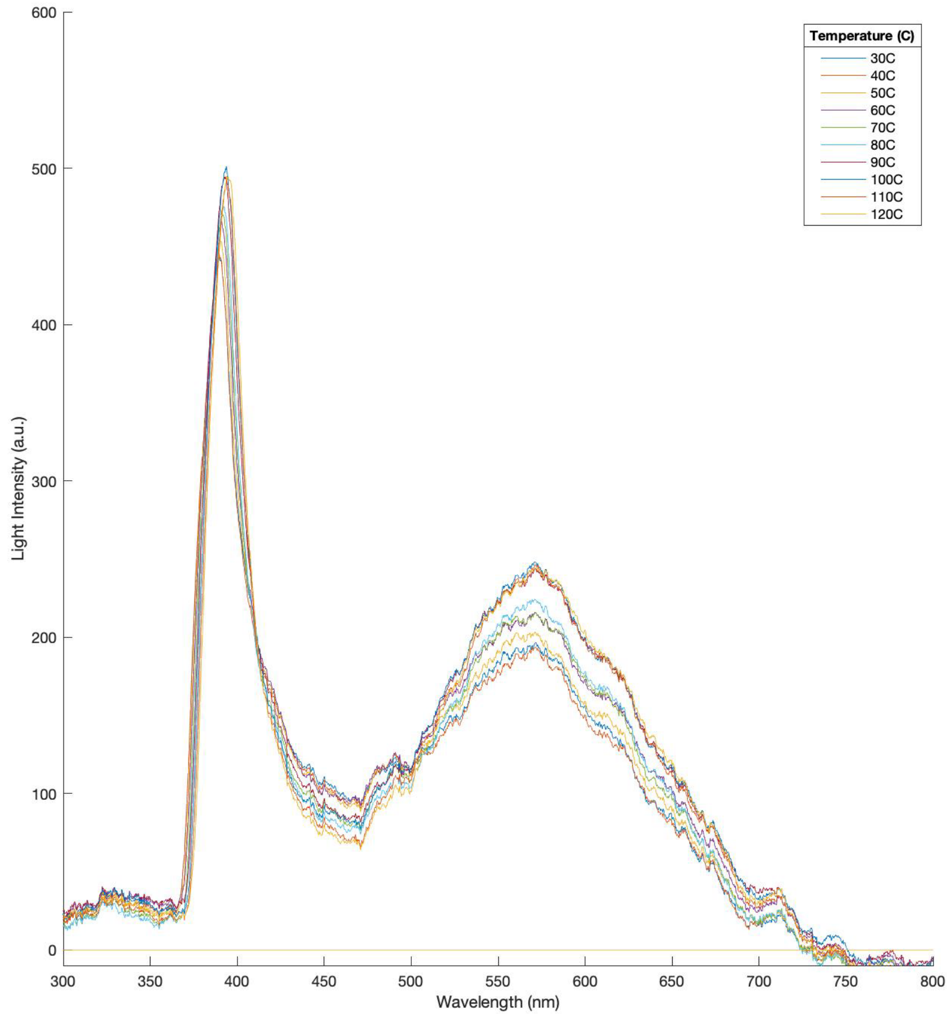

Figure 45. Device C2 Post Initial Stress Test Peak Spectra at 1.0A Varying Temperature

EL spectrum measurements were taken again ranging from 100 mA to 3 A with the TEC set to a constant temperature of 30C, as shown in Figure 46. The light intensity across all temperatures is suppressed compared to the original pre-stress measurements reported in Figure 19. A potential cause of this change is damage inflicted on the diode during the stress cycle, resulting in a collection of traps creating greater amounts of non-radiative recombination and thus less release of energy in the form of light through radiative recombination. Another observation is that the intensity and temperature relation observed in the pre-stress measurements, wherein an increase in temperature resulted in a lower intensity, is no longer true. In the post-stress EL spectrum

measurements, as temperature increases, intensity increases, with a slight increase in wavelength.

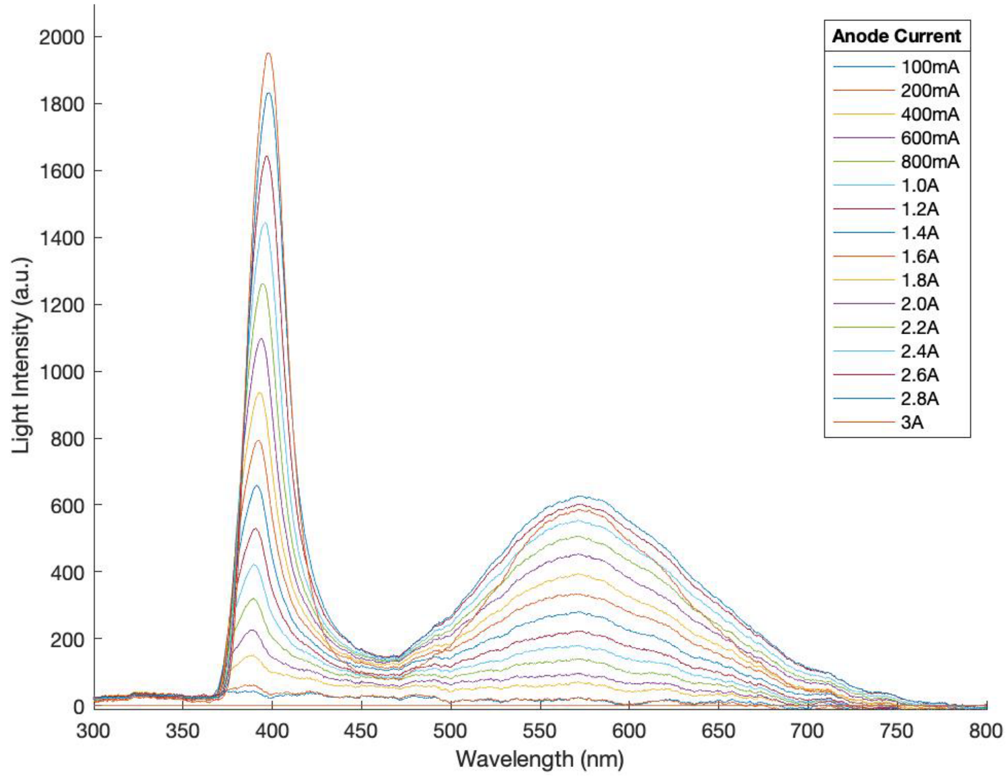

Figure 46. Device C2 Post Initial Stress GaN EL Spectra at 30C Varying Currents

Device C2 was tested again after the post-stress, post-rest EL spectrum data were collected. All stress test parameters for the next stress test were the same as those of the previous test, apart from stress temperature, which was increased to 100 C. Initial I-V-T measurements for this test are consistent with values expected for a PN diode shown in Figure 47 and Figure 48, unlike the initial measurements for the initial pre-stress test on this device that were affected by a high-resistance connection in the signal path. On-state resistance was calculated at 3.96 Ω using I-V measurements from data collected at 1A and 30 C.

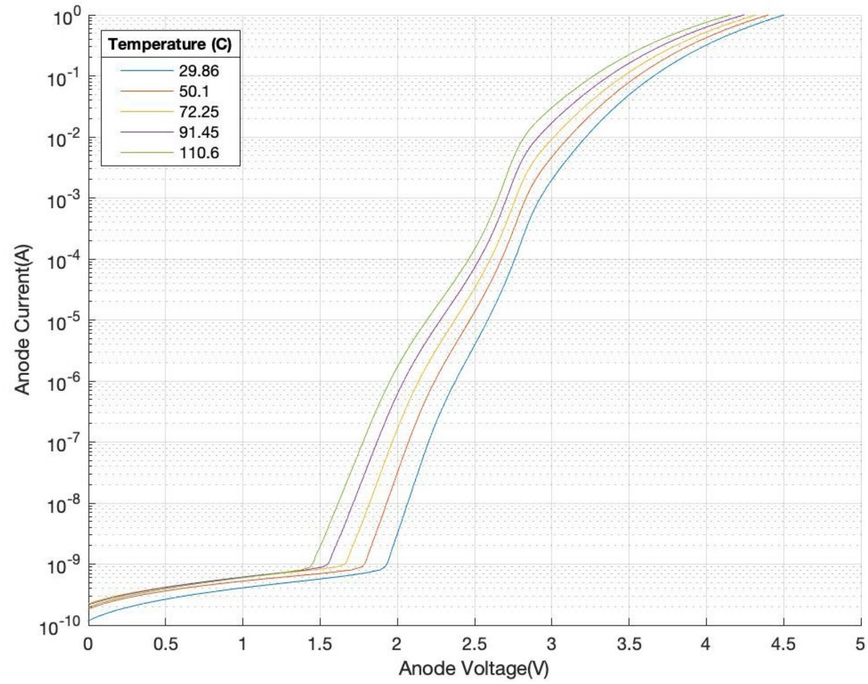

Figure 47. Device C2 Forward Bias Curves for Second Stress Test

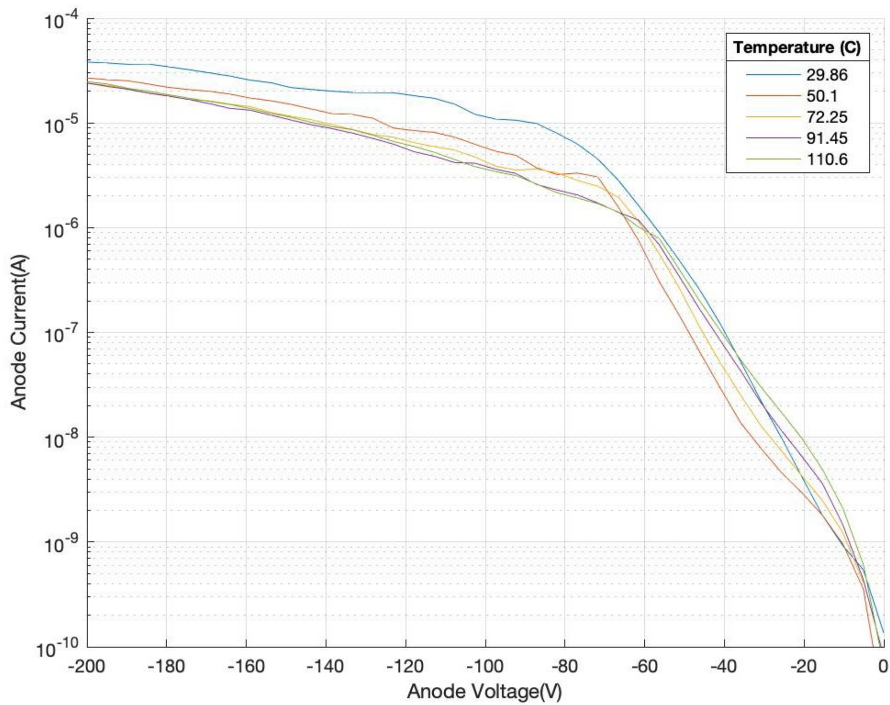

Figure 48. Device C2 Reverse Bias Curves for Second Stress Test

E. RESULTS OF SECOND STRESS TEST OF DEVICE C2

The I-V-T data collected for the second stress shown in Figure 49 and Figure 50 test showed slight changes, with on-state resistance calculated at 4.12 Ω from data collected at 1 A and 30 C. Anode voltage steadily increased over the duration of the constant current stress test, starting at 5.17 V and rising to 5.75 V at the end of the test.

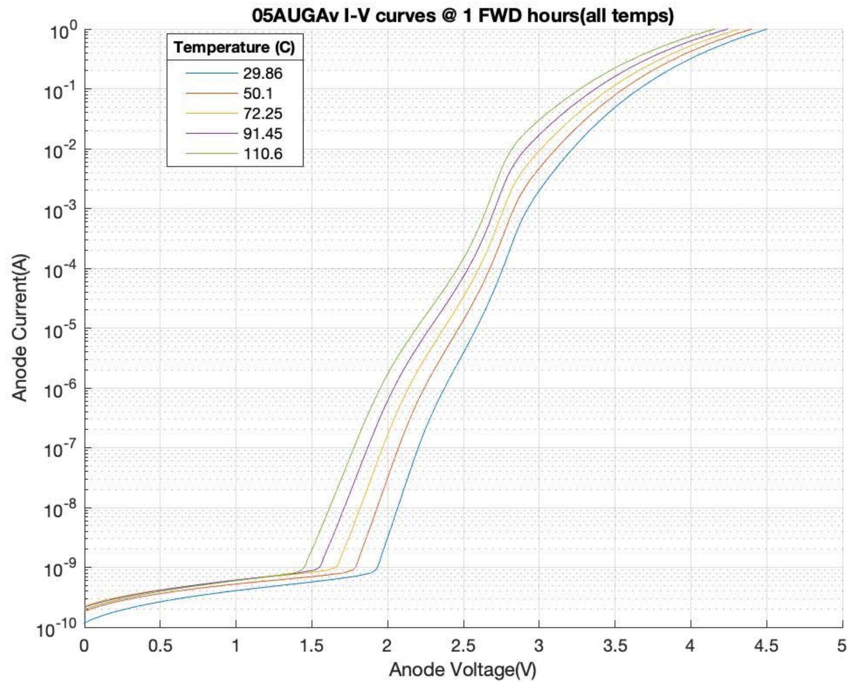

Figure 49. Device C2 Forward Bias Curves Post Second Stress Test

Leakage current did not rise appreciably over the duration of the second stress test shown in Figure 50, rising by tens of microamps vs. the results of the first test showing the uncharacteristic data that showed magnitudes of change. The EL spectrum data for this stress test in Figure 51 indicate further degradation, with the final three hours of EL spectrum peaks at 342.6 a.u., 215.7.2 a.u. and 207.5 a.u. compared to the initial three-hour peaks being at 476.0 a.u., 466.1 a.u. and 461.8 a.u.

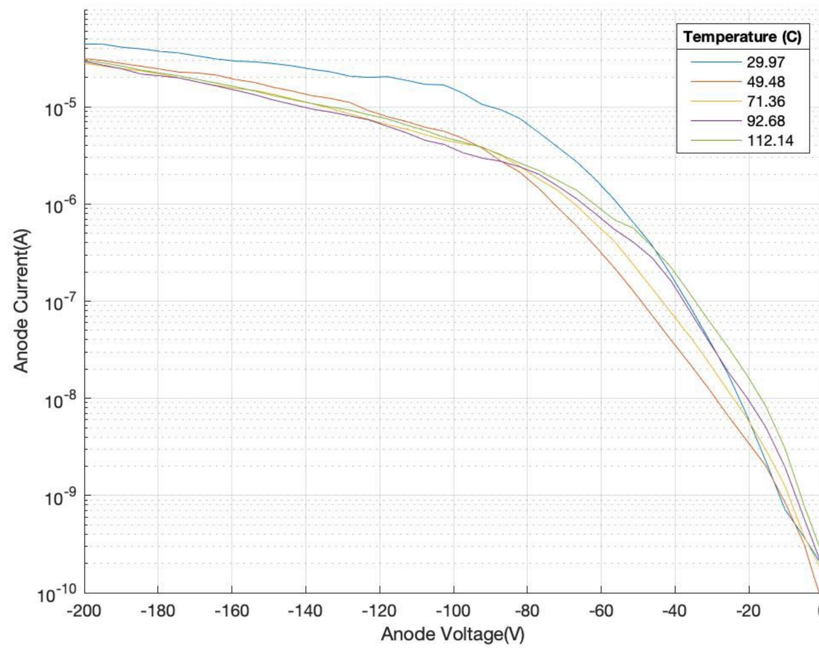

Figure 50. Device C2 Reverse Bias Curves Post Second Stress Test

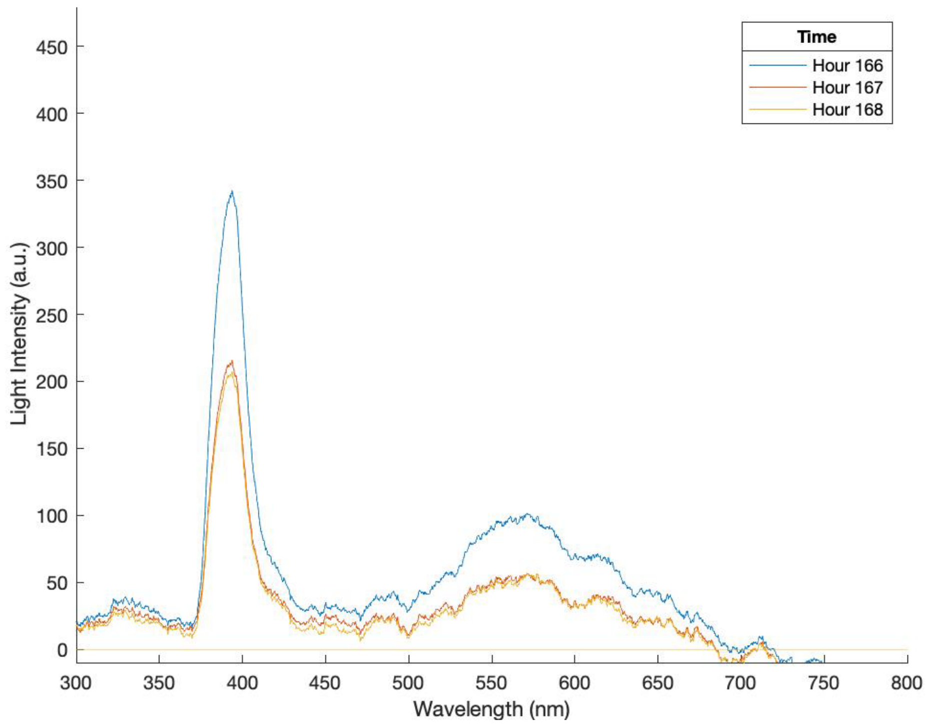

Figure 51. Device C2 Final Three Hours of EL Spectra Data Post Second Stress

EL spectrum measurements were taken again ranging from 100 mA to 3 A with the TEC set to a constant temperature of 30 C as shown in Figure 52. The post-stress peaks were again suppressed, consistent with the results from the first stress test, and the band-to-band peaks at 100 mA and 200 mA were almost indiscernible due to degradation.

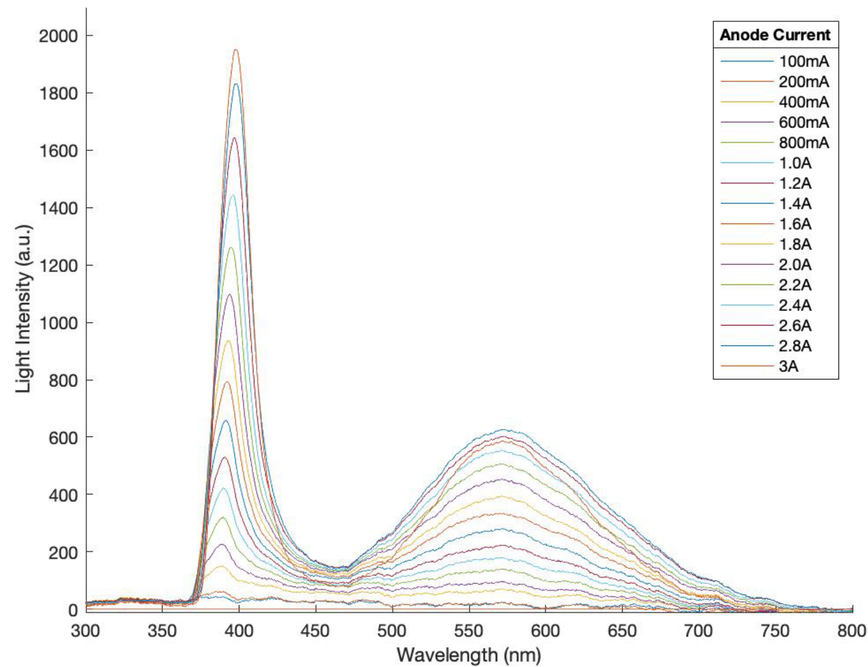

Figure 52. Device C2 Post Second Stress Test GaN Peak Spectra at 30C Varying Current

EL spectrum measurements were also taken at a constant current of 1A, and TEC temperature was varied from 30 C to 110 C, shown below in Figure 53. As with the first stress test, all band-to-band peaks and carbon impurity peaks are suppressed, with a notable inversion in temperature dependence across all temperatures. Initial results showed intensity decreasing with rising temperature, with a rightward shift in peak wavelength intensity. In this case, peak intensity rose with temperature.

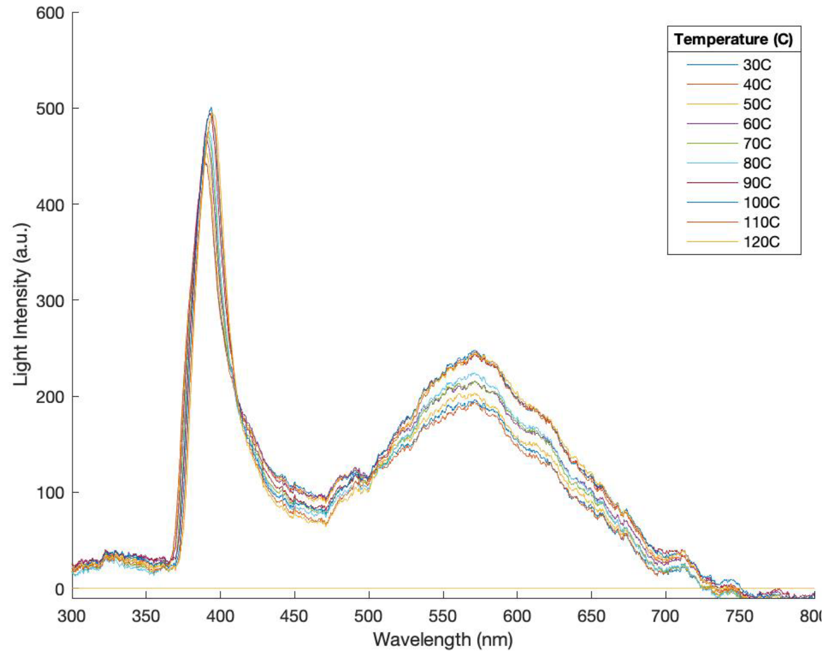

Figure 53. Device C2 Post Second Stress Test GaN Peak Spectra at 1.0A Varying Temperature

F. RESULTS OF STRESS TEST ON DEVICE C3

On-state resistance was calculated from measurements at 30 C and 1 A and found to be 3.77 Ω. Over the duration of the 84-hour stress test, leakage current rose from approximately 3 nA to 90 nA at 30 C, while forward voltage at 1 A rose from 3.4 V to 4.4 V, with post stress I-V-T measurements shown in Figure 54 and Figure 55.

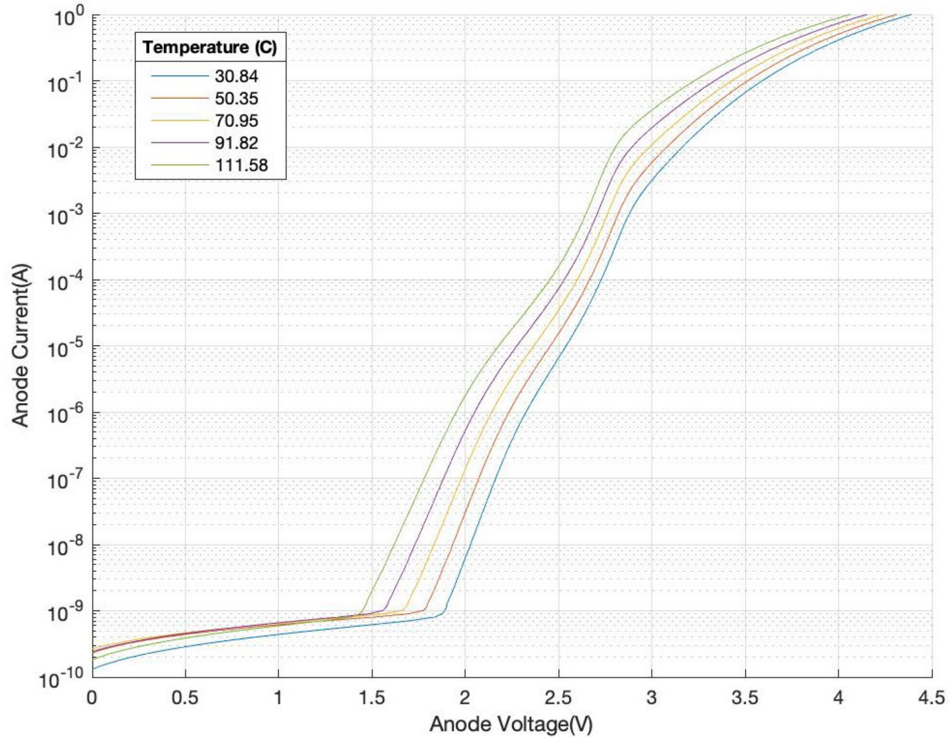

Figure 54. Forward Bias Curves for Device C3 Post Stress Test

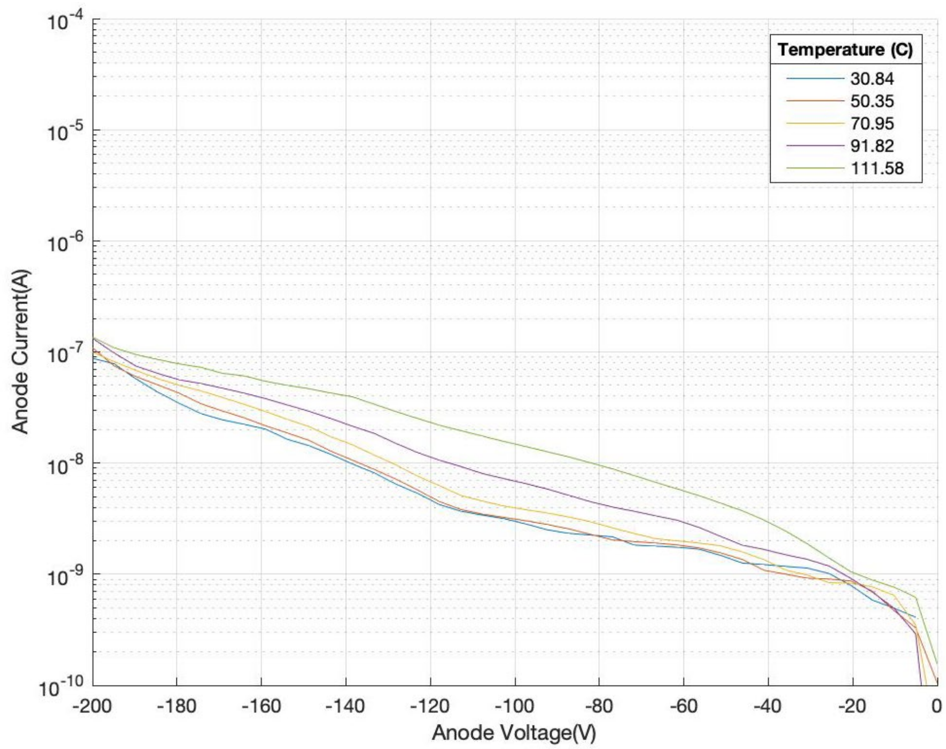

Figure 55. Reverse Bias Curves for Device C3 Post Stress Test

EL spectrum measurements in Figure 56 taken post stress for device C3 again show a degradation to the emitted light intensity across all currents sampled, with the peak at 100 mA barely discernible.

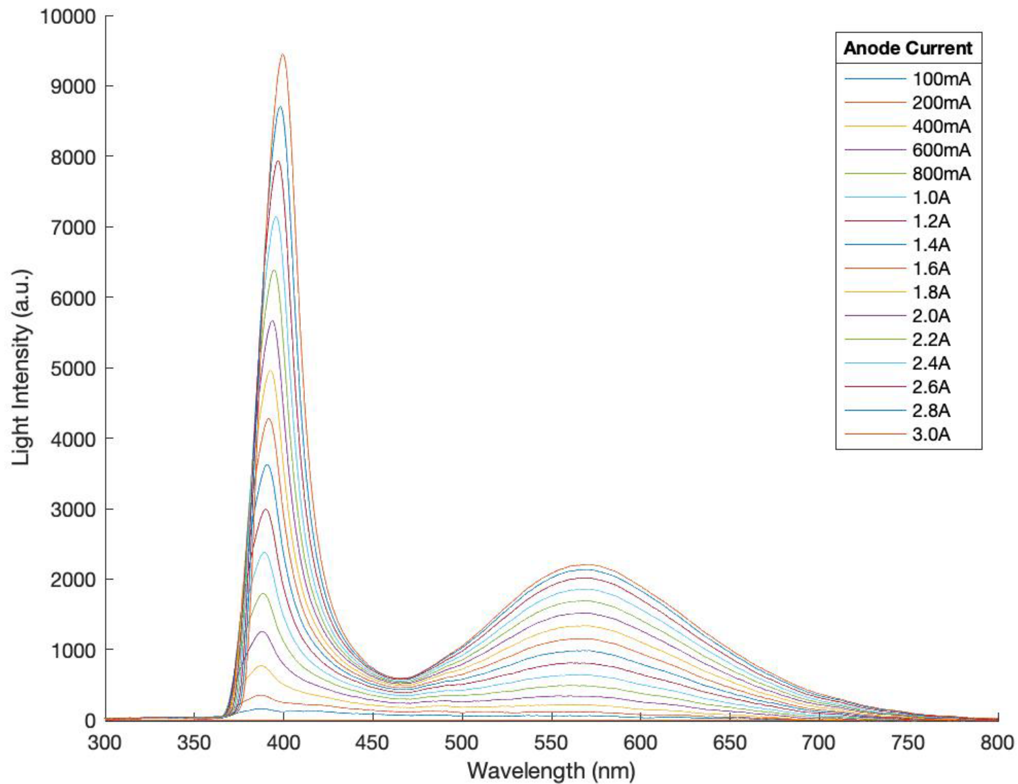

Figure 56. Device C2 Post Second Stress Test GaN Peak Spectra at 30C Varying Current

EL spectrum measurements for device C3 at varying temperatures and current fixed at 1 A again show a degradation to the emitted light intensity. As with device C2, several inversions in the spectral data take place with a rightward shift in the peak intensity for each temperature, illustrated in Figure 57.

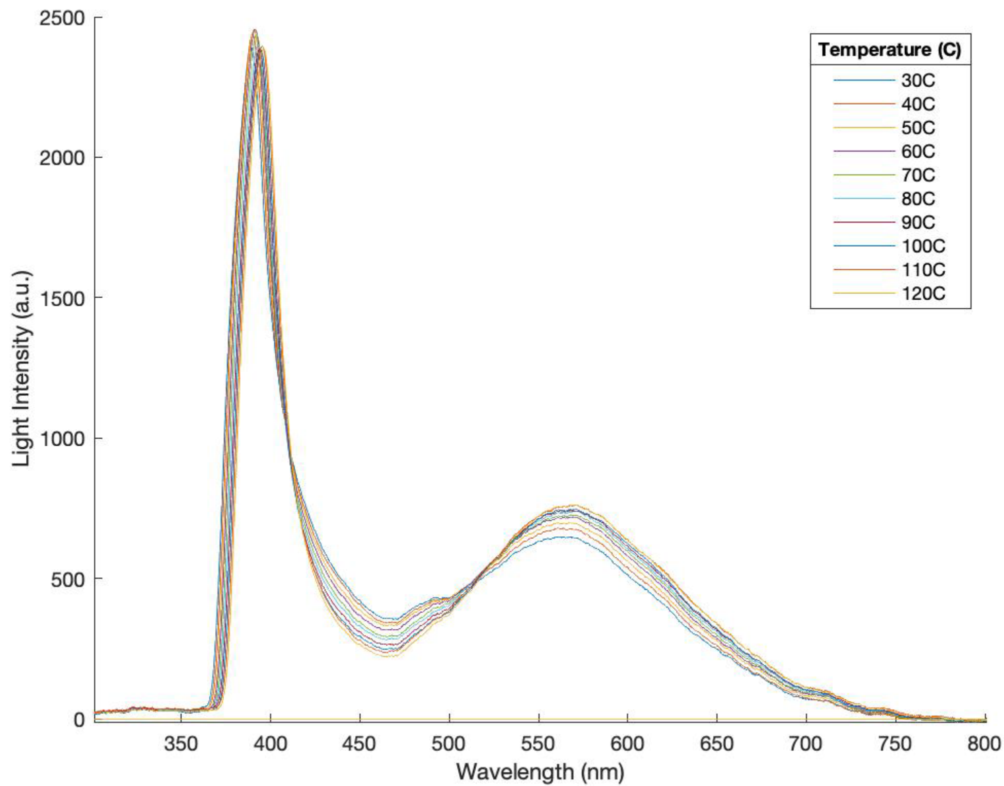

Figure 57. Device C3 Post Second Stress Test GaN Peak Spectra at 1A Varying Temperature

G. ANALYSIS OF STRESS TEST RESULTS ON COMMERCIAL DEVICES

The initial pre- and post-stress EL spectrum data collected for device C2 show a clear degradation in the intensity of light emitted from the power diode. From pre-stress to post-stress measurements in the first test, the peak intensity measured at 1 A at 90 C dropped from 2987.2 a.u. to 494.4 a.u, with final peak intensity being 16.5% of the original value. The current and temperature sweep EL spectra collected at pre- and post-stress timepoints show a decrease in peak intensity, as well as an inversion of the peaks at the temperatures between 30 C and 120 C observed in Figure 58, and a rightward shift in the wavelength of peak intensity, shown in Figure 59.

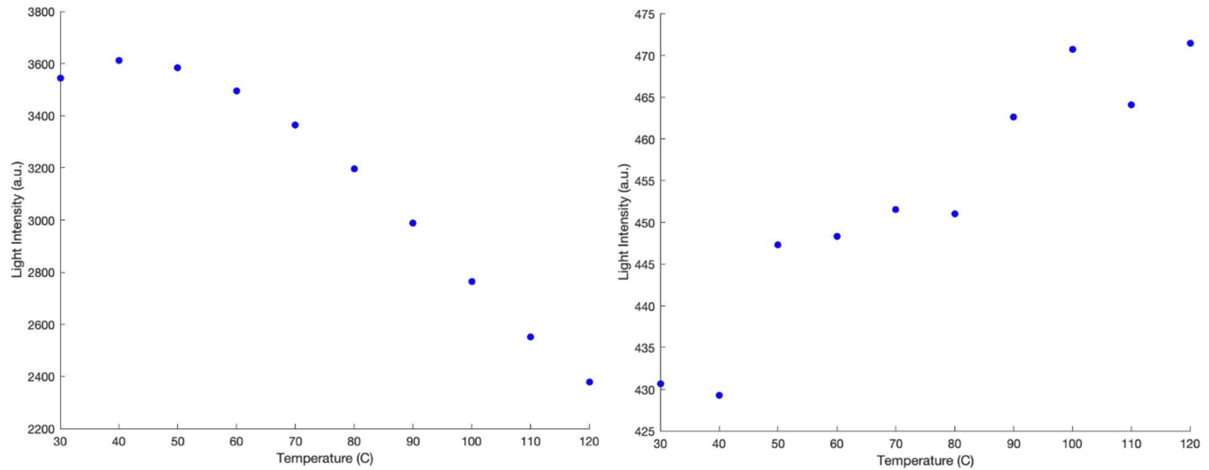

Figure 58. Device C2 Intensity vs. Intensity for Pre-stress (left) and Post-stress (right) at 1a and Varying Temperature

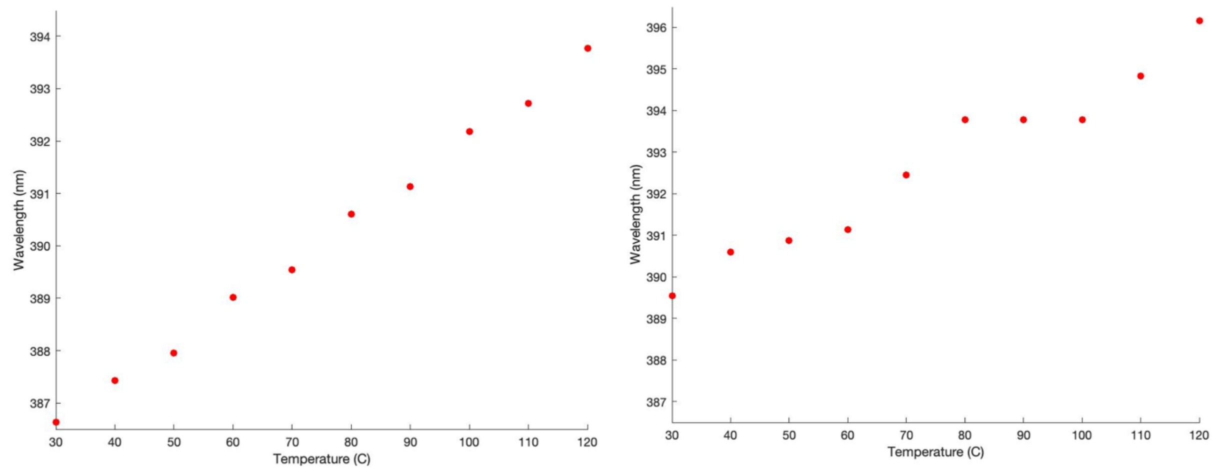

Figure 59. Device C2 Wavelength vs. Intensity for Pre-stress (left) and Post-stress (right) at 1a and Varying Temperature

Though the first pre-stress electrical measurements from device C2 were skewed due to a high-resistance connection, the data collected for the reverse-biased measurements show leakage current to be in the hundreds of nanoamps-to-microamps range. The data collected after the second stress cycle show leakage current now in the tens-of-microamps range over the temperatures sampled, showing degradation of the diode over time under a constant current and elevated temperature stress.

Pre- and post-stress electrical measurements for device C3 were characteristic of a GaN PN diode, and comparison of results showed degradation of the device. Reverse bias leakage current pre-stress was 3.5 nA at 30 C, while that post-stress was 90 nA at 30 C, an increase of 25.7 times the original value. As with that of device C2, the intensity of device C3 dropped between pre- and post-stress measurements, with peak intensity measured at 90 C and 1 A decreasing from 2531.5 a.u. to 2386.9 a.u., a 5.7% decrease. This change is not as marked as the change in C2, which can be attributed to the 84-hour stress interval for C3; in contrast, the C2 intervals were 168 hours each. The pre- and post-stress temperature EL spectrum sweeps revealed the peak intensity for given temperatures undergoing a slight inversion in temperature dependence and peak intensity in Figure 60. Even with a shorter duration test for C3, the rightward shift in the peak wavelength at varying temperatures was present, as illustrated in Figure 61.

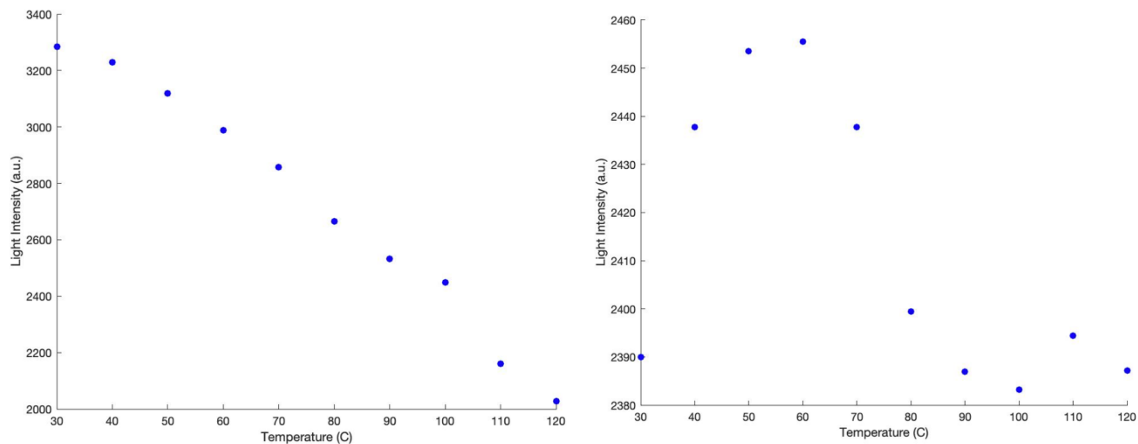

Figure 60. Device C3 Intensity vs. Temperature for Pre-stress (left) and Post-stress (right) at 1 A and Varying Temperature

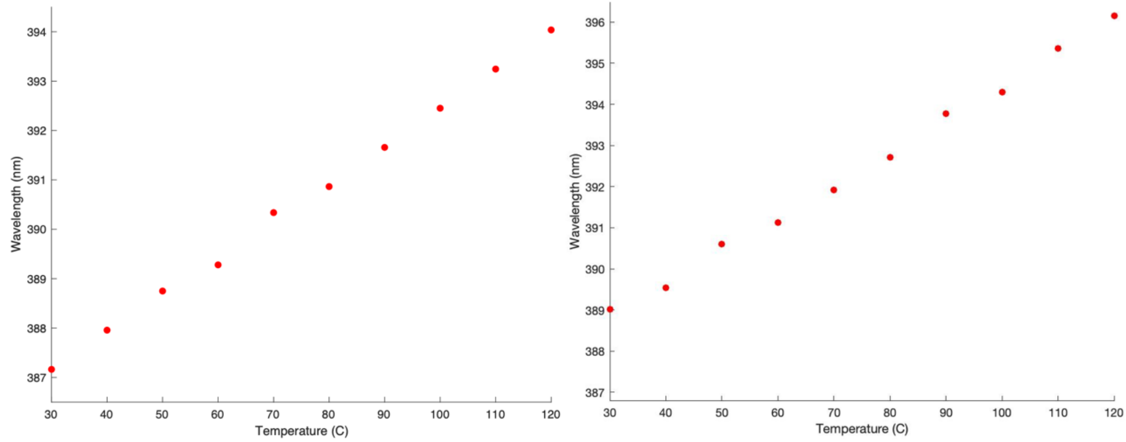

Figure 61. Device C3 Wavelength vs. Temperature for Pre-stress (left) and Post-stress (right) at 1A and Varying Temperature

Pre-stress, peak intensity dropped as temperature was increased over the range of 30 C to 120 C, while post stress the opposite was true, with peak intensity being expressed at 120 C and the lowest intensity at 30 C. The overall degradation in light output due to the stress may be attributed to defects building up and causing traps; these changes would lend more towards non-radiative recombination vs. radiative recombination, resulting in diminished light output, as well as elevated temperatures seeing higher intensity post-stress due to changes within the crystal structure of the diode. Data showing the change in band-to-band peak intensity and the wavelength shifts from pre- and post-stress data are shown in Appendix C.

VI. CONCLUSION AND FUTURE WORK

A. CONCLUSION

This study was conducted using GaN PN diodes optimized for power electronics. While power devices are not optimized for light emission, the EL of these devices was sufficient to collect spectrum data and track the peak intensity degradation over time in concert with changing I-V characteristics during heat- and current-induced stress. This result shows how stress applied to a GaN power diode over time causes the known migration and propagation of pre-existing defects in the crystal structure of the diode, leading to reduced radiative recombination, resulting in lower intensity of light being emitted. The changes in electrical characteristics coincide with the reduced light output and show that though the device still functions as a diode, over time the performance may be affected because of the stress. This information, applied to large-volume HTOL testing coupled with EL spectral analysis, can be applied to power systems designed in the future to monitor the intensity and shift in wavelength to diagnose device health in systems utilizing PN junctions (diodes, HEMTs, etc.) with a direct bandgap that emit light sufficient to analyze the spectrum; notably, this would require the packaging for the devices be designed such that a fiber may be placed to couple the light emitted to be analyzed via a spectrometer.

This work complements reliability studies done on commercial-grade GaN PN diodes by Kizilyalli et al. in 2015 [10]. Constant-current HTOL stress tests performed by Kizilyalli's group demonstrated the capacity to develop high-quality GaN devices with low leakage currents and small changes in on-state resistance as seen with the reliability tests on devices C2 and C3. The long-duration, constant-current stress tests performed in this study showed mΩ changes in on-state resistance, as well as maintaining sub-mA leakage current profiles over the duration of the test. This thesis furthers the study of GaN PN diode reliability by examining the change in EL spectra over time caused by current- and temperature-induced aging.

Raising the understanding and reliability of WBG power devices, in this case specifically GaN devices, would allow for further miniaturization of power electronics while increasing power efficiency and reliability, with the ability to remotely monitor/ control passively with EL spectra. The result would allow platforms with restricted space and reliability requirements, such as ships, submarines, UUVs, and seabed systems, to operate with more reliable and more efficient power sources, translating to more dependable equipment and enhanced operational endurance.

B. FUTURE WORK

Recommendations for future work include modifications to the updated HTOL system, as well as conducting HTOL stress tests with EL spectrum analysis on larger volumes of devices to aid in the study of device reliability.

The updated HTOL system would benefit from modifications to the HTOL LabVIEW program to allow collection of EL spectrum data from multiple devices at a time. The hardware for this capability is already installed but was not exploited due to the scarcity of DUTs available for the experiment. Collecting I-V-T and EL spectrum measurement data for batches of devices at a time would allow for further research into the reliability of GaN power diodes and investigation of how stress affects light output over time based on stress conditions (stress current, temperature, duration, etc.).

Another modification that would benefit this system would be upgrading the capacity of the DC power supplies currently installed. The ability to stress diodes at extreme temperatures and at room temperature conditions over a greater current range would allow testing of more robust devices and evaluation of the effects on the EL spectra for commercial devices already on hand at higher currents. The upgraded current capacity for the updated HTOL switch matrix is 16 A, vs. the 3.2 A maximum output of the power supplies presently installed in the system.

Updating the PC used as the control system with internet connectivity would allow for remote monitoring of system parameters, which would allow researchers to detect a testing issue earlier in the process. Had remote access been enabled, the high-resistance connection could have been diagnosed earlier in the test of device C2, which

would have allowed for the test to be halted and troubleshot. More broadly, this change would allow issues to be recognized even if personnel access to the building is restricted due to extenuating circumstances, such as was the pandemic-related instance in this experiment.

The test system would benefit from redesigning the switch matrix to minimize noise due to EMI during I-V-T measurements. High-quality GaN power devices are expected to have very low leakage current at voltages the Keysight B1500A scope is capable of sampling, which may be below the noise floor of picoamps to nanoamps that the system has in its current state of design.

THIS PAGE INTENTIONALLY LEFT BLANK

APPENDIX A. LABVIEW HTOL INITIALIZATION PANES

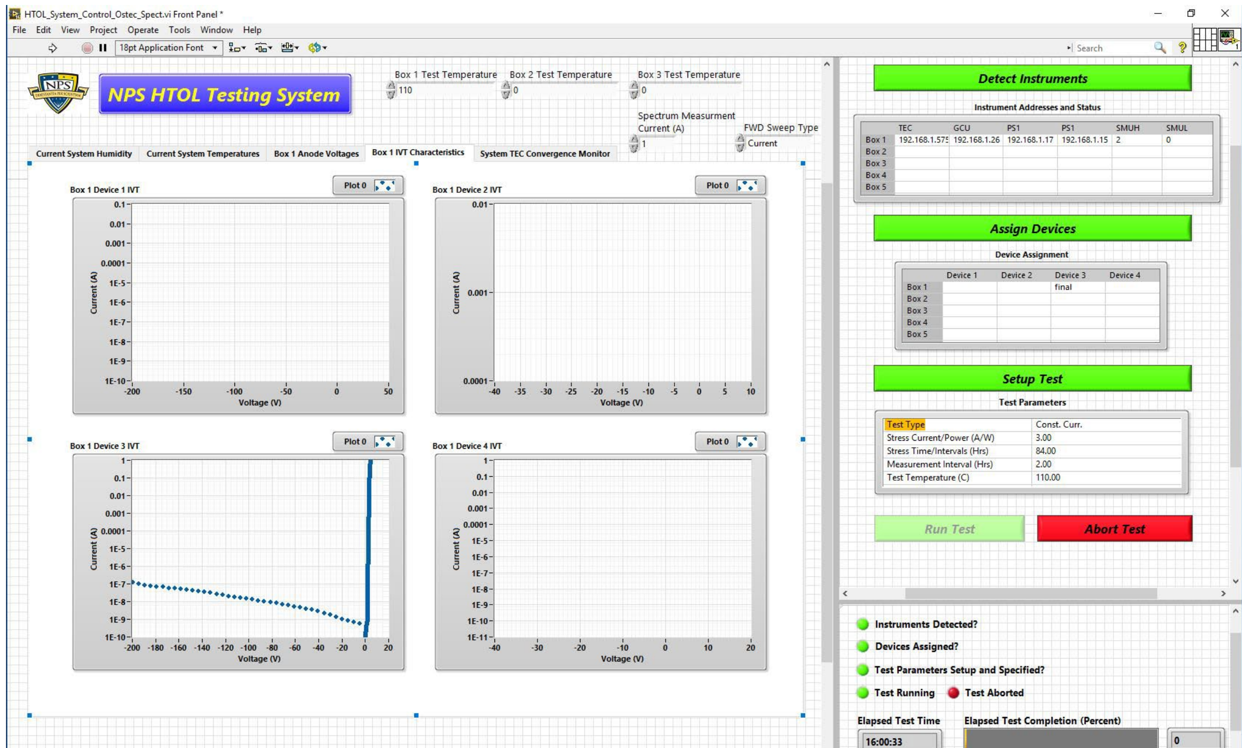

Figure 62. Screen Capture of HTOL EL Spectra Testing System Main User Interface in LabVIEW

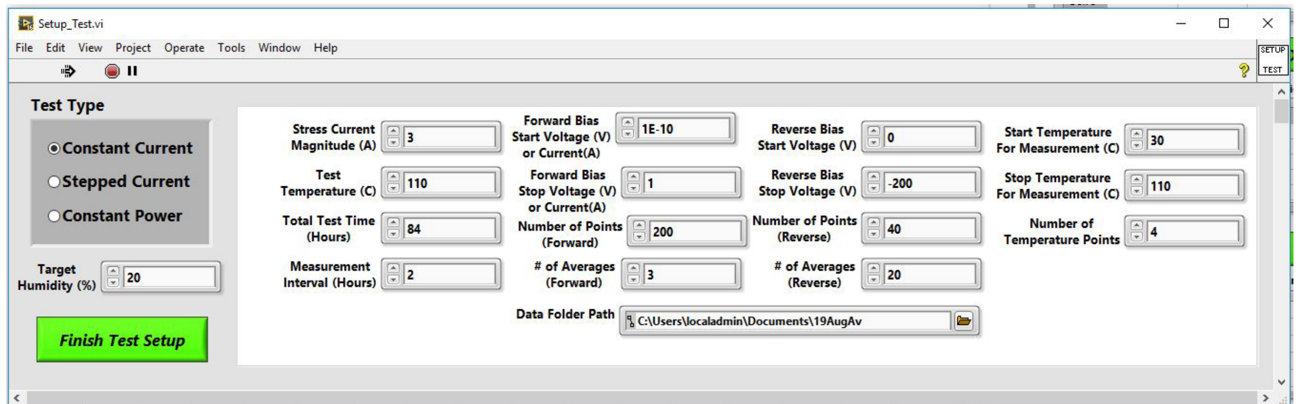

Figure 63. Screen Capture of HTOL EL Spectra Testing Parameters Setup Panel In LabVIEW

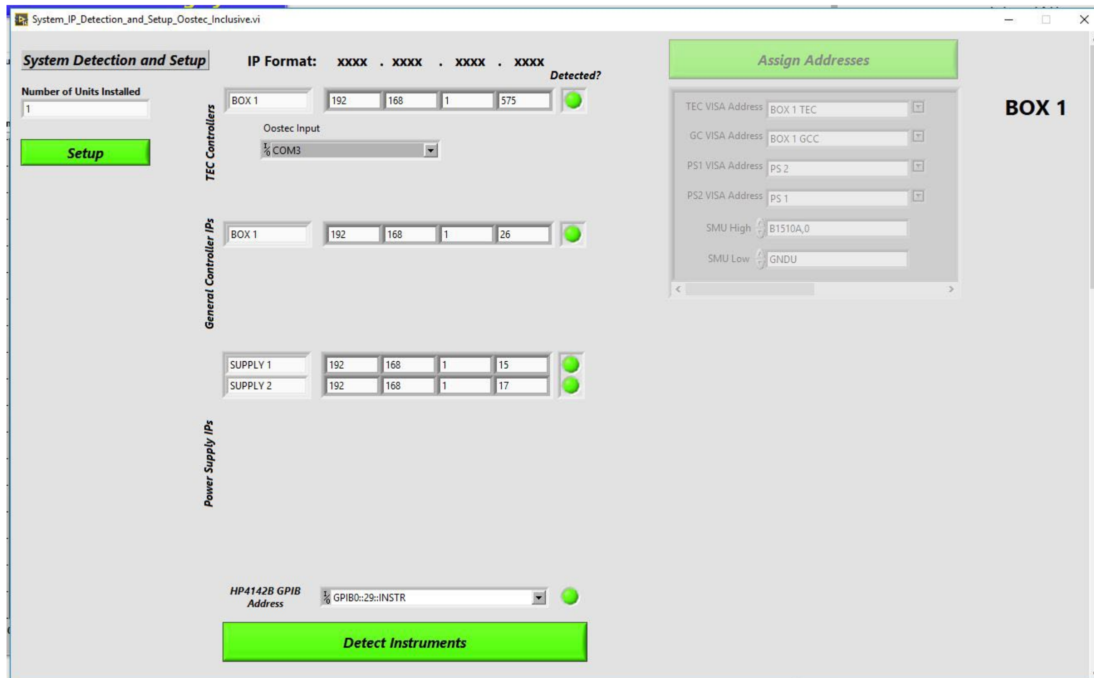

Figure 64. Screen Capture of HTOL EL Spectra Testing Sub-system Setup Panel in LabVIEW

APPENDIX B. LABVIEW SPECTROSCOPY ADDITION

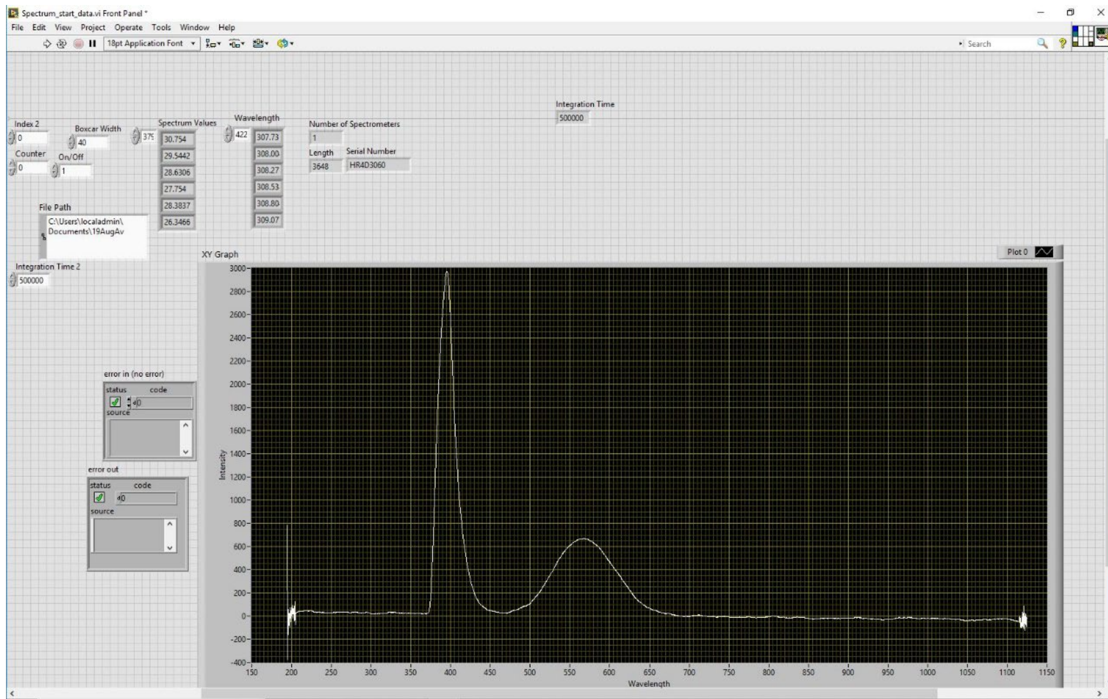

Figure 65. Screen Capture of HTOL EL Spectra Testing System Spectrometer Integration SubVI Front Panel in LabView

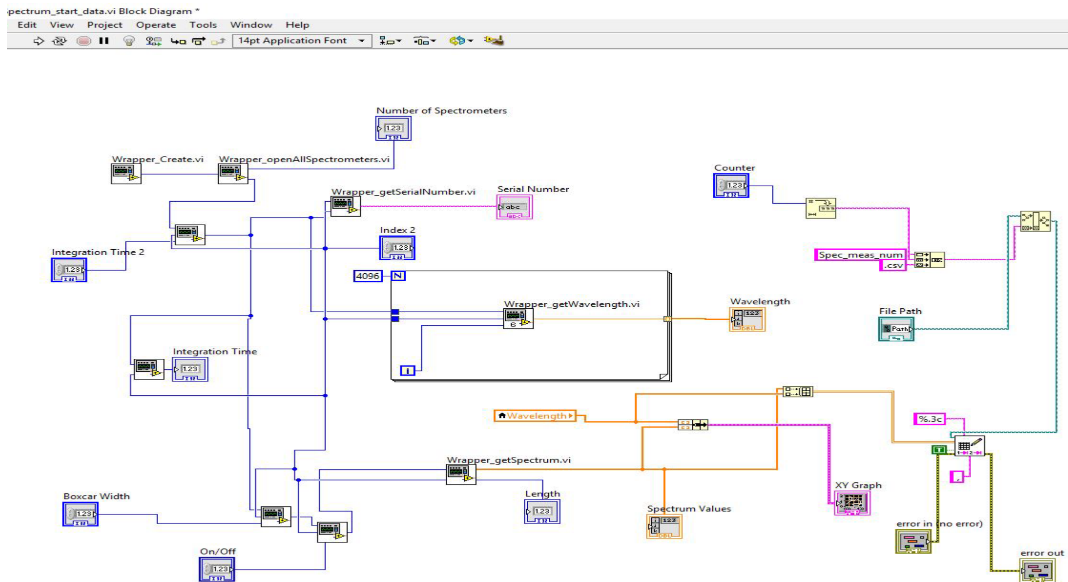

Figure 66. Screen Capture of HTOL EL Spectra Testing System Spectrometer Integration Block Diagram in LabVIEW

THIS PAGE INTENTIONALLY LEFT BLANK

APPENDIX C. COMMERCIAL DEVICE SPECTRAL DATA VS. INTENSITY PRE AND POST STRESS

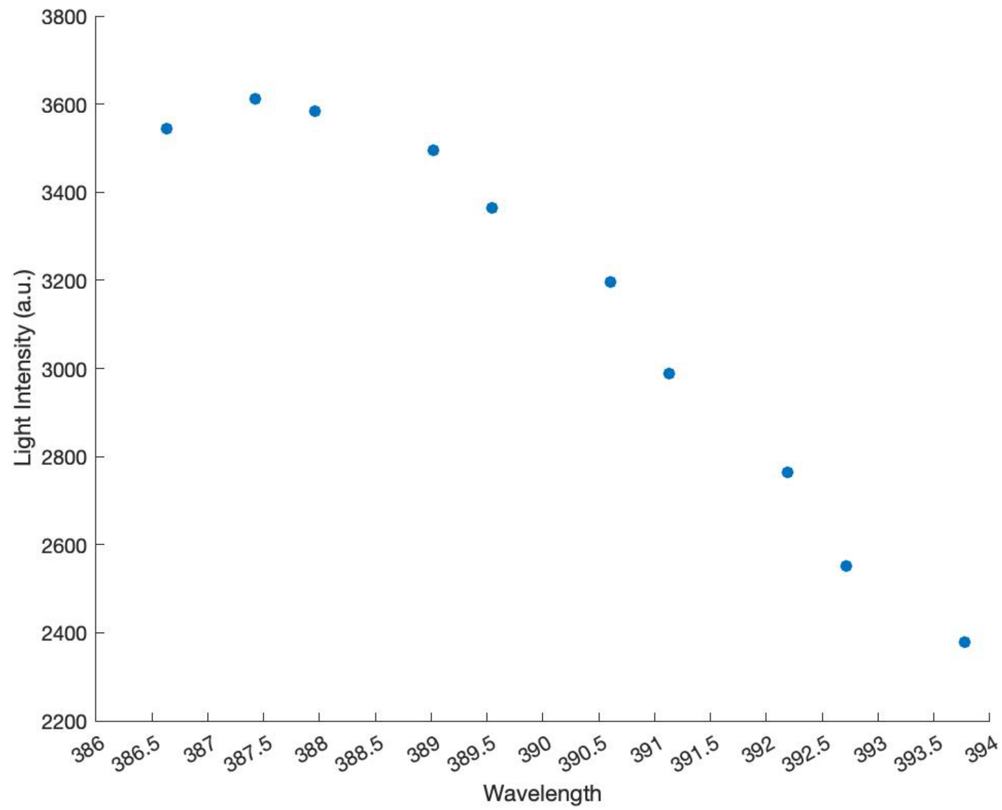

Figure 67. Device C2 Pre-stress Band-to-band Peak Intensity vs. Wavelength

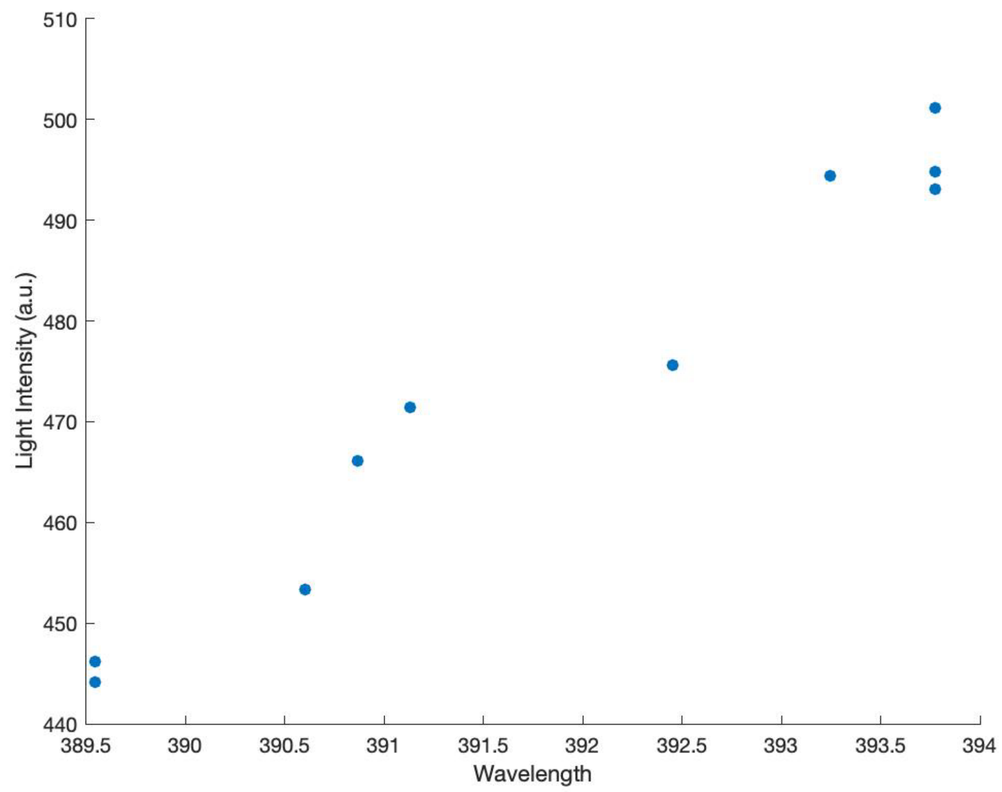

Figure 68. Device C2 Post-stress Band-to-band Peak Intensity vs. Wavelength

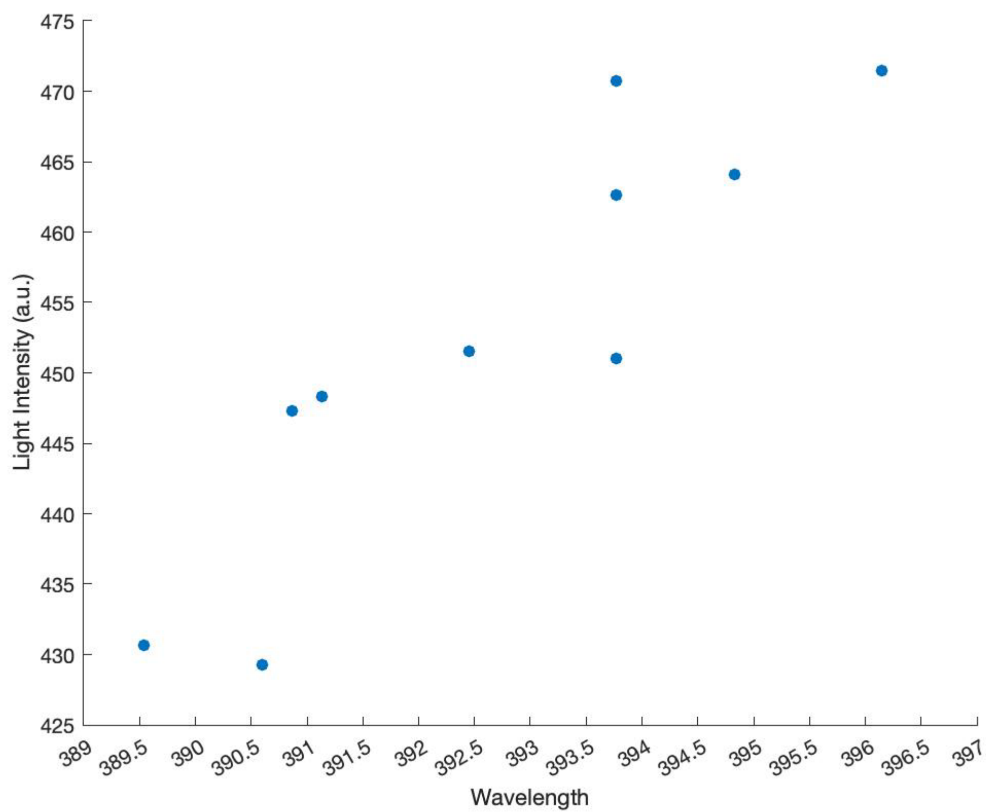

Figure 69. Device C2 Post Second Stress Band-to-band Peak Intensity vs. Wavelength

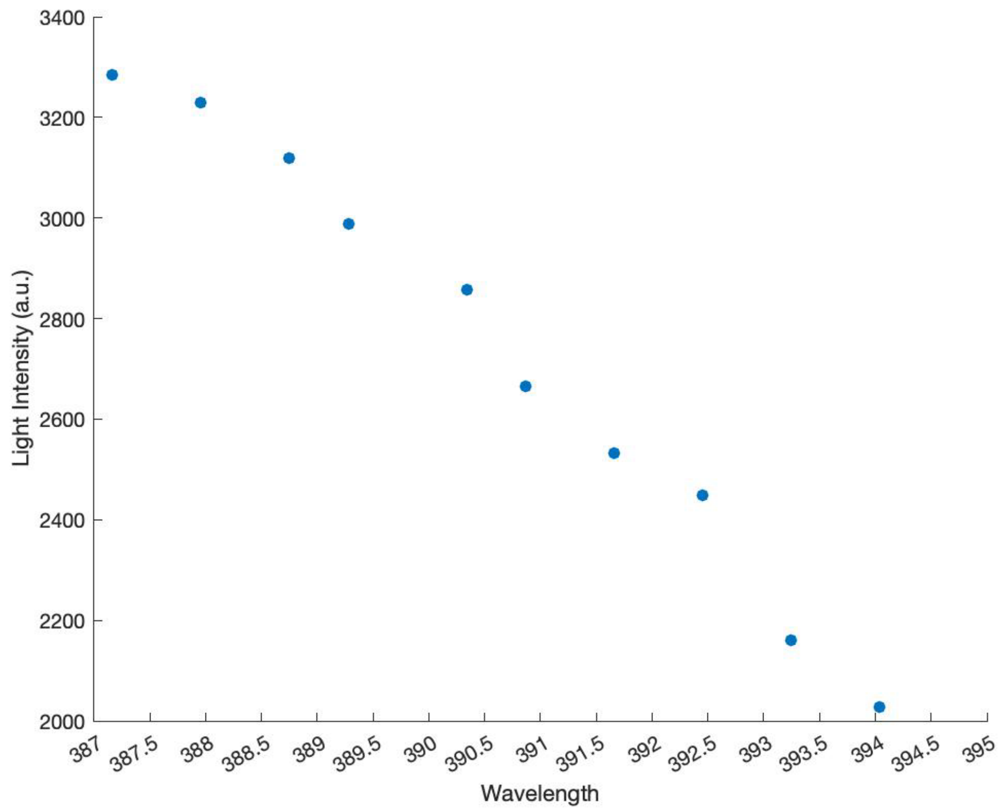

Figure 70. Device C3 Pre-stress Band-to-band Peak Intensity vs. Wavelength

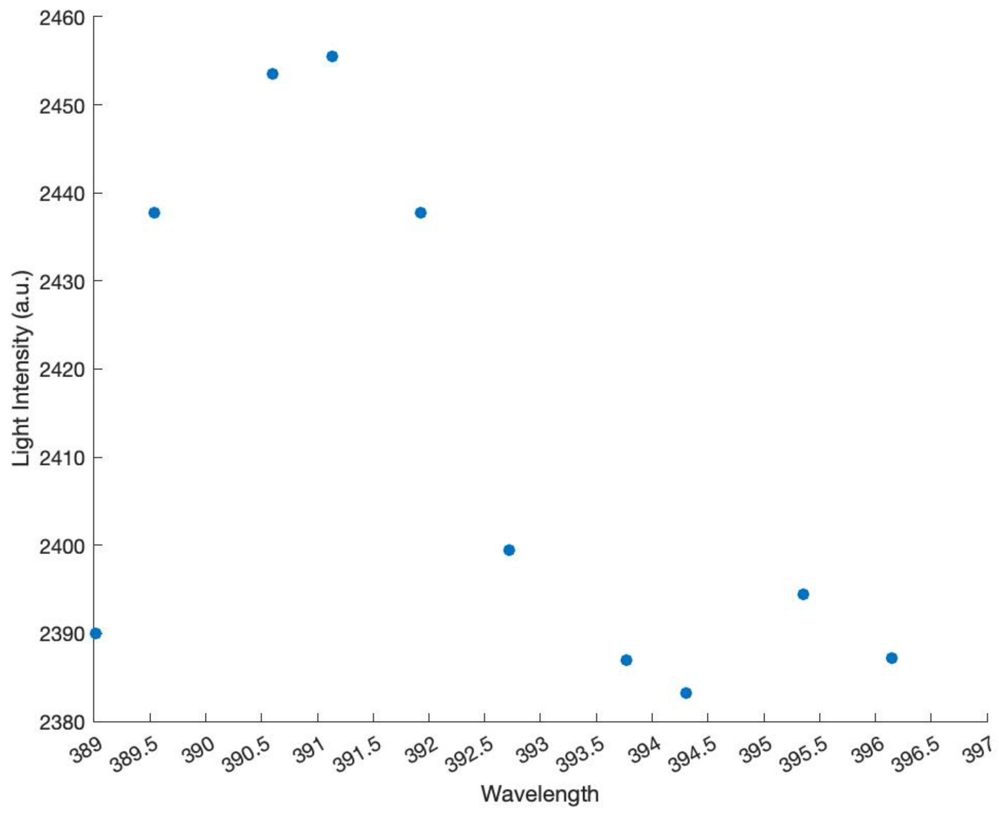

Figure 71. Device C3 Post-stress Band-to-band Peak Intensity vs. Wavelength

THIS PAGE INTENTIONALLY LEFT BLANK

LIST OF REFERENCES

[1] Jeff Smith, "Future Naval Applications for Unmanned Undersea Vehicles," *Ocean News Technol.*, pp. 48–50, 2020.

[2] G.-J. Su, "Comparison of Si, SiC, and GaN based Isolation Converters for Onboard Charger Applications," 2018, pp. 1233–1239. doi: 10.1109/ECCE.2018.8558063.

[3] Office of the Chief of Naval Operations Washington, DC, "The Navy Unmanned Undersea Vehicle (UUV) Master Plan," WASHINGTON DC, 2004. [Online]. Available: https://apps.dtic.mil/sti/citations/ADA511748

[4] D. Burg and J. H. Ausubel, "Moore's Law revisited through Intel chip density," *PLoS One*, vol. 16, no. 8, Aug. 2021 [Online]. Available: https://doi.org/10.1371/journal.pone.0256245.

[5] R. Mitova, R. Ghosh, U. Mhaskar, D. Klikic, M.-X. Wang, and A. Dentella, "Investigations of 600-V GaN HEMT and GaN Diode for Power Converter Applications," *IEEE Trans. Power Electron.*, vol. 29, no. 5, pp. 2441–2452, May 2014, https://doi.org/10.1109/TPEL.2013.2286639.

[6] Y. Zhang, "Comparison Between Competing Requirements of GaN and SiC Family of Power Switching Devices," *IOP Conference Series.Materials Science and Engineering,* vol.738, *(1),* 2020. Available: https://libproxy.nps.edu/login?url=https://www.proquest.com/scholarly-journals/comparison-between-competing-requirements-gan-sic/docview/2561994618/se-2. DOI: https://doi.org/10.1088/1757-899X/738/1/012004.

[7] C. Robinson, "Electrooptical characteristics of SiC MOSFET body diode and GaN power diode," M.S. thesis, Dept. of Elec. and Comp. Eng., NPS, Monterey, CA, USA. 2022.

[8] L. Liu and J. H. Edgar, "Substrates for gallium nitride epitaxy," *Mater. Sci. Eng. R Rep.*, vol. 37, no. 3, pp. 61–127, Apr. 2002 [Online]. Available: https://doi.org/10.1016/S0927-796X(02)00008-6.

[9] K. Fu *et al.*, "Investigation of GaN-on-GaN vertical p-n diode with regrown p-GaN by metalorganic chemical vapor deposition," *Applied physics letters*, vol. 113, no. 23, p. 233502, Dec. 2018 [Online]. Available: https://doi.org/10.1063/1.5052479

[10] I. C. Kizilyalli, P. Bui-Quang, D. Disney, H. Bhatia, and O. Aktas, "Reliability studies of vertical GaN devices based on bulk GaN substrates," *Microelectronics and reliability*, vol. 55, no. 9–10, pp. 1654–1661, [Online], 2015. https:// doi.org/ 10.1016/j.microrel.2015.07.012.

[11] B. A. Clemmer, "A Reliability Study on the Effects of HTOL and High-Current Density Stress Testing on Commercial-Grade Vertical N-Type Pd/Gan Schottky Diodes," M.S. thesis, Dept. of Elec. and Comp. Eng., NPS, Monterey, CA, USA, 2021.

[12] M. A. Broeg, "Current and temperature sensing via light emission from GaN PN junctions," M.S. thesis, Dept. of Elec. and Comp. Eng., NPS, Monterey, CA, USA, 2019.

[13] T. J. Flack, B. N. Pushpakaran, and S. B. Bayne, "GaN Technology for Power Electronic Applications: A Review," *J. Electron. Mater.*, vol. 45, no. 6, pp. 2673–2682, Jun. 2016 [Online]. Available: https://doi.org/10.1007/s11664-016-4435-3.

[14] P. G. Neudeck, R. S. Okojie, and L.-Y. Chen, "High-temperature electronics - a role for wide bandgap semiconductors?," *Proc. IEEE*, vol. 90, no. 6, pp. 1065–1076, Jun. 2002 [Online]. Available: https://doi.org/10.1109/ JPROC.2002.1021571.

[15] K. Nelkovski, "A GaN Roundup: RF MMICs, Power ICs, and SOIC Drivers Keep the Ball Rolling," All About Circuits, December 22, 2021 [Online]. Available: https://www.allaboutcircuits.com/news/a-gallium-nitride-roundup-rf-mmic-power-ic-and-soic-drivers-keep-ball-rolling/ (accessed Aug. 01, 2022).

[16] B. J. Baliga, "Power semiconductor device figure of merit for high-frequency applications," in *IEEE Electron Device Letters*, vol. 10, no. 10, pp. 455–457, Oct. 1989 [Online]. Available: https://doi.org/10.1109/55.43098

[17] U. Mishra and J. Singh, *Semiconductor Device Physics and Design*. Dordrecht, Netherlands: Springer, 2007 [Online]. https://doi.org/10.1007/978-1-4020-6481-4.

[18] W. Bi, H. Kuo, P. Ku, and B. Shen, *Handbook of GaN Semiconductor Materials and Devices*, 1st ed. Milton: CRC Press, [Online] 2018. https://doi.org/10.1201/ 9781315152011.

[19] J. Muth *et al.*, "Absorption coefficient, energy gap, exciton binding energy, and recombination lifetime of GaN obtained from transmission measurements," *Applied physics letters*, vol. 71, no. 18, pp. 2572–2574, 1997, [Online]. https://doi.org/10.1063/1.120191.

[20] F. Olivier, A. Daami, C. Licitra, and F. Templier, “Shockley-Read-Hall and Auger non-radiative recombination in GaN based LEDs: A size effect study,” *Appl. Phys. Lett.*, vol. 111, no. 2, pp. 22104, 2017 [Online]. Available: https://doi.org/10.1063/1.4993741.

[21] J.-H. Yang, L. Shi, L.-W. Wang, and S.-H. Wei, “Non-Radiative Carrier Recombination Enhanced by Two-Level Process: A First-Principles Study,” *Sci. Rep.*, vol. 6, no. 1, Art. no. 1, Feb. 2016 [Online]. Available: https://doi.org/10.1038/srep21712.

[22] Engineering LibreTexts, “Auger Recombination,” Nov. 03, 2018 [Online]. Available: https://eng.libretexts.org/Bookshelves/Materials_Science/Supplemental_Modules_(Materials_Science)/Solar_Basics/C._Semiconductors_and_Solar_Interactions/IV._Recombination_of_Charge_Carriers/3._Auger_Recombination (accessed Aug. 02, 2022).

[23] J. Piprek, “Efficiency droop in nitride-based light-emitting diodes,” *Physica status solidi. A, Applications and materials science*, vol. 207, no. 10, pp. 2217–2225, [Online]. 2010. https:// doi.org/10.1002/pssa.201026149.

THIS PAGE INTENTIONALLY LEFT BLANK

INITIAL DISTRIBUTION LIST

1. Defense Technical Information Center
   Ft. Belvoir, Virginia

2. Dudley Knox Library
   Naval Postgraduate School
   Monterey, California